



University of KwaZulu-Natal
College of Agriculture, Engineering and Science

DEVELOPMENT OF NEURO-FUZZY STRATEGIES FOR PREDICTION AND MANAGEMENT OF HYBRID PV-PEMFC- BATTERY SYSTEMS

by

Ntumba Marc-Alain Mutombo

Thesis submitted in fulfilment of the academic requirements for the degree of Doctor of
Philosophy in Electrical Engineering

Supervisor : Prof. Freddie L. Inambao

Co-supervisor : Dr Remy Tiako

12th July 2017

“As the candidate’s Supervisors we agree/~~do not agree~~ to the submission of this dissertation”.

Prof. Freddie Inambao



.....

NAME OF SUPERVISOR

SIGNATURE

Dr. Remy Tiako



.....

NAME OF CO-SUPERVISOR

SIGNATURE

DECLARATION 1 – PLAGIARISM

I, **Ntumba Marc-Alain Mutombo**, declare that:

1. The research reported in this dissertation, except where otherwise indicated, is my original research.
2. This dissertation has not been submitted for any degree or examination at any other university.
3. This dissertation does not contain other persons' data, pictures, graphs or other information, unless specifically acknowledged as being sourced from other persons.
4. This dissertation does not contain other persons' writing, unless specifically acknowledged as being sourced from other researchers. Where other written sources have been quoted, then:
 - a. Their words have been re-written but the general information attributed to them has been referenced.
 - b. Where their exact words have been used, then their writing has been placed in italics and inside quotation marks, and referenced.
5. This dissertation does not contain text, graphics or tables copied and pasted from the Internet, unless specifically acknowledged, and the source being detailed in the dissertation and in the References sections.

Signed



.....

DECLARATION 2 – PUBLICATIONS

DETAILS OF CONTRIBUTION TO PUBLICATIONS that form part and/or include research presented in this dissertation (include publications in preparation, submitted, in press and published and give details of the contributions of each author to the experimental work and writing of each publication).

Publication 1: **N. M-A. Mutombo**, F. L. Inambao, and R. Tiako, “Photovoltaic systems growing,” *Proceedings of the 1st International Conference on Clean Energy for Sustainable Growth in Developing Countries*, Botswana International University of Science and Technology, 16-18 September, 2015, Gaborone, Botswana (**PRESENTED**)

Publication 2: **N. M-A Mutombo**, Inambao F.L. and Remy Tiako: “Design and Analysis of Grid-Connected Photovoltaic System for Residential Applications Case Study of Durban, South Africa”, *African Journal of Science, Technology, Innovation and Development*, (**SUBMITTED**).


Publication 3: **N. M-A Mutombo**, F. L. Inambao, and G. Bright, “Performance analysis of thermosyphon hybrid photovoltaic thermal collector,” *Journal of Energy of Southern Africa*, Vol 27 No 1, pp 28-38, February 2016.

Publication 4: **N. M-A Mutombo**, F. L. Inambao, and R. Tiako, “Fuel cells development, applications and market”, *ARPJ Journal of Engineering and Applied Sciences*, (**SUBMITTED**).

Publication 5: **N. M-A Mutombo**, F. L. Inambao, R. Tiako, and S. A. O. Ilupeju, “Energy management for stand-alone hybrid photovoltaic-PEM fuel cells systems,” *International Journal of Applied Engineering Research*, (**IN PRESS**).

Publication 6: **N. M-A Mutombo**, F. L. Inambao, R. Tiako, and S. A. O. Ilupeju, “Neuro-fuzzy strategies for prediction and management of hybrid PV-PEMFC batteries systems,” *International Journal of Engineering Research in Africa*, (**UNDER REVIEW**).

In all these papers, I, Ntumba Marc-Alain Mutombo was the main and corresponding author, whilst Prof. Freddie L. Inambao and Dr Remy Tiako were the co-authors and my research supervisor and co-supervisor, respectively and Dr Samuel A. O. Ilupeju was a co-author

Signed: 

ACKNOWLEDGEMENTS

I would particularly like to thank my supervisor Prof Freddie L. Inambao for his enthusiasm, encouragement, persistent support and guidance in all aspects of this research work. My gratitude is also due to Dr Remy Tiako who agreed to be my second supervisor, for his advice and guidance.

This dissertation is not only a result of my own devotion and determination, but is largely a credit to my wife Sidonie Mangabu, my sweet daughter Pricilla Mwa-Mujinga, my son Ethaniel Mutombo, my son Emmanuel Ilunga, my father Polycarpe Mutombo, my mother Therese Mujinga, my brother Jean-Claude Mutombo and my friend and brother Evans Eshiemogie Ojo and my other relatives for their love, encouragement and support.

I would also like to express my heartfelt thanks to all my colleagues in the Green Energy Solutions Research Group (GES) for making helpful suggestions throughout the duration of my studies.

ABSTRACT

Many clean electricity sources are available and one of the most important is sunlight. Sunlight can be converted into electricity by the use of photovoltaic (PV) systems. High output electrical energy can be obtained from photovoltaic (PV) systems subjected to high irradiance. PV systems alone cannot cover electricity demand, especially at low sunlight. To remediate this situation different back-up systems are used; some of which damage the environment. In addition, variability of the solar insolation often leads to load energy flow management problems which tend to shorten the battery lifespan; but optimal solutions from the existing classical techniques for dealing with such non-linearity are usually insufficient. Thus, the motivation for this study.

The study has investigated the design and implementation of a neuro-fuzzy system for the prediction and management of energy flow for hybrid photovoltaic systems equipped with fuel cells and battery storage as back-up for household demand; especially in winter when solar irradiance is low and as a result the PV out is low. This was achieved by reviewing trends in the development of PV systems to highlight the various efficiency improvement methods and their future market potentials. The theoretical design and simulation study was performed with specific component models of the system in order to develop a typical energy management strategy of a grid-connected residential PV system, based on household demand case study for Durban – South Africa; to assess the performance and to establish energy flow control strategies for a PV Proton Exchange Membrane Fuel Cell (PEMFC) system.

Conclusively, an adaptive neuro-fuzzy interference system (ANFIS) for the management and control of the energy flow of different components of a hybrid photovoltaic-battery fuel cell system was developed. The system was compared with an artificial neural network (ANN); and the results from the two systems correlated very well for a typical non-linear system, which is difficult to model with classical control techniques. The system developed does not only manage power flows but also prolongs battery lifetime while taking environmental parameters, namely: solar insolation and ambient temperature into consideration.

TABLE OF CONTENT

DECLARATION 1 – PLAGIARISM.....	iiii
DECLARATION 2 – PUBLICATIONS	iv
ACKNOWLEDGEMENTS	v
ABSTRACT.....	vi
LIST OF FIGURES	x
LIST OF TABLES	xii
LIST OF APPENDICES	xiii
INTRODUCTION	1
CHAPTER 1 : PHOTOVOLTAIC SYSTEMS GROWING	4
Abstract	4
1.1 Introduction.....	5
1.2 Photovoltaic systems	5
1.2.1 Solar cells.....	5
1.2.2 Efficiency and performance	6
1.2.3 Environmental impact of PV technology	8
1.2.4 Applications	8
1.3 Evolution of PV capacities	9
1.4 Economy	10
1.5 Conclusion	11
References	12
CHAPTER 2 : DESIGN AND ANALYSIS OF GRID-CONNECTED PHOTOVOLTAIC SYSTEM FOR RESIDENTIAL APPLICATION – CASE STUDY, DURBAN, SOUTH AFRICA.....	15
Abstract	15
2.1 Introduction.....	16
2.2 South Africa and the electrical energy challenge	16
2.2.1 South Africa’s electricity production.....	16
2.2.2 Electricity crisis in South Africa.....	17
2.2.3 Electricity crisis strategic plan	17
2.2.4 South Africa solar irradiance and tilt angle	17
2.3 Photovoltaic module	18
2.3.1 Modelling of photovoltaic module.....	19
2.3.2 The PV I-V curve under standard test conditions (STC).....	20
2.3.3 Effects of temperature and solar irradiance on I-V curves	21
2.3.4 Determination of cell temperature and average efficiency	23
2.4 Design of photovoltaic system for a modest Durban household	23
2.4.1 Load determination	23
2.4.2 Grid connected photovoltaic array sizing	24
2.5 Grid connected PV system simulations	25
2.6 Economics of the PV system	30
2.6.1 Cost of PV system and energy delivery	30
2.6.2 Loan terms and income tax	31

2.6.3	Financing of the PV system	31
2.7	Conclusion and recommendations	34
	References	35
CHAPTER 3 : PERFORMANCE ANALYSIS OF THERMOSYPHON HYBRID PHOTOVOLTAIC THERMAL COLLECTOR.....		37
CHAPTER 4 : FUEL CELLS DEVELOPMENT, APPLICATIONS AND MARKET		49
	Abstract	49
4.1	Introduction.....	50
4.2	Types of fuel cells.....	50
4.2.1	Proton exchange membrane fuel cells	50
4.2.2	Phosphoric acid fuel cell.....	50
4.2.3	Solid oxide fuel cell	51
4.2.4	Alkaline fuel cell.....	51
4.2.5	Molten carbonate fuel cell	51
4.2.6	Direct methanol fuel cell.....	52
4.2.7	Summary of fuel cell types	52
4.3	Evolution of fuel cells.....	52
4.4	Efficiency of fuel cell	53
4.5	Applications.....	55
4.5.1	Power	55
4.5.2	Cogeneration	56
4.5.3	Fuel cell electric vehicles (FCEVs)	56
4.6	Markets and economics	57
4.7	Conclusion	60
	References	61
CHAPTER 5 : ENERGY MANAGEMENT FOR STAND ALONE HYBRID PHOTOVOLTAIC PEM FUEL CELLS SYSTEMS		64
	Abstract	64
5.1	Introduction.....	65
5.2	System description and size.....	65
5.3	System configuration	67
5.4	System modelling	68
5.4.1	Photovoltaic model	68
5.4.2	Fuel cell model.....	69
5.4.3	Battery model.....	69
5.4.4	Electrolyser model	70
5.4.5	Power conditioning	70
5.5	Energy management	70
5.6	Simulations and analysis of results.....	72
5.7	Conclusion	77
	References	78
CHAPTER 6 : NEURO-FUZZY STRATEGIES FOR PREDICTION AND MANAGEMENT OF HYBRID PV-PEMFC-BATTERIES SYSTEMS.....		81
	Abstract	81
6.1	Introduction.....	82
6.2	Review of artificial intelligence applied to photovoltaic and fuel cell systems	82
6.3	Description and operation of the system	84
6.4	Control strategies	85

6.5	Artificial neural networks	86
6.5.1	Algorithm and structure	86
6.5.2	Simulation and validation of ANN model	87
6.6	Neuro-fuzzy control strategies.....	91
6.6.1	Neuro-fuzzy algorithm and structure	91
6.6.2	Simulation and validation of ANFIS model	92
6.7	Comparison of ANN model and ANFIS model obtained.....	96
6.8	Conclusion	99
	References	100
CHAPTER 7 : CONCLUSION		103
APPENDICES		104

LIST OF FIGURES

Figure 1.1: Schematic block diagram of a PV cell	5
Figure 1.2: PV cell, module and array	6
Figure 1.3: The ‘ultimate’ and two ‘nominal’ Shockley-Queisser efficiencies [4]	7
Figure 1.4: Evolution of global PV cumulative installed capacity 2000-2013 [19]	9
Figure 1.5: Global PV cumulative scenario until 2018.....	10
Figure 1.6: Global annual market scenarios until 2018 [34]	11
Figure 2.1: A typical laminated module structure	18
Figure 2.2: Photovoltaic cells, modules and an array	18
Figure 2.3: A simplified equivalent circuit for a PV cell.....	19
Figure 2.4: Q PEAK PV module I-V and P-V characteristic curves at STC simulated with Matlab	20
Figure 2.5: Q PEAK PV module I-V curve at STC simulated with Matlab	21
Figure 2.6: I-V characteristic curves for PV module under various irradiance levels at 25 °C temperature and 1 m/s wind speed simulated with Matlab.....	22
Figure 2.7: I-V characteristic curves for PV module under various cell temperature levels at 1 kW/m ² insolation and 1 m/s wind velocity simulated with Matlab	22
Figure 2.8: PV array simulation results for particular summer day of 04/12/2010	26
Figure 2.9: PV array simulation results for particular summer day of 29/12/2010	27
Figure 2.10: PV array simulation results for particular winter day of 14/06/2011	28
Figure 2.11: PV array simulation results for particular winter day of 28/06/2011	29
Figure 2.12: Average cost of residential PV systems for modest household demand in Durban	31
Figure 2.13: PV system loan balance and loan interest over 20 years.....	32
Figure 2.14: PV system variation of electricity cost over 20 years	33
Figure 2.15: PV system tax savings over 20 years	33
Figure 4.1: Evolution of fuel cells by cell type.....	53
Figure 4.2: Evolution of fuel cells power by cell type.....	54
Figure 4.3: Evolution of fuel cells by application.....	55
Figure 4.4: Evolution of fuel cells power by application.....	55

Figure 4.5: Production ratio of fuel cells by application	58
Figure 4.6: Production ratio of fuel cells by cell type.....	58
Figure 4.7: Evolution of fuel cells by region	58
Figure 4.8: Evolution of fuel cells power by region	59
Figure 5.1: Hybrid PV-PEMFC electrolyser system equipped with a battery bank.....	67
Figure 5.2: Hybrid PV-PEMFC topology	67
Figure 5.3: Flowsheet diagram of the PV-PEMFC hybrid system energy management.....	71
Figure 5.4: Simulation results for summer day of 2010/12/22	73
Figure 5.5: Simulation results for summer day of 2010/12/29	74
Figure 5.6: Simulation results for winter day of 2011/06/07.....	75
Figure 5.7: Simulation results for winter day of 2011/06/28.....	76
Figure 6.1: Block diagram of developed global model [14].....	83
Figure 6.2: Hybrid PV PEMFC topology [5]	84
Figure 6.3: Flow chart energy management [5].....	86
Figure 6.4: ANN performance	88
Figure 6.5: ANN error autocorrelation	88
Figure 6.6: ANN input-error cross-correlation	89
Figure 6.7: ANN time-series response.....	89
Figure 6.8: ANN regression.....	90
Figure 6.9: ANN structure	90
Figure 6.10: First-order Sugeno fuzzy model with two rules [38]	92
Figure 6.11: ANFIS properties	93
Figure 6.12: ANFIS membership functions.....	93
Figure 6.13: ANFIS training error	94
Figure 6.14: ANFIS training data time-series.....	94
Figure 6.15: ANFIS checking data time-series.....	95
Figure 6.16: ANFIS structure	96
Figure 6.17: Time-series response of ANN for different weather conditions	97
Figure 6.18: Time-series response of ANFIS for different weather conditions	98

LIST OF TABLES

Table 1-1: Properties of the principal semiconductors with photovoltaic applications [4]	6
Table 1-2: The current best reported efficiencies of different types of solar cells [4].....	7
Table 2-1: Daily electrical use and kWh used per month for a modest household	24
Table 2-2: Array description.....	25
Table 2-3: Summary of the results from simulation of PV system.....	29
Table 2-4: PV components cost	30
Table 2-5: The tax rates applicable to individuals for the tax year 2012/2013.....	31
Table 2-6: System electricity cost and net economic benefit in the first year	32
Table 4-1: Summary of fuel cell types.....	52
Table 5-1: PV array parameters	66
Table 5-2: Fuel cell parameters.....	66
Table 5-3: Battery parameters.....	66
Table 5-4: Simulation results for stand-alone PV generator.....	76
Table 5-5: Simulation results for stand-alone hybrid PV-PEMFC generator.....	77
Table 6-1: ANFIS information.....	95
Table 6-2: The rmse values of the ANN and ANFIS networks.....	96

LIST OF APPENDICES

Appendix A:	ANFIS membership functions	104
Appendix B:	ANFIS inputs – output surfaces	105
Appendix C:	Design and Analysis of Grid-Connected Photovoltaic System for Residential Applications Case Studied of Durban, South Africa	107
Appendix D:	Fuel cells development, applications and market	108
Appendix E:	Energy management for stand-alone hybrid photovoltaic-PEM fuel cells systems	109
Appendix F:	Neuro-fuzzy strategies for prediction and management of hybrid PV PEMFC batteries systems	110
Appendix G:	Matlab code to load data set for simulation	111
Appendix H:	Matlab code to calculate module current under given voltage, irradiance and temperature	112
Appendix I:	Matlab code to determine the maximum power point of the PV module	114
Appendix J:	Matlab function calculates the output power of the PV module or array	115
Appendix K:	Matlab code to determine the energy management of the hybrid photovoltaic fuel cells system equipped with batteries bank	116
Appendix L:	Solving an input-output time-series problem with a time delay neural network	122
Appendix M:	Matlab code to predict power supplied to the load time-series adaptive neuro-fuzzy interference system	125

INTRODUCTION

A better performance of photovoltaic (PV) generators is obtained at high solar insolation. But at high insolation, the temperature of the PV system increases and leads to the drop of the performance of the system making the system unable to supply the load. The problem becomes more difficult with irregular insolation when the system experience variation in output, which is not good for the user. One of the solutions to overcome this problem may be to couple the PV generator with a proton exchange membrane fuel cell (PEMFC) system particularly for stand-alone systems for household demand. One of the challenges in this type of system is the prediction and management of energy flow between different components of the system and the load, especially if more than three sources are involved.

The advance in research and the development of the knowledge of hybrid systems in the field of renewable energy and their non-linear behaviour have led to the application of artificial intelligence techniques to deal with modelling, prediction, management and control of the flow of energy from different components of those systems.

In this thesis, an adaptive neuro-fuzzy interference system (ANFIS) for the management and control of energy flow of a hybrid photovoltaic-fuel cell-batteries system is developed. The ANFIS structure obtained is compared to an artificial neural network (ANN).

Aims and objectives

In order to achieve the desired power demand, the PV will act as a primary power plan while the fuel cell and the battery will act as first and secondary auxiliary power units respectively.

The aim of this research project is to investigate the feasibility of using an electrical hybrid system consisting of a PV, a fuel cells (FC) stack and battery pack for a stand-alone power system and implement a neuro-fuzzy strategy for management of the power sharing between different components and the load.

The objectives of the project were to:

- Review previous work on renewable energy hydrogen systems, focusing on the stand-alone hybrid photovoltaic fuel cell systems.
- Investigate the possibility of best hybrid system configuration and coupled system topology for household demand.
- Develop a computer simulation model of the complete hybrid system and an algorithm for optimising the overall energy transferred and ensure battery lifetime.
- Develop a neuro-fuzzy strategy for the system and compare the results of the system performance to an artificial neural network.

Research questions

- Research question: Can neuro-fuzzy strategies be used to predict and manage hybrid PV-PEMFC battery
- Research sub-questions:
 - 1) What is the best hybrid system configuration and coupled system topology for household demand?
 - 2) What is the control strategy for better energy efficiency and system performance for the power sharing of different components of the system?

- 3) How close are the results obtained from the developed management strategy to the expectation?

Contribution to knowledge

The novelty of this work can be summarised as follows:

- Development of an Intelligent Energy Management System to manage the power supply from photovoltaic, fuel cells and battery and to meet the power requirement for the variation of load.
- Integration of the complete hybrid photovoltaic fuel cell battery system to operate in real time and the neuro-fuzzy management in one environment; and to simulate the system for the specific application.
- Take into account environmental parameters namely solar insolation and ambient temperature on the performance of the system.

Outline of the thesis

The thesis is composed of the following chapters:

1. Photovoltaic systems growing: This chapter presents the growing of photovoltaic technology by listing different methods to improve the efficiency and performance of solar cells, as well as the environmental and economic advantages and disadvantages of photovoltaic systems.
2. Design and analysis of a grid-connected photovoltaic system for residential application – case study, Durban, South Africa: This chapter presents the design and simulation of a photovoltaic system for household demand for South Africa. The design is based on a particular case of Durban weather conditions and simulated with the Matlab package.
3. Performance analysis of thermosyphon hybrid photovoltaic thermal collector: The purpose of this chapter is to present the behaviors of water in the thermosyphon hybrid photovoltaic thermal systems as a method to improve the performance of photovoltaic systems when exposed to environmental parameter variation and to provide the advantage of cooling photovoltaic modules with water using rectangular channel profiles for the thermal collector.
4. Fuel cell development, applications and market: This chapter is a review of types of fuel cells, their applications and their economy. Different types of fuel cells are presented and their efficiency and operating temperature compared, the progress of the different types and applications are presented as well as the market, the economy and projections for the future.
5. Energy management for stand-alone hybrid photovoltaic-PEM fuel cells systems: This chapter presents the energy management for the control of energy flow for a PV-PEMFC system in a particular case of household demand in Durban, South Africa.
6. Neuro-fuzzy strategies for prediction and management of hybrid PV-PEMFC battery systems: In this chapter, an adaptive neuro-fuzzy interference system (ANFIS) for the management and control of energy flow of a hybrid photovoltaic-battery fuel cells system is developed. The ANFIS structure obtained is compared to an artificial neural network (ANN).

7. Conclusion: This chapter concludes the thesis by presenting the results from the research and gives recommendations for further work.

CHAPTER 1 : PHOTOVOLTAIC SYSTEMS GROWING

PUBLICATION 1

Ntumba Marc-Alain Mutombo^a; Freddie L. Inambao^b; Remy Tiako^c

^{a,c} University of KwaZulu-Natal, School of Engineering, Discipline of Electrical Engineering, Howard College Campus, Durban, South Africa (209520511@stu.ukzn.ac.za; Tiako@ukzn.ac.za)

^b University of KwaZulu-Natal, School of Engineering, Discipline of Mechanical Engineering, Howard College Campus, Durban, South Africa (inambaof@ukzn.ac.za)

Abstract

Solar energy is a renewable energy source which is growing in production as well as in use. This is due mostly to the environmental and economic advantages that have allowed this technology to become the third most common renewable energy source after hydro and wind, based on installed capacity [1]. Technological improvements, the increase of the industrial production, falling of the price of kWh and its low environmental impact have made solar cell technology more attractive and one of the most important renewable energy source currently and this is likely to continue for years to come.

This paper presents the growth of photovoltaic technology by listing different methods to improve the efficiency and performance of solar cells, as well as the environmental and economic advantages and disadvantages of photovoltaic systems.

Key words: Solar cell, Efficiency, Cost, Electrical energy, Growing, Environment, Economy

1.1 Introduction¹

Electricity is needed in everyday life, and the scope for solar cell systems keeps increasing with the most important being power stations, buildings, stand-alone and grid-connected systems. Solar energy can be converted into direct current. This process of conversion is made by use of semiconducting material with photovoltaic effect. Solar energy is a renewable energy source which is growing in production and use. The effective process of conversion of solar energy into electricity by solar cells is based on the properties of the semi-conductor material used in the manufacture of solar cells, the most important properties being: the band gap, the absorption coefficient, the refractive coefficient, the electron affinity, the lattice constant, and the thermal expansion coefficient. The choice of semi-conductor material is based on energetic efficiency and low cost. Research has been focused on the improvement of solar cell efficiency and cost by considering its environmental impact. Research and field results have proven that photovoltaic systems are clean energy sources in terms of environmental impact and the price of this technology keeps decreasing following Swanson's law. Graphs of global evolution of installed capacity, global markets and the predictions from 2000 to 2013 (Figure 1.4) and projections to 2018 (Figure 1.5) are given. The economic and environmental advantages and disadvantages of photovoltaic systems are discussed.

1.2 Photovoltaic systems

The first photovoltaic cell was developed in 1954 by Daryl Chapin, Calvin Fuller and Gerard Pearson at Bell labs, USA. This silicon based device could convert enough solar energy into electricity for household appliances [2]. The term 'photovoltaic' refers to the flow of current due to the transduced light energy, which is the operating mode of a photodiode device. Based on their structure and operating mode, all photovoltaic devices can be considered as some type of photodiode.

1.2.1 Solar cells

Solar cell is constituted of different layers as shown in Figure 1.1.

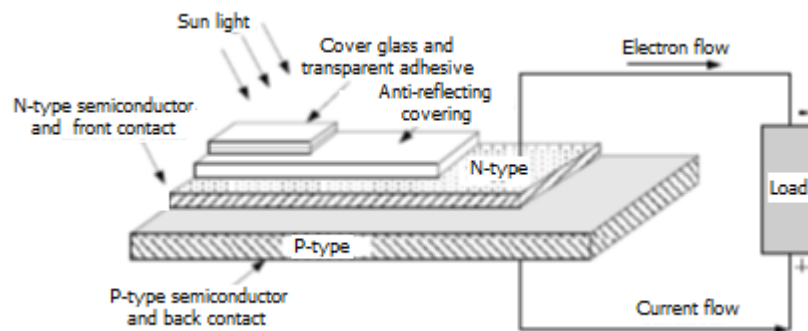


Figure 1.1: Schematic block diagram of a PV cell

¹ Although each chapter is an individual publication, for the purposes of this thesis subheadings and captions have been numbered consecutively according to chapter number.

Based on energy demand, PV cells can be connected in series to increase the voltage or in parallel to increase the current. Cells connected together produce a PV module, PV modules connected together produce an array, and multiple arrays are connected to build a solar power plant. Figure 1.2 shows a PV Cell, module and array.

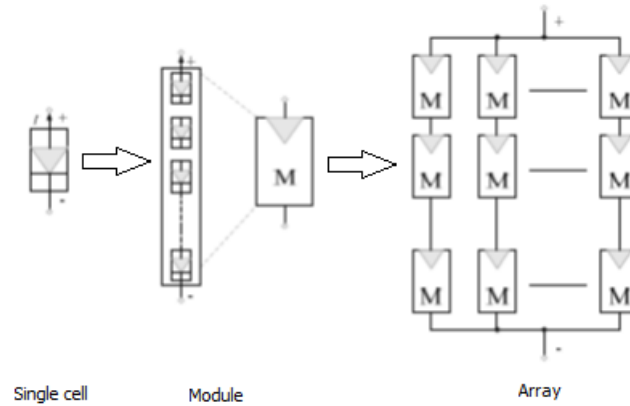


Figure 1.2: PV cell, module and array

Most common materials used in the manufacturing of photovoltaic solar cells are monocrystalline silicone [3]. Other semiconductor materials can also be used. Table 1.1 gives some properties of the semiconductor materials commonly used in photovoltaic applications.

Those values are provided at the temperature of 300 K. The values of bandgap are given with index i and d as indirect and direct respectively.

1.2.2 Efficiency and performance

The solar cell efficiency is measure by solar cell ability to convert solar energy into useful energy for human consumption.

Table 1-1: Properties of the principal semiconductors with photovoltaic applications [4]

Materials	Bandgap E_g (eV)	Absorption coefficient	Refractive coefficient
c-Si	1.12(i)	11.9	3.97
GaAs	1.42(d)	13.18	3.90
InP	1.35(d)	12.56	3.60
a-Si	≈ 1.8 (d)	≈ 11	3.32
CdTe	1.45-1.5(d)	10.2	2.89
CuInSe ₂ (CIS)	0.96- 1.04(d)		
Al _x Ga _{1-x} As ($0 \leq x \leq 0.45$)	$1.424 + 1.247x$ (d)	$13.18 - 3.12x$	
Al _x Ga _{1-x} As ($0.45 \leq x \leq 1$)	$1.9 + 0.125x + 0.143x^2$		

The ultimate and two nominal Shockley-Quiesser efficiencies for different semiconductor materials are shown in Figure 1.3. The black-body radiation with temperature $T = 6000$ K was used [4].

As can be seen from Table 1.2, solar cell efficiency varies from 6% to 44.0% depending to type of semiconductor used [5] but the efficiency of commercial solar cells in the market is in the

range of 14% to 22% [6] [7]. The most efficient solar cell so far was manufactured by Solar Junction in April 2011. This solar cell is a multi-junction concentrator solar cell with an efficiency of 43.5% [8].

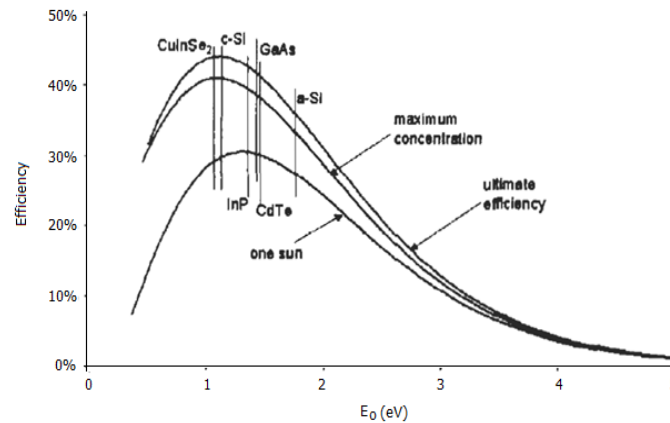


Figure 1.3: The ‘ultimate’ and two ‘nominal’ Shockley-Queisser efficiencies [4]

Sharp Corporation achieved an efficiency of 35.8% in 2009, using a triple-junction manufacturing technology without concentrator [9]. The same design was also used by Boeing Spectrolab to achieve an efficiency of 40.7%. The use of a concentrator in solar cell manufacturing may reduce the cost of solar.

Table 1-2: The current best reported efficiencies of different types of solar cells [4]

Solar Cells	Efficiency (%)	Current Density (mA/cm ²)	Open Circuit Voltage (V)
Crystalline: single junction			
c-Si	24.7	.2	0.706
GaAs	25.1	28.2	1.022
InP	21.9	29.3	0.878
Crystalline: multijunction			
GaInP/GaAs/Ge tandem	31.0	14.11	2.548
Thin-film: single junction			
CdTe	16.5	25.9	0.845
CIGS	18.9	34.8	0.696
Thin-film: multijunction			
a-Si/a-SiGe tandem	13.5	7.72	2.375
Photoelectrochemical			
Dye-sensitised TiO ₂	11.0	19.4	0.795

There have been many attempts to reduce the costs of solar cells and modules to make them both competitive and efficient. The energy conversion efficiency of photovoltaic materials

needs to be increased by improving their electrical, optical and structural properties by choosing semiconductor material with appropriate energy gaps that match the solar spectrum [10].

The best performance of photovoltaic systems is obtained when they face the sun. Increasing the time they face the sun can be achieved by use of solar trackers with an increase of about 20% in the winter season and an increase of about 50% in the summer season. For static mounted systems, sun paths must be analyzed, and modules be set at a tilt angle equal to the latitude. The better performance of this type of system can be obtained by setting the tilt angle for winter and summer seasons. The efficiency of photovoltaic system can be improved by combining solar cell systems and thermal collectors to form hybrid photovoltaic thermal collectors (PV/T) systems. These systems combine photovoltaic cells which combine solar energy into electrical energy at about 14% to 22% and the remainder of energy in the form of heat is removed from the system by a thermal absorber to cool the photovoltaic system and improve its efficiency. The capture of both electrical energy and removal of heat for heating purposes allows these systems to have higher energy [13] and thus have higher overall energy efficiency than conventional solar photovoltaic or solar thermal systems [14].

1.2.3 Environmental impact of PV technology

Photovoltaic systems have been considered as an option to overcome problems related to the environmental caused by the fossil fuel combustion. Emissions related to different photovoltaic technologies are little compare to emissions obtained from traditional energy technologies [15]. The major environmental impact of photovoltaics comes from the production of the cells, a process in which the emissions of various toxic, flammable and explosive chemicals are involved.

With the growing demand for thin film module production to meet the demand in years to come, life cycle assessments (LCA) have to be conducted to evaluate the environmental impacts from such technologies. Many studies have been published in the field of LCA applied to thin film PV technologies. In a study conducted by Collier et al. in 2014, the LCA was applied to CZTS and Zn_3P_2 PV technologies for the first time. The four impacts analyzed in this study are the primary energetic demand, the green effect potential, the fresh water used and the eco-toxicity impact. For the four impacts mentioned above, it has been found that the performance of CdTe and Zn_3P_2 were better than for CIGS and CZTS. More details can be found in [15].

1.2.4 Applications

Solar systems are used in many areas as main suppliers of electrical energy, as well as functioning as backup sources. World production of photovoltaic devices is allocated mostly to power stations, buildings, standalone and grid connected systems. To date, the Desert Sunlight Solar Farm and the Topaz Solar Farm are the largest photovoltaic power stations. Built by the American company First Solar, these stations using thin-film CdTe PV modules have a nominal capacity of 550 MW each [16]. The use of building-integrated photovoltaics (BIPV) in new domestic and industrial buildings has considerably increased. This technology is used in building as principal or auxiliary source of electrical energy [17]. The areas where the cost to connect to utility grid is high have seen an increase in the use of solar powered remote fixed devices.

1.3 Evolution of PV capacities

Compared to 13 TW consumed in 2005 by humans, the sunlight reaching the surface of the Earth is almost 10 000 times that on average [18], which leads to the conclusion that in years to come solar energy can become the primary source of energy. With a density of about 170 W/m², solar electrical generation has the highest power density compared to other renewable energy systems [18].

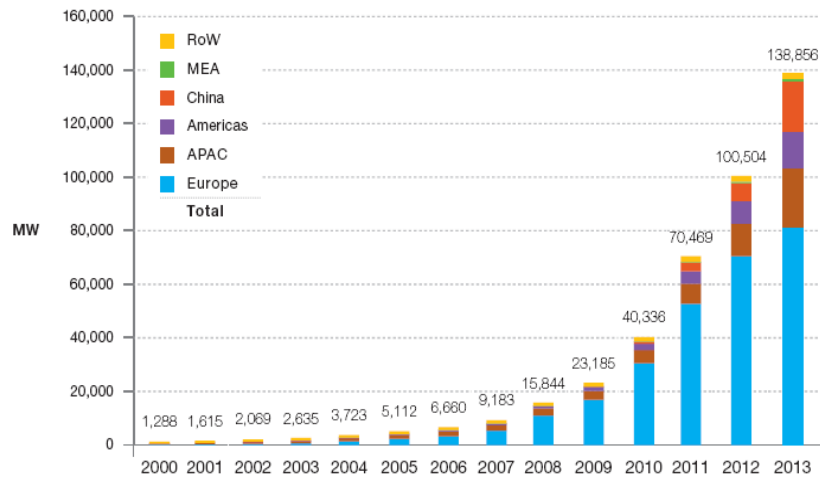


Figure 1.4: Evolution of global PV cumulative installed capacity 2000-2013 [19]

Figure 1.4 shows the evolution of global PV cumulative installed capacity from 2000 to 2013 in which cumulative installed capacity for the Americas, Europe, China, Asia Pacific (APAC), Middle East and Africa (MEA) and Rest of the World (ARoW) is given. It can be seen that in 2013 the worldwide installed solar PV increased by 38% to 139 GW which is about 160 TWh of energy generated and represents 0.85% of world electricity demand. Early in 2015, the worldwide installed solar PV increased to 200 GW, 40 times more than installed solar PV in 2006 [20]. Solar photovoltaics are developing quickly and worldwide capacity was estimated to be up to 177 GW by the end of 2014. With the total electrical power output capacity of 200 billion kWh in a calendar year, the world's PV capacity represents 1% of global electricity demand. The number of countries using solar photovoltaic is about 100 [21] [22]. Throughout the world, photovoltaics is the third most important renewable energy source after hydro and wind, based on installed capacity [1].

Figure 1.5 shows the global PV cumulative installed capacity scenario until 2018. The prediction made for 2018 shows a net increase of photovoltaic installed capacity to double or even triple i.e. to 430 GW. The European Photovoltaic Industry Association (EPIA) projects photovoltaic to meet 10% to 15% of Europe's energy demand in 2030 [23] [24]. By 2050, over 20% of electricity demand could be supplied by photovoltaics [25].

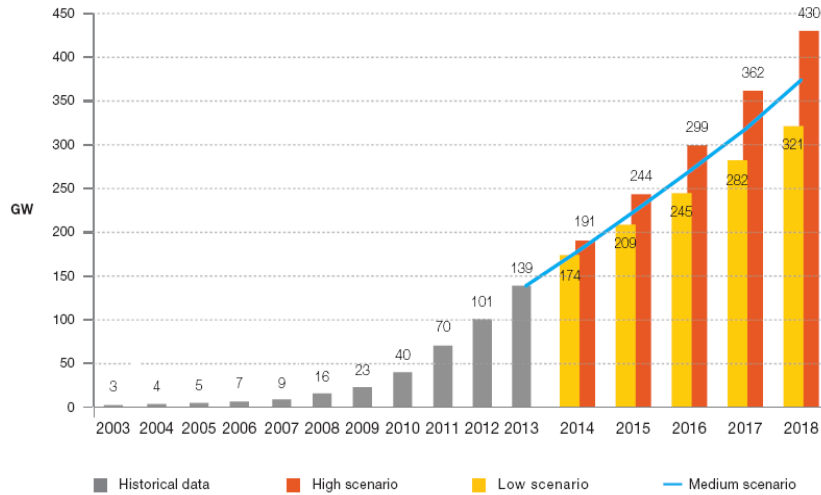


Figure 1.5: Global PV cumulative scenario until 2018

1.4 Economy

Driven by the advance of technology, the increase in production at industrial scale and sophistication, the price of photovoltaics has fallen considerably from the first cells produced [26] [27], and the levelized cost of electricity (LCOE) of PV has become competitive against the traditional sources of electricity in many geographic regions [28].

Since 2008, the price of the photovoltaics has dropped considerably. For the crystalline silicon solar cell for example, the price has fallen from \$76.67 /W in 1977 to an estimation of \$0.74 /W in 2013 [29] which is evidence confirming Swanson's law which stipulates that solar cell prices decrease by 20% each time industrial capacity doubles [29]. The average price of solar cells presented by Solarbuzz group was from \$3.50 /W to 2.43 /W by 2011 [30]. From summer 2008 to 2011, the price of solar panels fell by 60% based on the Bloomberg New Energy Finance estimation, putting solar power on the same level of competition with the retail price of electricity in many higher insolation countries. A study noting the fall of the price of electricity by 75% from 2007 to 2012 has been published [31] without specifying if the figure was only for United States or globally. Renewable energy technology is becoming cheaper while fossil fuels price generally are becoming more expensive. For large scale installations, prices below \$1.00 /W have been reached. In April 2012, the price of €0.60 /W (an equivalent to \$0.78 /W) for a panel was published for a large scale five years market [32]. By the end of 2012, the best class of module fell to \$0.50 /W and is expected to fall to \$0.36 /W by 2017 [33].

Figure 1.6 shows the global annual market scenarios until 2018. A low market scenario remains constant from 2014 to 2015 to 35 GW and increases to 39 GW by 2018, while a high market scenario shows a net increase from 52 GW to 69 GW. PV remains a policy-driven business, where political decisions considerably influence potential market take-off or decline [34].

Photovoltaic generators can operate for 100 years or more [35] with limited maintenance after their start-up, which means that the operating cost for any PV power plant is very low compared to existing technologies. The lower the solar energy price is compared to conventional energy,

the more attractive it is to utilities and users. However, only a small budget is allocated to research for the development of solar cells compared to fossil and nuclear energy.

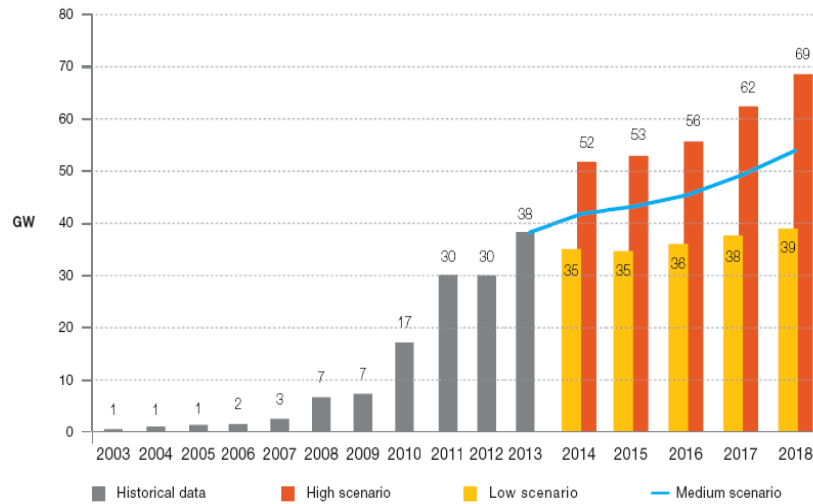


Figure 1.6: Global annual market scenarios until 2018 [34]

Nevertheless, concentrating photovoltaic cells with a very high efficiency of about 40% are already at the experimental stage [36] and efficiency is increasing rapidly while the price of quantity produced falls rapidly [37]. Technological advances, amelioration of the manufacturing process and industrial restructuring promises future decreases of the price of photovoltaics [26].

1.5 Conclusion

Research and field results have proven that photovoltaic systems are clean energy sources for the environment, and the price of this technology keeps decreasing following Swanson's law. Their lower efficiency can be improved by choosing semi-conductor material with appropriate energy gaps that match the solar spectrum and the use of solar concentrators with an appropriate and low cost as possible sinks in solar cells manufacturing. The environmental impact of photovoltaic technology, particularly for thin film module technology, can be improved by the use of LCA. Technological improvements, the increase of industrial production, falling prices per kWh and a small environmental impact have made solar cell technology more attractive and one of the most important renewable energy sources now and for the future.

References²

- [1] European Photovoltaic Industry Association (EPIA), “Global market outlook for photovoltaics until 2016,” 2012.
- [2] MrSolar.com, “Photovoltaic effect,” 12 December 2010. [Online]. Available: <http://www.mrsolar.com/photovoltaic-effect/>. [Accessed 13 06 2015].
- [3] M. Z. Jacobson, “Review of solutions to global warming, air pollution, and energy security,” *Energy and Environmental Science*, vol. 2, pp. 148-173, 2009.
- [4] T. Markvart and L. Castafier, *Practical Handbook of Photovoltaics: Fundamentals and Applications*. Amsterdam: Elsevier, 2003, pp. 97-132.
- [5] UDaily, “UD-led team sets solar cell record, joins DuPont on \$100 million project,” University of Delaware, [Online]. Available: <http://www.udel.edu/PR/UDaily/2008/jul/solar072307.html>. [Accessed 13 06 2015].
- [6] O. Schultz, A. Mette, R. Preu, and S. W. Glunz, “Silicon solar cells with screen-printed front side metallization exceeding 19% efficiency: The compiled state-of-the-art of PV solar technology and deployment,” in *European Photovoltaic Solar Energy Conference*, Milan, 2007.
- [7] Z. Shahan, “Sunpower panels awarded Guinness world record,” 20 June 2011. [Online]. Available: <http://www.reuters.com/article /2011/06/20/idUS110444863620110620>. [Accessed 13 06 2015].
- [8] E. Wesoff, “Update: solar junction breaking CPV efficiency records, raising \$30m,” 15 April 2011. [Online]. Available: <http://www.greentechmedia.com/articles/read/solar-junction-setting-new-cpv-efficiency-records>.
- [9] Sharp, “Sharp develops solar cell with world's highest, conversion efficiency of 37.9%,” Sharp, [Online]. Available: <http://sharp-world.com/corporate/news/130424.html>. [Accessed 13 06 2015].
- [10] S. K. Deb, “Recent developments in high-efficiency PV cells,” in *World Renewable Energy Congress VI*, Brighton, U.K, 2000.
- [11] J. Yu, Y. Zheng, and J. Huang, “Towards high performance organic photovoltaic cells: a review of recent development in organic photovoltaics,” *Polymers*, vol. 6, pp. 2473-2509, 2014.
- [12] Y. Sun, G. C. Welch, W. L. Leong, C. J. Takacs, G. C. Bazan, and A. J. Heeger, “Solution-processed small molecule solar cells with 6.7% efficiency,” *Nature Materials*, vol. 11, no. 1, pp. 44-48, 2011.

² Referencing styles per chapter are retained because they are consistent with the publication concerned.

- [13] A. Mojiri, R. Taylor, E. Thomsen, and G. Rosengarten, "Spectral beam splitting for efficient conversion of solar energy - A review," *Renewable and Sustainable Energy Reviews*, vol. 28, pp. 654-663, 2013.
- [14] M. J. M. Pathak, P. G. Sanders, and J. M. Pearce, "Optimizing limited solar roof access by exergy analysis of solar thermal, photovoltaic, and hybrid photovoltaic thermal systems," *Applied Energy*, vol. 120, pp. 115-124, 2014.
- [15] V. M. Fthenakis, H. C. Kim, and E. Alsema, "Emissions from photovoltaic life cycles," *Environmental Science & Technology*, vol. 42, no. 6, pp. 2168-2174, 2008.
- [16] Renewable Energy World Editors, "DOE closes on four major solar projects," 2011.
- [17] Wisconsin Public Service Corporation, "Building integrated photovoltaics," [Online]. Available: <http://www.buildingsolar.com>. [Accessed 13 06 2015].
- [18] V. Smil, "Energy at the crossroads," in OECD Global Science Forum Conference on Scientific Challenges for Energy Research, Paris, 2006.
- [19] EPIA-European Photovoltaic Industry Association, "Global market outlook for photovoltaics 2014-2018," 2014.
- [20] T. Hunt, "The solar singularity is nigh," Greentech Media.
- [21] International Energy Agency (IEA), "2014 snapshot of global PV markets," 2015.
- [22] J. L. Sawin, E. Martinot, D. Barnes, A. McCrone, J. Roussell, R. Sims, and V. S. O'Brien, "Renewables 2011: global status report," REN21, 2011.
- [23] European Photovoltaic Industry Association (EIPA), "Market report 2013 (For EIPA Members only)," 2014.
- [24] European Photovoltaic Industry Association (EIPA), "Global market outlook for photovoltaics 2013-2017," 2013.
- [25] European Photovoltaic Industry Association (EIPA), "Solar photovoltaic electricity empowering the world," 2012.
- [26] M. Bazilian, I. Onyeji, M. Liebreich, I. MacGill, J. Chase, J. Shah, D. Gielen, D. Arent, D. Landfear, D. Landfea, and S. Zhengrong, "Re-considering the economics of photovoltaic power," *Renewable Energy*, vol. 53, pp. 329-338, 2013.
- [27] R. M. Swanson, "Photovoltaics power up," *Science Magazine*, vol. 324, no. 5929, pp. 891-892, 2009.
- [28] K. Branker, M. Pathak, and J. Pearce, "A review of solar photovoltaic levelized cost of electricity," *Renewable and Sustainable Energy Reviews*, vol. 15, pp. 4470-4482, 2011.
- [29] G. Carr, "Sunny uplands: alternative energy will no longer be alternative," 2012. [Online]. Available: <http://www.economist.com/news/21566414-alternative-energy-will-no-longer-be-alternative-sunny-uplands>. [Accessed 20 06 2015].

- [30] J. Quiggin, "The end of the nuclear renaissance," 2012. [Online]. Available: <http://nationalinterest.org/commentary/the-end-the-nuclear-renaissance-6325>. [Accessed 20 06 2015].
- [31] K. Wells, "Solar energy is ready. The U.S. isn't," 2012. [Online]. Available: <http://www.bloomberg.com/bw/articles/2012-10-25/solar-energy-is-ready-dot-the-u-dot-s-dot-isnt>. [Accessed 20 06 2015].
- [32] SolarServer, "Chinese PV producer Phono Solar to supply German system integrator Sybac Solar with 500 MW of PV modules," *Solar Magazine*, 2012. [Online]. Available: <http://www.solarserver.com/solar-magazine/solar-news/archive-2012/2012/kw18/chinese-pv-producer-phono-solar-to-supply-german-system-integrator-sybac-solar-with-500-mw-of-pv-modules.html>. [Accessed 16 07 2015].
- [33] N. Rinaldi, "Solar PV module costs to fall to 36 cents per watt by 2017," *GreenTechSolar*, 18 06 2013. [Online]. Available: <http://www.greentechmedia.com/articles/read/solar-pv-module-costs-to-fall-to-36-cents-per-watt>. [Accessed 15 04 2015].
- [34] European Photovoltaic Industry Association (EIPA), "Global market outlook for photovoltaics 2014-2018," 2014.
- [35] Hi Energy People, "Advantages and disadvantages of solar energy," [Online]. Available: <http://www.hienergypeople.com/advantages-and-disadvantages-of-solar-energy/>. [Accessed 27 06 2015].
- [36] Fraunhofer Institute for Solar Energy Systems ISE, "41.1% efficiency multi-junction solar cells," 2009. [Online]. Available: <http://www.renewableenergyfocus.com/view/753/fraunhofer-41-1-efficiency-multi-junction-solar-cells/>. [Accessed 27 06 2015].
- [37] U. Bossel, "Does a hydrogen economy make sense?," in *The IEEE*, 2006.
- [38] Fraunhofer Institute for Solar Energy Systems ISE, "Photovoltaics report," Fraunhofer, 2014.

CHAPTER 2 : DESIGN AND ANALYSIS OF GRID-CONNECTED PHOTOVOLTAIC SYSTEM FOR RESIDENTIAL APPLICATION – CASE STUDY, DURBAN, SOUTH AFRICA

PUBLICATION 2

Ntumba Marc-Alain Mutombo^a; Freddie L. Inambao^b; Remy Tiako^c

^{a,c} University of KwaZulu-Natal, School of Engineering, Discipline of Electrical Engineering, Howard College Campus, Durban, South Africa (209520511@stu.ukzn.ac.za; Tiako@ukzn.ac.za)

^b University of KwaZulu-Natal, School of Engineering, Discipline of Mechanical Engineering, Howard College Campus, Durban, South Africa (inambaof@ukzn.ac.za)

Abstract

With its economic growth and increase in population, South Africa needs more electrical energy than ever before. The supply of electrical energy for mining companies has been prioritised over domestic use, penalising families with blackouts and neglecting remote areas. Nevertheless, the surface of the country is irradiated by large amounts of sunlight, therefore photovoltaic systems are one option among other renewable energy technologies to remediate this situation, particularly for remote areas and for household electricity demand. Solar power is considered to be one of the most reliable sources of renewable energy available today.

This paper presents the design and simulation of a photovoltaic system for household demand in South Africa. The design is based on a particular case of Durban weather conditions and simulated with the Matlab package. After an economic analysis, it was found that the system could meet the need for electrical energy in summer time based on sunlight received, but in winter time the performance was low. To compensate for low irradiance, the system could be coupled with other renewable energy technologies such as a fuel cell system to make a hybrid system.

Keywords: design, analysis, photovoltaic, array, economy

2.1 Introduction

The worldwide need for electrical energy increases every day because of the lifestyle demands of humans. With a gross domestic product (GDP) of US\$ 495 billion based on purchasing power parity, South Africa is the most industrialized nation in Africa with a population of 48 million over 1.2 million km² (Niez 2010). Even though the country is one of the most highly electrified countries in Africa, only 75% of the population has regular access to electrical energy.

South Africa has vast natural resources of coal (Pereira, Sena, Freitas and Silva 2011). As the most developed African country, with high electrical energy production and consumption, South Africa has most of its electrical energy produced through coal-fired power stations. Unfortunately, this technology has significant environmental implications with adverse effects on human health and ecosystems (Cristóbal, Guillén-Gosálbez, Jiménez and Irabien 2012) due particularly to greenhouse gases generated by this technology. The majority of this energy is transported to and distributed in big cities, leaving remote areas without electricity.

Considering the surface irradiation in South Africa, photovoltaic systems are one option amongst other renewable energy technologies to remediate this situation particularly for remote areas and household electricity demands.

2.2 South Africa and the electrical energy challenge

In 2008, the International Energy Agency reported that more than 1.5 billion people did not have access to electricity (Niez 2010). Over 85% of this total are rural residents, with the majority of them living in remote areas of developing countries (Pereira, Sena, Freitas and Silva 2011).

2.2.1 South Africa's electricity production

In the next 25 years, world electricity demand is expected to increase rapidly particularly in emerging countries. As one of lowest cost energy sources, coal still until today a main energy source (Cristóbal, Guillén-Gosálbez, Jiménez and Irabien 2012) for same developed and growing economy countries.

South Africa has vast natural resources of coal, gold and diamonds, and the country's use of electricity is the highest in Africa due to its mining industries (Pereira, Sena, Freitas and Silva 2011).

Using its own coal resources and intensive and continuous public sector investment in production and transmission, the price of electricity in South Africa is one of the lowest in the world (Hammed, Kafayat and Ramos 2009). Even though the country is one of the most highly electrified country in Africa, only 75% of the population has regular access to electrical energy (Pereira, Sena, Freitas and Silva 2011).

The South African public utility company Eskom which is the biggest producer of electricity in Africa, is also placed among the top seven utilities in the world producing electrical energy. Eskom runs a number of important power plants including Kendal Power Station, one of the biggest coal-fired power stations in the world (Schmidt n.d.). Unfortunately, this technology has significant environmental implications such as the reduction of natural resources, global environmental impacts and pollution with adverse effects on ecosystems (Cristóbal, Guillén-Gosálbez, Jiménez and Irabien 2012).

2.2.2 Electricity crisis in South Africa

The provision of electrical energy in any society is an important public service, and can be seen as an essential right in the context of social equity and justice. Access to electricity promotes social integration and accessibility of other essential services. In South Africa where 40% of the population is poor, it is necessary to analyze the program of electrification for provision of universal access to electricity for poor and rich alike, and the impact this has on the economy (Pereira, Sena, Freitas and Silva 2011).

Since 1994, the desire of the government to assure general access to electricity and economic development has increased South African electricity demand at the rate of 4% per year (Hammed, Kafayat and Ramos 2009). By 2007, South Africa's electricity reserve which is the difference between electricity produced and demand had dropped down from 25% in 2001 to between 8% and 10% (Hammed, Kafayat and Ramos 2009). Since 2007, Eskom has been unable to meet the demand for electricity (Inglesi-Lotz 2010). This electricity over-demand compared to supply had a negative impact on the South African government objective of growing the economy at 6% per year between 2010 and 2014 (Hammed, Kafayat and Ramos 2009). In 2008, South Africa experienced a major electricity disaster. All fields of use endured blackouts all over the country resulting in substantial economic losses. The National Energy Regulator of South Africa (NERSA) revealed that 50 billion Rands was lost to the economy because of the blackouts (Inglesi-Lotz 2010).

2.2.3 Electricity crisis strategic plan

To improve the inadequate electricity capacity, Eskom planned to spend 343 billion Rands between 2008 and 2013. With the objective of boosting economic growth by increasing electricity demand by 4% per year, an extra 1.3 trillion Rands will be needed by Eskom until 2025 to provide the infrastructure to meet the increasing demand (Hammed, Kafayat and Ramos 2009).

To deal with electricity demand and supply and to support energy conservation, Eskom and the government decided that electricity tariffs should be used as a strategic instrument. Research indicates that the demand for electricity drops after tariff increases (Inglesi-Lotz 2010). In the third quarter of 2009, Eskom made representation to NERSA for an augmentation of the electricity tariffs to finance their present plans and projects to come. At the end of September 2009, the made by NERSA was made public: an estimated 25% increment of the electricity tariff per year during the following three years (Inglesi-Lotz 2011).

2.2.4 South Africa solar irradiance and tilt angle

The position of the sun in the sky changes over the course of the year. One of the ways to improve the efficiency of energy output of solar systems such as photovoltaic panels, solar water heaters and buildings' thermal mass is to tilt the panels at the optimum angle according to the time of year (Bellingham, Davies and Human 2009).

South Africa's optimum tilt angle does not follow the latitudinal gradient. It increases from about 24° in the Northern part of the country towards the Southeast where it reaches values up to 35° (Suri, Cebecauer and Skoczek 2012). For Durban, Bellingham, Davies and Human (2009) propose the best angle for overall annual solar energy harvesting to be 35° to the horizontal.

There are two ways to position solar energy converter devices: the fixed system and the tracking system. The tracking system follows the daily displacement of the sun to maximize the solar insolation received while the fixed system is fixed at the same position for the whole the year, either to supply the highest regularly energy over a year e.g. for grid-connected PV arrays or to supply the highest minimal energy of a day throughout the year e.g. for battery charging purposes.

For Durban, Becker proposes an optimal elevation tilt angle of 30° HYE (Bekker 2007). Zawilska and Brooks (2011) recorded and analyzed solar radiometry and chose meteorological conditions for Durban over an entire year of 2007, based on flat-plate collectors tilted at an angle of latitude 29.867° south. They obtained 13% increase in energy availability, supporting the value of an appropriate tilt angle in Durban (Zawilska, Brooks 2011).

2.3 Photovoltaic module

The voltage produced by an individual solar cell is 0.5 V to 0.6 V which is too little for any application. To get useful and adequate voltage, cells are wired in series, all encased in tough, weather-resistant packages which is the PV module. A typical laminated module structure is shown in Figure 2.1.

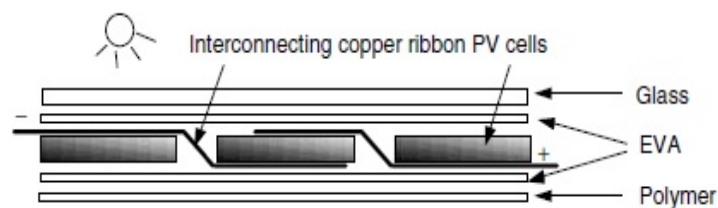


Figure 2.1: A typical laminated module structure

To increase the current or the voltage at the terminals of photovoltaic generator, multiple modules can be connected in parallel or series respectively as an array, the product of output voltage and output current is the array output power. Such arrangement of modules is shown in Figure 2.2 (Masters 2004).

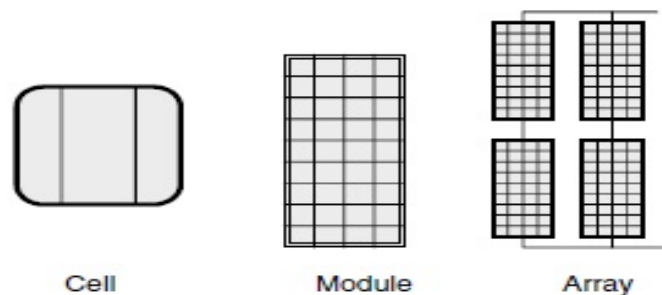
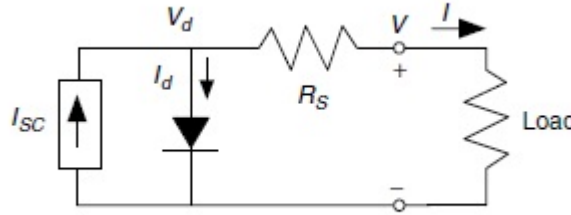


Figure 2.2: Photovoltaic cells, modules and an array

2.3.1 Modelling of photovoltaic module

As PV cells are wired in series to produce module voltage, the strategy of modelling the PV module is the same as modelling solar cells. The only difference is that voltages produced are divided by the number of cells in the PV module, other parameters remaining the same. Two main models are mostly used: the one diode model and the two diode model, each model having advantages and disadvantages (Ishaque, Salam and Taheri. 2011). Without detailed experiment results on the photovoltaic generator obtained in advance, the one diode model is to be used in this particular case. The electrical circuit for a one diode model is illustrated in Figure 2.3.

Figure 2.3: A simplified equivalent circuit for a PV cell



The photovoltaic cell can therefore be modelled using equations (1) and (2) below:

$$I = I_{sc} - I_o \left(e^{q \left(\frac{V + IR_s}{AkT} \right)} - 1 \right) \quad (1)$$

Where I (A) is the cell current which is the same as the module current, I_{sc} (A) is the short circuit current which is equal to photocurrent, I_o (A) is the dark saturation current, q is the electronic charge (1.602×10^{-19} C), k is the constant of Boltzmann (1.381×10^{-23} J/K), A is the idealizing factor, T (K) is the temperature of the cell, V (V) is the cell voltage and R_s (Ω) is the shunt resistance.

The equation for R_s is deduced by differentiating equation (1) and then rearranging it in terms of R_s :

$$R_s = -\frac{dV}{dI} - \frac{AkT/q}{I_o e^{q \left(\frac{V + IR_s}{AkT} \right)}} \quad (2)$$

At the open circuit, the voltage $V = V_{oc}$ and the current $I = 0$ so that equation (2) gives the value of R_s as:

$$R_s = -\left. \frac{dV}{dI} \right|_{V_{oc}} - \frac{AkT/q}{I_o e^{\frac{qV_{oc}}{AkT}}} \quad (3)$$

Where $-\left. \frac{dV}{dI} \right|_{V_{oc}}$ the slope of the I - V curve at the V_{oc} obtained from the I - V curve in the solar cell datasheet, V_{oc} is the open-circuit voltage of the cell found in the solar cell datasheet.

The introduction of a series resistance in the model makes the numerical solution of the current equation unsolvable, reference to equation (1). An approximate solution to this equation is

obtained by using the Newton Raphson method which converges quickly for positive as well as for negative current values (Walker 2000).

2.3.2 The PV I-V curve under standard test conditions (STC)

In the design of a PV array and in the determination of PV modules, important parameters for solar cells and PV modules are provided by manufacturers. Those parameters are represented in Figure 2.4. In this figure, curves of current against voltage and electrical power against voltage are represented.

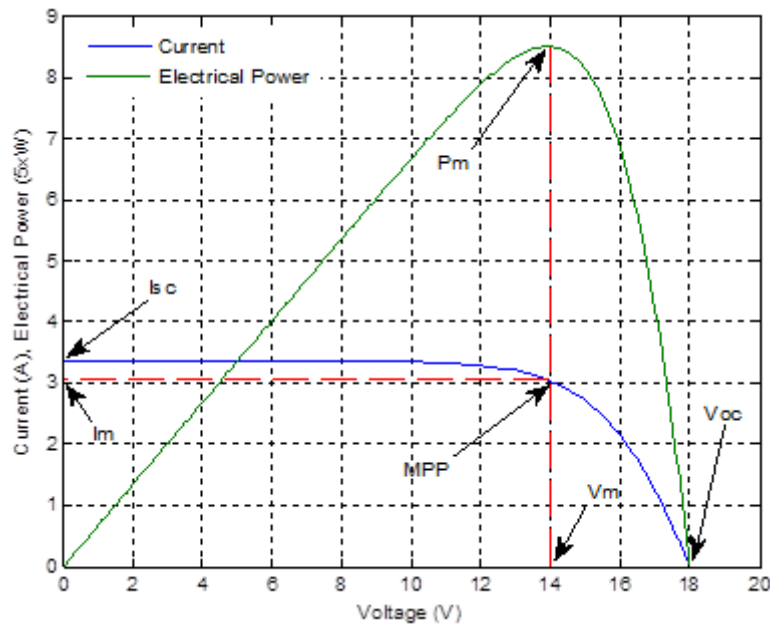


Figure 2.4: Q PEAK PV module I-V and P-V characteristic curves at STC simulated with Matlab

It can be found that for a specific PV module, the power is zero at the two extremities of the power-voltage curve. The left point with the power equal to zero is the short-circuit point where the voltage is zero and the current is equal to the short-circuit current I_{sc} and the right point with the power equal to zero is the open-circuit point, the current I is zero and the voltage is equal to the open-circuit voltage V_{oc} . The electric power is the maximum at a point at the knee of the power-voltage curve where the tangent dE/dV is zero. This point represents the maximum power point (MPP) (Masters 2004). The values of voltage and current corresponding to this point are the maximum voltage V_m and the maximum current I_m . The maximum power is obtained from equation (4):

$$E_m = I_m V_m \quad (4)$$

The maximum power point (MPP) is also determined by finding the biggest rectangle that will fit below the I-V curve as shown in Figure 2.5, as the electric power is defined as the product of voltage and the current, and the surface of the rectangle corresponds to the maximum power E_m (Masters 2004).

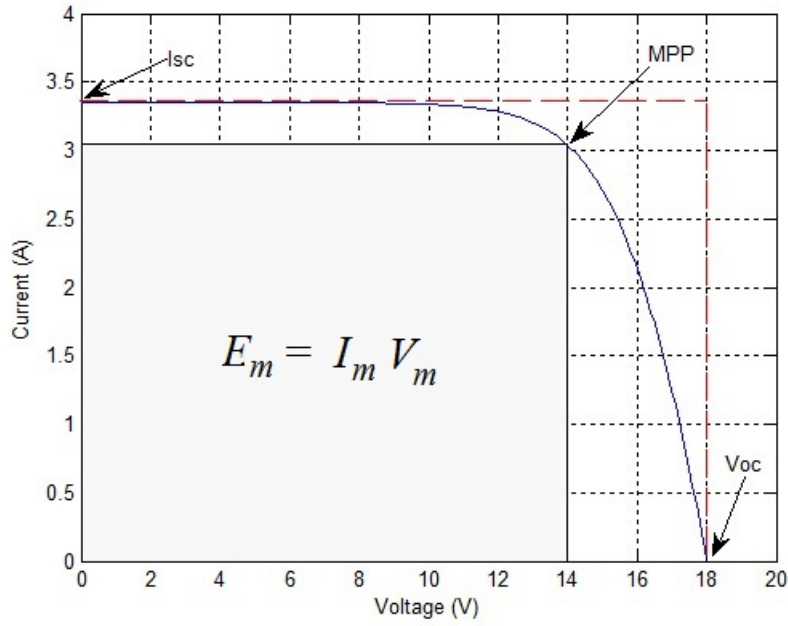


Figure 2.5: Q PEAK PV module I-V curve at STC simulated with Matlab

2.3.3 Effects of temperature and solar irradiance on I-V curves

Solar insolation and temperature have an impact on the I-V curves of the PV module. When insolation increases, short-circuit current increases in direct proportion while the open-circuit voltage increases by half of the previous increase for the same increment of the insolation. This curve can be seen in Figure 2.6 in which the behaviours of a PV module under various irradiance levels at ambient temperature of 25 °C and wind speed of 1 m/s are presented (Masters 2004).

The open-circuit voltage decreases considerably with an increase of cell temperature, while short-circuit current increases slightly as shown in Figure 2.7. Therefore, perhaps, this explains why photovoltaic have better performance on cold, clear days than hot ones.

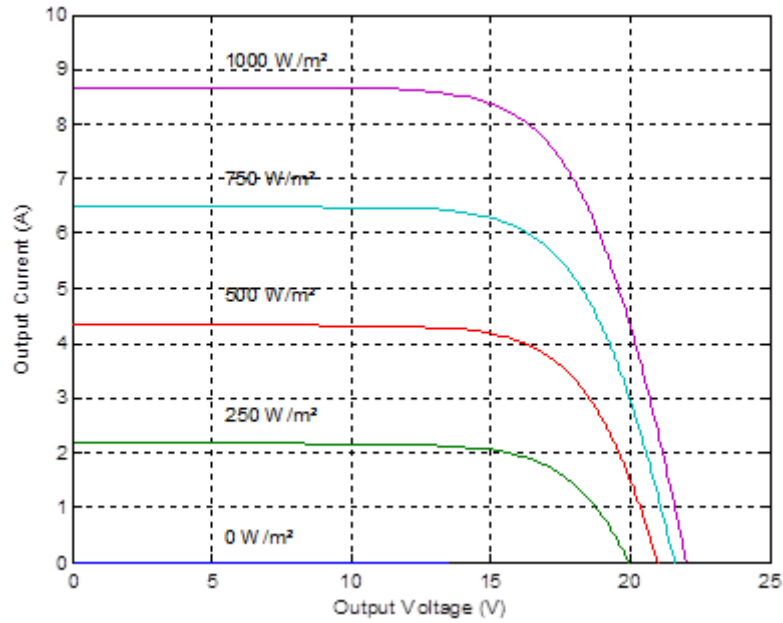


Figure 2.6: I-V characteristic curves for PV module under various irradiance levels at 25 °C temperature and 1 m/s wind speed simulated with Matlab

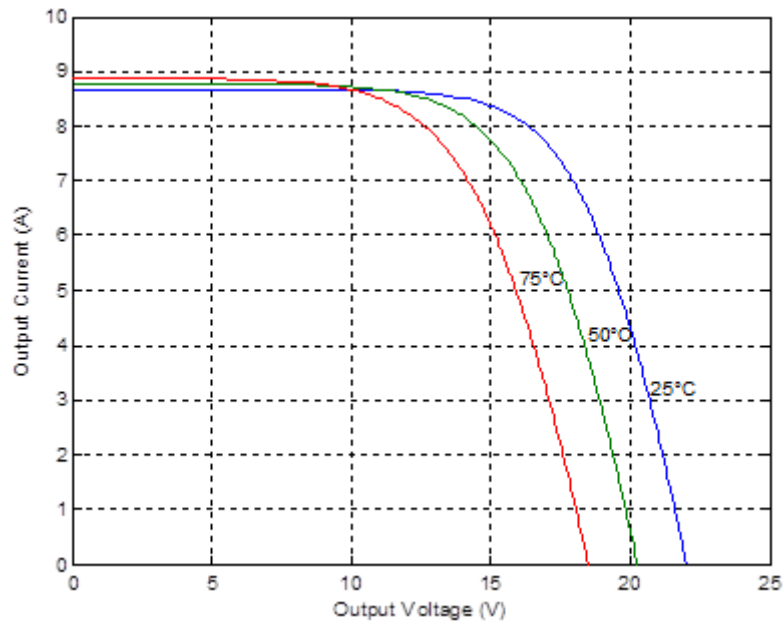


Figure 2.7: I-V characteristic curves for PV module under various cell temperature levels at 1 kW/m² insolation and 1 m/s wind velocity simulated with Matlab

For crystalline silicon cells, for each increase of one degree Celsius in temperature, the open-circuit voltage decreases by about 0.37% and the short-circuit current increases roughly by 0.05%. The consequence of this heating up of solar cells is that the MPP rises slightly and moves to the left with the MPP dropping about 0.5% per degree Celsius resulting in a important change in performance as the temperature of the solar cell changes (Masters 2004). A good model of the efficiency of photovoltaic module considers these effects.

2.3.4 Determination of cell temperature and average efficiency

Cell temperature has a negative impact on the efficiency of the PV module and must be curbed. The influence of temperature on I-V characteristics and consequently on the electrical efficiency of the PV module has been presented. Therefore it is important to determine the temperature of the PV module which is the same as the temperature of solar cells for any analysis of its performance. This is commonly determined using the Normal Operating Cell Temperature (NOCT) (Mattei, Notton, Cristofari, Muselli and Poggi 2006). The NOCT is the cell temperature in module lighting by the insolation of 0.8 kW/m² at ambient temperature of 20 °C and wind speed of 1 m/s. The NOCT value is given by manufacturers of solar cells (Masters 2004). The temperature of the PV module at different conditions is determined using the expression below:

$$T_c = T_a + \frac{NOCT-20}{0.8} G \quad (5)$$

Where T_c (°C) is the cell temperature, T_a (°C) is the ambient temperature and G (kW/m²) is the solar insolation.

The most common model of efficiency is given by the following Evans-Florschuetz correlation given in equation (6):

$$\eta = \eta_r [1 - \lambda(T_c - T_r)] \quad (6)$$

Where η_r (%) is the reference module efficiency, T_r (°C) is the reference temperature of 25 °C, λ (1/K) is the temperature coefficient of the PV module and T_c (°C) is the cell temperature.

PV module electrical energy, E , as function of temperature is given by:

$$E = \eta AG \quad (7)$$

where A is the PV module surface (m²).

The model for prediction of the performance of PV module in term of electrical output power in field, as the deviation from the standard test conditions as reported by the manufacturers, is obtained in the same manner as above (Skoplaki and Palyvos 2009).

2.4 Design of photovoltaic system for a modest Durban household

Electricity is used for a number of objectives ranging from everyday domestic needs for the use of electrical appliances to industrial purposes for production through to commercial uses. Between 1994 and 1999, approximately 2.8 million households in South Africa have been connected to the national electricity network. The acceleration of electrification of households anticipates an increase in electricity demand for residential use (Ziramba 2008). It is estimated that by 2025 approximately 11.4 million households in South Africa will be connected (Davidson, Tyani and Afrane-Okesse 2002).

2.4.1 Load determination

To make a decision in the electricity sector, the prediction of daily peak demand is very important (Sigauke and Chikobvu 2011). This is accomplished by selecting items that are often used to determine the average load for designing the PV system for modest household demand. Based on electrical rating, hours used per day, and days used per month, the following

household appliances have been considered from the Eskom residential tariff: computer, geyser, heater: two bars, hotplate: two plates, kettle, lighting: ten FLC, microwave oven, M-net decoder/DVD player, refrigerator with freezer, television: 51cm color, toaster. Items not enumerated will be those used based on the energy management of home owner or user. The electrical rating, hours used, days used and kWh used for those items are given in Table 2.1. The total of energy hours used is 692.3 kWh/month or 8307.6 kWh/ year.

Table 2-1: Daily electrical use and kWh used per month for a modest household

Electrical Appliances	Electrical Rating (Watts)	Hours Used Per Day	Days Used Per Month	kWh Used Per Month
Computer	480	2	15	14.4
Geyser	2000	5	30	300
Heater: 2 Bar	1000	5	15	75
Hotplate: 2 Plate	1500	3	30	135
Kettle	2000	0.5	30	30
Lighting: Single 100 W	100	5	30	15
Microwave Oven	1000	1	20	20
M-Net Decoder / DVD Player	25	6	30	4.5
Refrigerator (With Freezer)	400	6.5	30	78
Television: 51cm Colour	80	6	30	14.4
Toaster	800	0.5	15	6

2.4.2 Grid connected photovoltaic array sizing

The design of the grid-connected photovoltaic system studied is based on the method presented by Masters (2004) where it is explained in detail. The Q-PEAK 250 monocrystalline solar module was used as the PV generator in this study.

The design of the PV generator is based on a roof top non-tracking fixed orientation array. The maximum average irradiation for a year was obtained at a tilt angle of 29°, as explained previously. The average irradiance on the horizontal surface is 5.18 kWh/m²/day at a tilt angle of 29° as per NASA surface meteorological data (NASA n.d.). Using the peak hour approach with the impacts of temperature, inverter efficiency, and module mismatch and dirt considered to be 25% lost, for an efficiency of 75%, the electrical energy of the array at standard test condition is 5.8585 kW for a total number of 24 modules used.

The architecture of modules in the array is led by the choice of the converter and the size of the grid. For large grid connected systems, each string of modules can be connected to its own inverter in the same way as the single module-inverter topology. This makes the system modularised, so that maintenance can be done on certain parts of the system without disconnecting the whole system. In addition, installation costs are lower because of using many small inverters instead of one large central inverter (Masters 2004). To connect 24 PV panels in a string, there are seven possible combinations. By using a SMA Solar inverter, the best option is to use two Sunny Boy 3000TL inverters instead of one mini central 6000TL inverter for 5858.5 W, as explained above. Based on the array output energy and MPP voltage range, four strings of six modules each arranged into an array are obtained. With six modules per string, the STC rated voltage would be 180.06 V.

The Sunny Boy 3000TL inverter has one MPP tracker with two string plugs for the maximum input current of 17 A, an MPP voltage range of 188V-440 V, and a maximum current per string of 17 A. The STC rated voltage for two strings for one MPP tracker is 180.06 V. This is in the range of 180-280 V and a maximum input current of 16.82 A which is less than 17 A. It is

important to limit the maximum open-circuit voltage of the strings for the inverter to operate safely. That voltage must be less than the highest DC voltage that can be supported by the inverter. With two strings of six modules in parallel at each input of the inverter, the total voltage is about 180.06 V and is much less than the limit of 550 V of the inverter.

But V_{oc} increases when the PV cells temperature is less than the PV cells temperature at the Standard Test Condition of 25 °C. It can be figured that on a cold time with a severe and cold wind, and poor insolation, cell temperature can approach the ambient temperature and can be less than 25 °C, with a temperature coefficient for the open-circuit voltage of -0.32%, and the lowest recorded temperature of 6 °C (Washington Post 2012). Assuming the ambient and PV cell temperatures being equals, the open-circuit voltage $V_{oc,m}$ at one MPP tracker would now be 190.9864 V. This is still below the 550 V limit of this inverter. The other motive to verify the open-circuit voltage of a grid-connected array under strongest cold ambient conditions on the site is to limit the open-circuit voltage to a value less than 600 V as specified by the National Electrical Code for one or two households (Masters 2004). The array designed satisfied this constraint, and 24 modules arranged in 4 strings, with each string constituted of modules is suitable to be used for this purpose.

By considering the Q-PEAK 250 monocrystalline solar module dimensions, the roof area required for 24 modules with a fixed orientation is 42.60 m² with a DC standard test conditions rated power of 6000 W for the array. Assuming a 25% de-rating for AC and using the 5.18 kWh/m²day average solar radiation for Durban, the system is predicted to produce 8508.15 kWh/year.

Referring to the results obtained, the system can produce 8508.15 kWh/year. From Table 2.1 above, it is evident that the electrical power required by a modest Durban house is 8307.6 kWh/year, therefore the PV system can easily meet the requirements of the household electricity demand. The designed results for the PV generator are given in the Table 2.2.

Table 2-2: Array description

Module Type	Q-PEAQK 250 Monocrystalline Silicon
Array Size	42.60 m ²
Number of Strings	24
Number of Modules per String	6
Maximum Voltage at MPP (V_{PM})	180.06 V
Open Circuit Voltage (V_{OC})	222.90 V
Maximum Current at MPP (I_{PM})	33.64 A
Short Circuit Current (I_{SC})	A

2.5 Grid connected PV system simulations

A grid connected PV system to provide electricity for modest Durban household demand was designed. The simulation was undertaken to predict its performance before economic analysis and implementation can be done. The simulation of the system at different environmental parameters allows understanding of the system's behaviour in outdoor conditions. Based on the mathematical model of a one diode model, the grid connected PV array was simulated using Matlab software. The average results from the simulations were compared to those found in the literature. Results for different days in terms of energy and efficiency are presented and discussed below.

An array of 24 Q PEAK 250 PV modules for PV system was used for simulation. The system was tilted at 29.867° and weather data for two particular summer days (04/12/2010 and 29/12/2010) and two particular winter days (14/06/2011 and 28/06/2011) were used. The environmental parameters were obtained from the Greater Durban Radiometric network (GRADRAD) for solar irradiance, and Weather Analytics for ambient temperature and wind velocity. The simulations results are given in Figures 2.8, 3.9, 3.10 and 2.11.

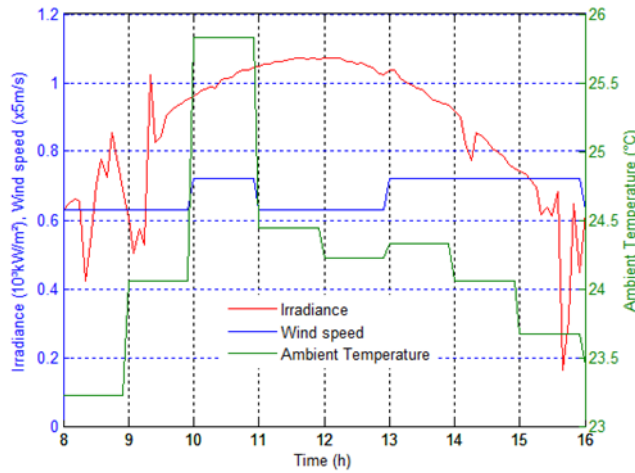


Figure 2.8.1: Weather condition for particular day of 04/12/2010

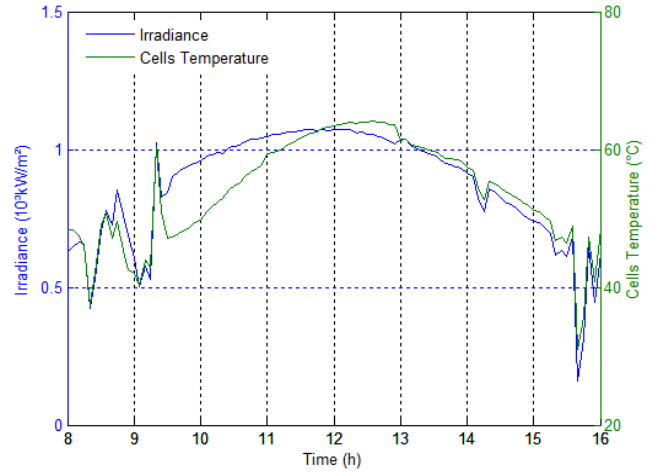


Figure 2.8.2: Irradiance and cell temperature behaviors on 04/12/2010

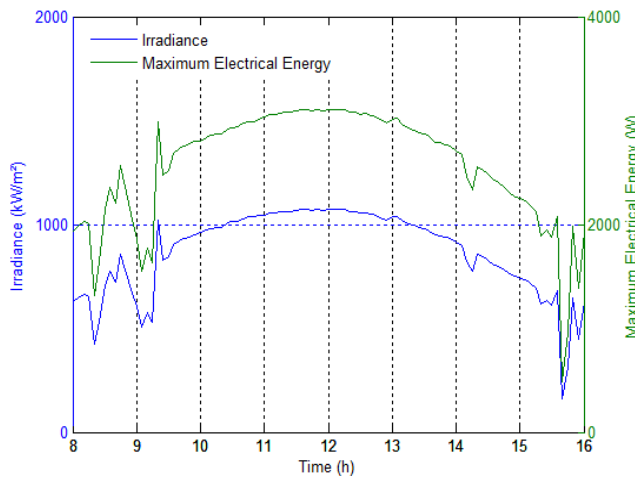


Figure 2.8.3: Irradiance and maximum electrical energy behaviors on 04/12/2010

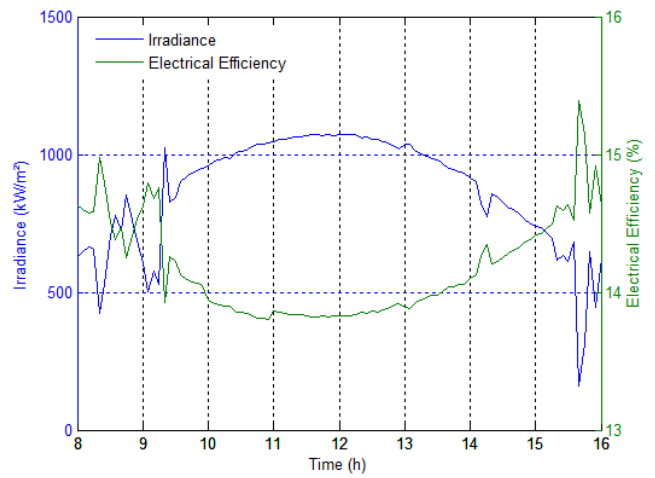


Figure 2.8.4: Irradiance and electrical efficiency on 04/12/2010

Figure 2.8: PV array simulation results for particular summer day of 04/12/2010

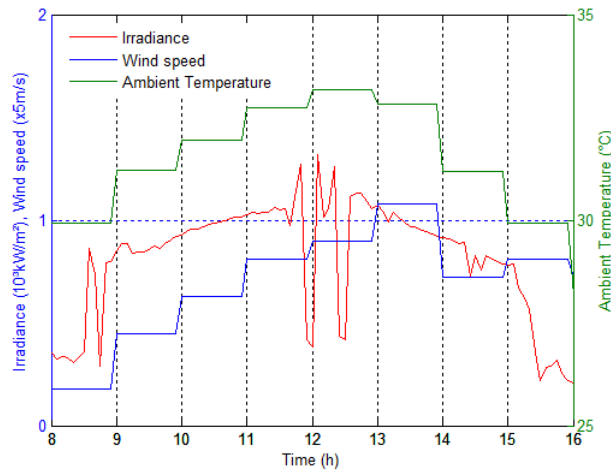


Figure 2.9.1: Weather condition for particular day of 29/12/2010

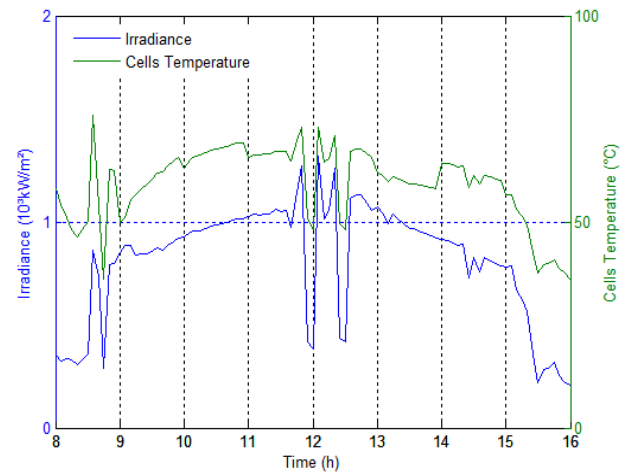


Figure 2.9.2: Irradiance and cell temperature behaviors on 29/12/2010

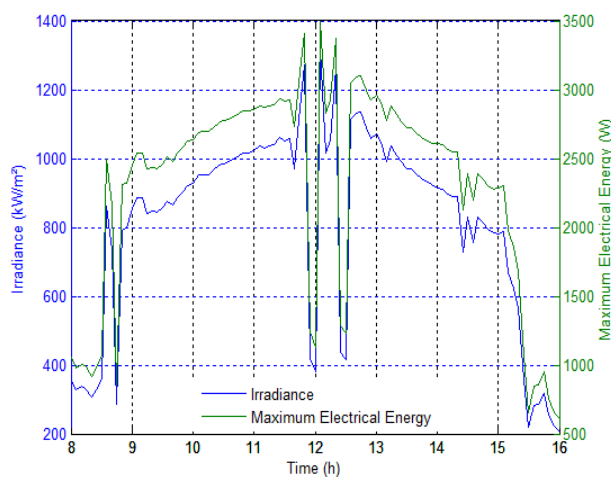


Figure 2.9.3: Irradiance and maximum electrical energy behaviors on 29/12/2010

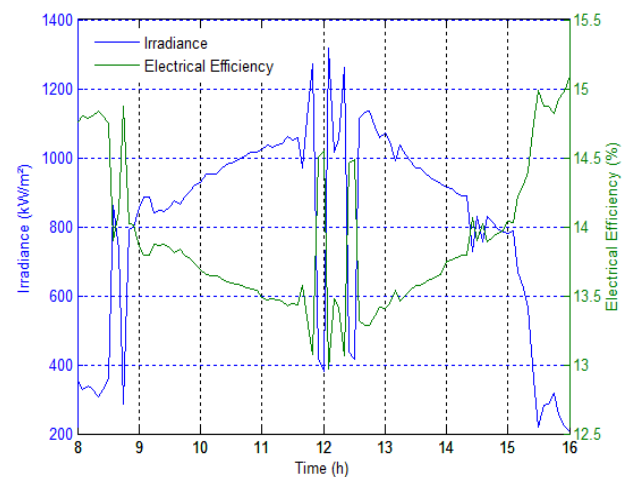


Figure 2.9.4: Irradiance and electrical efficiency on 29/12/2010

Figure 2.9: PV array simulation results for particular summer day of 29/12/2010

The simulation results can be interpreted that array temperature and array maximum electrical energy follow irradiance, while array temperature and array maximum electrical energy variations follow solar insolation variation, and the array efficiency drop-offs with an increase of irradiance. This is justified by the increase of array temperature with insolation. The average array temperature is around 30 °C with peaks of about 41.6 °C and 40.8 °C on 14/06/2011 and 28/06/2011 (winter days) respectively; and around 50 °C with peaks of about 61 °C and 78 °C on 04/12/2010 and 29/12/2010 (summer days) respectively. The average summer maximum electrical energy is above 3100 W and is twice greater than the average of about 1200 W in winter, while efficiency of about 14% is obtained in summer and about 15% in winter.

These results are justified by the behavior of array temperature and array electrical energy against insolation as well as the behavior of efficiency against array temperature, as explained previously. The summary of simulation results is given in Table 2.3.

From the simulation results it is evident that the array design can supply the electrical energy for household demand in the Durban area. But the performance of the system will be low in

winter due to low insolation. That will require extra energy from other sources such as diesel, hydrogen, wind etc. By combining those sources with photovoltaic systems, hybrid systems can be built and energy supply improved.

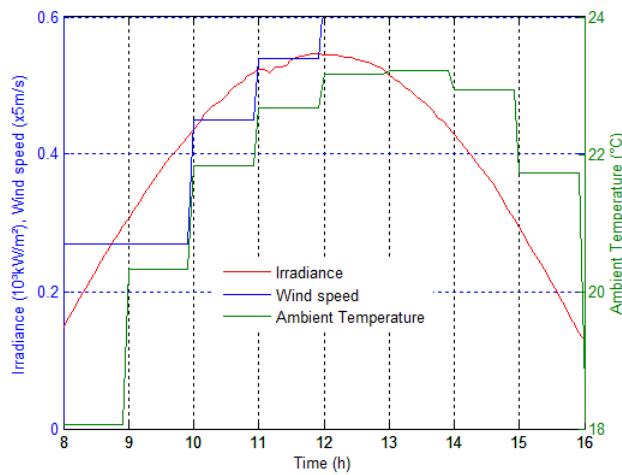


Figure 2.10.1: Weather condition for particular day of 14/06/2011

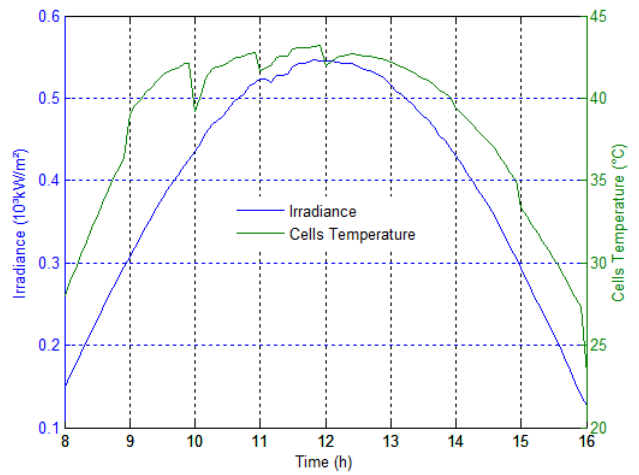


Figure 2.10.2: Irradiance and cell temperature behaviors on 14/06/2011

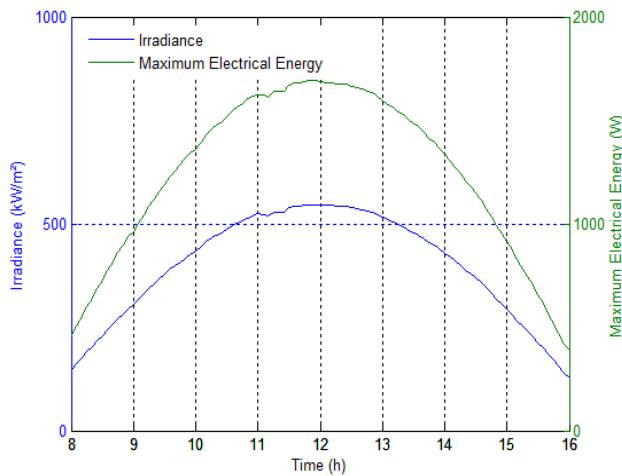


Figure 2.10.3: Irradiance and maximum electrical energy behaviors on 14/06/2011

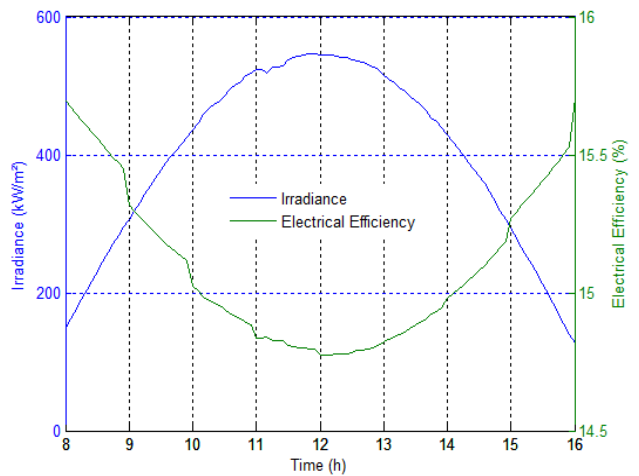


Figure 2.10.4: Irradiance and electrical efficiency on 14/06/2011

Figure 2.10: PV array simulation results for particular winter day of 14/06/2011

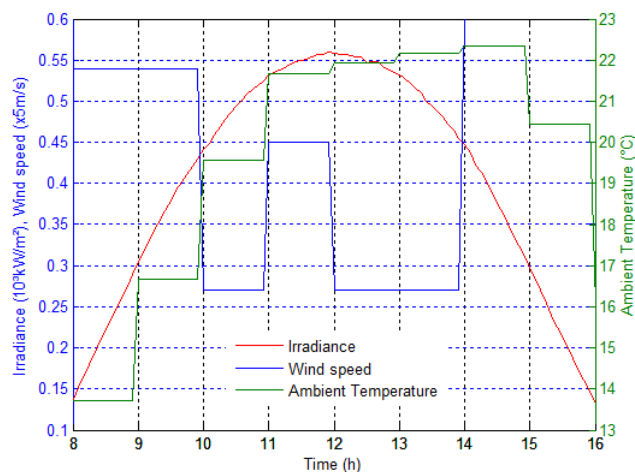


Figure 2.11.1: Weather condition for particular day of 28/06/2011

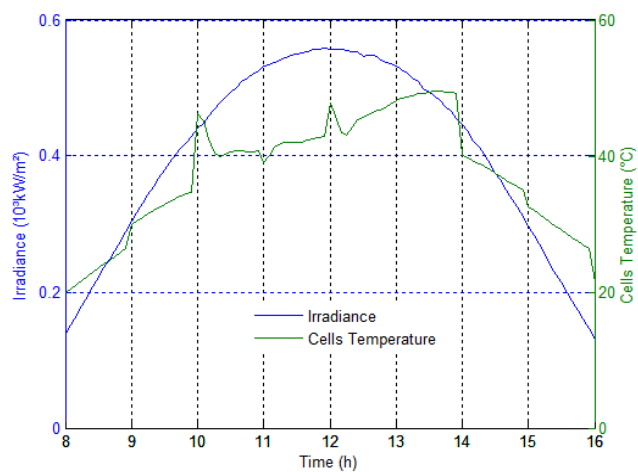


Figure 2.11.2: Irradiance and cell temperature behaviors on 28/06/2011

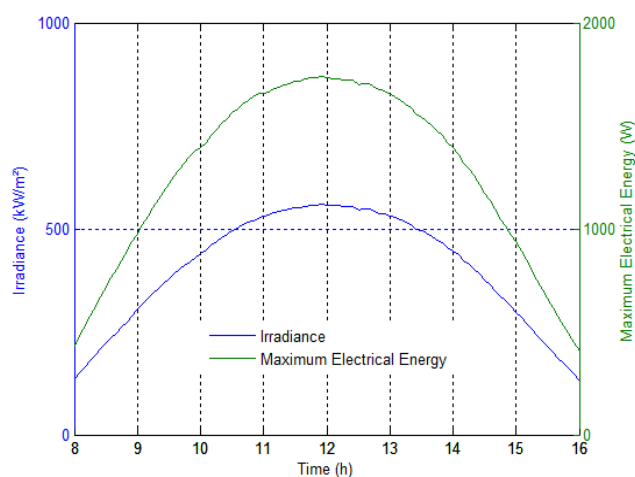


Figure 2.11.3: Irradiance and maximum electrical energy behaviors on 28/06/2011

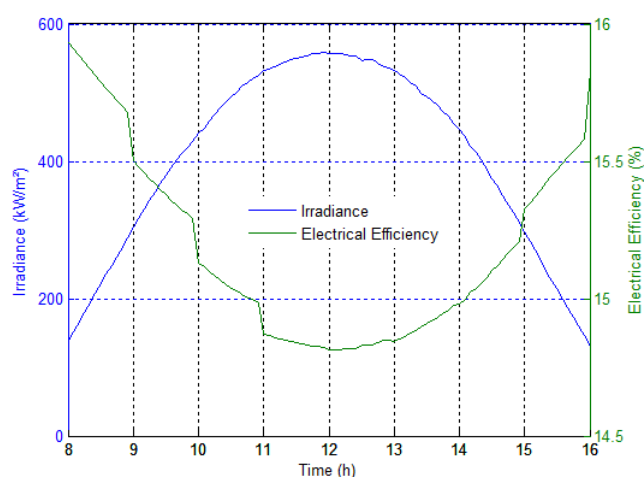


Figure 2.11.4: Irradiance and electrical efficiency on 28/06/2011

Figure 2.11: PV array simulation results for particular winter day of 28/06/2011

Table 2-3: Summary of the results from simulation of PV system

Measured Parameters		Summer		Winter	
		04/12/2010	29/12/2010	14/06/2011	28/06/2011
Cell temperature (°C)	Average	53.6	59	35.2	33.5
	Minimum	29.1	35	22.8	18.3
	Maximum	61.0	78	41.6	40.8
Maximum electrical power (W)	Average	2568.7	2308	1242.6	1273.3
	Minimum	488.5	611	387.2	407.2
	Maximum	3106.8	3495	1693.4	1741.8
Electrical efficiency (%)	Average	14.2	14	15.1	15.2
	Minimum	13.8	13	14.8	14.8
	Maximum	15.4	15	15.7	15.9

2.6 Economics of the PV system

To complete the design, an economic analysis was performed based on the initial cost of the PV generator and the quantity of energy it will produce every year. The economic viability of the system ultimately depends on the price of the energy produced by the system which includes the possibility of tax credits, economic advantages and the mode in which the system is paid for (Masters 2004).

2.6.1 Cost of PV system and energy delivery

The cost of the system is obtained using the SUNSIM simulation results published by Bekker (2007). A major cost advantage is that the equipment is maintenance free apart from material degradation since there are no moving parts in the integrated PV systems (Chow, He, Ji and Chan 2007). Table 2.4 gives the cost for components of the PV system.

Table 2-4: PV components cost

SYSTEM DESCRIPTION	PV Component Cost (Rand)
Collector frame and support	21,090.85
PV modules	210,908.52
Inverters	46,868.56
Wiring and accessories	5,858.57
Transport and installation	23,434.28
Total cost	308,160.78

Design results show that to attend to the required household electricity demand, a 4500 W AC PV system should be used. The system must deliver 8508.15 kWh per year to a house that currently pays R0.94 per kWh, which is the Eskom energy cost without value added tax (VAT) (2012 residential tariffs).

From the design, we can see that the PV system is supposed to supply 8508.15 kWh/year. As can be seen from Figure 2.12, more than 70% of investment is allocated to the electricity generator, with 68% for PV modules and 15% for inverters for PV systems, with at least 85% to PV modules.

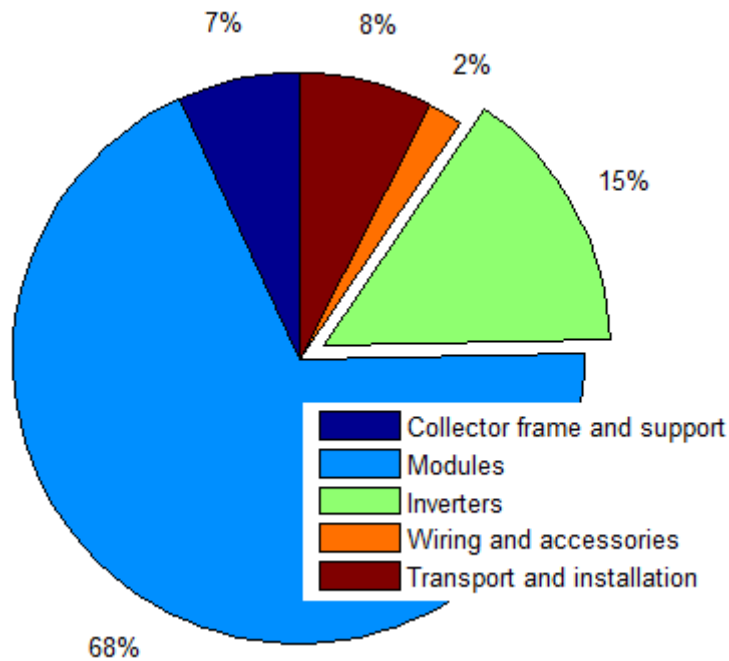


Figure 2.12: Average cost of residential PV systems for modest household demand in Durban

2.6.2 Loan terms and income tax

The following is assumed for the calculations below: the taxpayer earns R300 000 per year and so will be in the 22.23% tax bracket as seen in Table 2.5; the bank loan will be for a term of 20 years at an interest rate of 8.5% (SA Loans 2012); the system is eligible for a rebate of R50 per WAC.

Table 2-5: The tax rates applicable to individuals for the tax year 2012/2013

Taxable Income	Tax Rate
R0.00 - R160,000.00	18% of taxable income
R160,001.00 - R250,000.00	R 28,800 + 25% of taxable income
R250,001.00 - R346,000.00	R 51,300 + 30% of taxable income
R346,001.00 - R484,000.00	R 80,100 + 35% of taxable income
R484,001.00 - R617,000.00	R 128,400 + 38% of taxable income
R617,001.00	R 178,940 + 40% of taxable income

Source: SA Loans 2012

2.6.3 Financing of the PV system

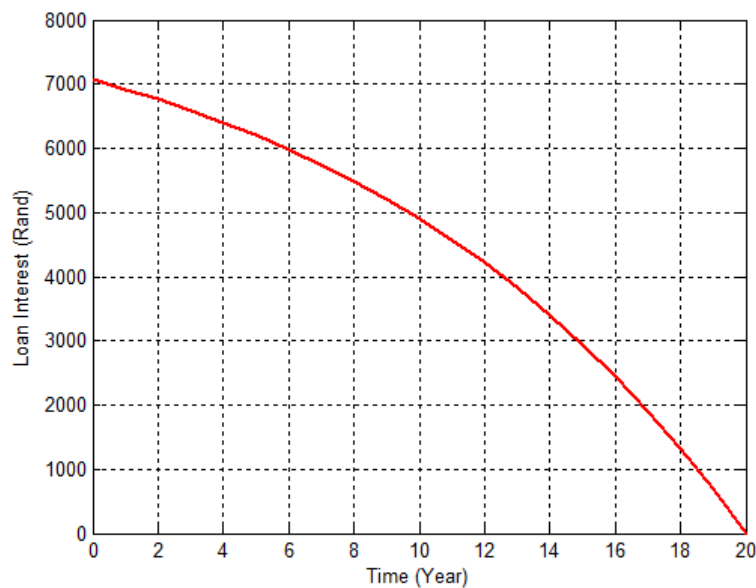
Financing of the PVC system is based on the determination of the net economic benefit. The net cost of the system, the annual load payment, annual cost and saving are calculated over 20 years. The energy cost is also determined and compared to the cost of energy from Eskom.

By using data from Sections 6.1 and 6.2, we obtain the cost of PV system electricity and the net economic benefit in the first year as given in Table 2.6.

Table 2-6: System electricity cost and net economic benefit in the first year

Parameter	PV
System power (kW)	4500.00
System power predicted (kWh/yr)	8508.15
Total cost (R)	308160.78
PV rebate (R/W)	50.00
Loan interest (i)	0.09
Number of years (n)	20.00
Tax rate (MTB)	0.22
Eskom electricity tariff (R/kWh)	0.94
Net cost (R)	83160.78
CRF (i,n)	0.11
Loan (R)	8787.68
Tax saving (R)	1571.36
System electricity cost (R/kWh)	0.85
System Net economic benefit (R)	756.67

Figure 2.13 represents the variation of loan balance and loan interest for the PV system over 20 year with utility electricity costs increasing at 5% each year. It can be seen that after twenty years, the balance is zero due to the savings realized over twenty years. While the utility electricity cost increases from R0.94 /kWh by 5% each year over 20 years to R2.49 /kWh, the PV system increases from R0.94 /kWh to R1.01 /kWh for 19 years then drops to R0 /kWh at the twentieth year as shown in Figure 2.14, which means free electricity at the twentieth year.

**Figure 2.13: PV system loan balance and loan interest over 20 years**

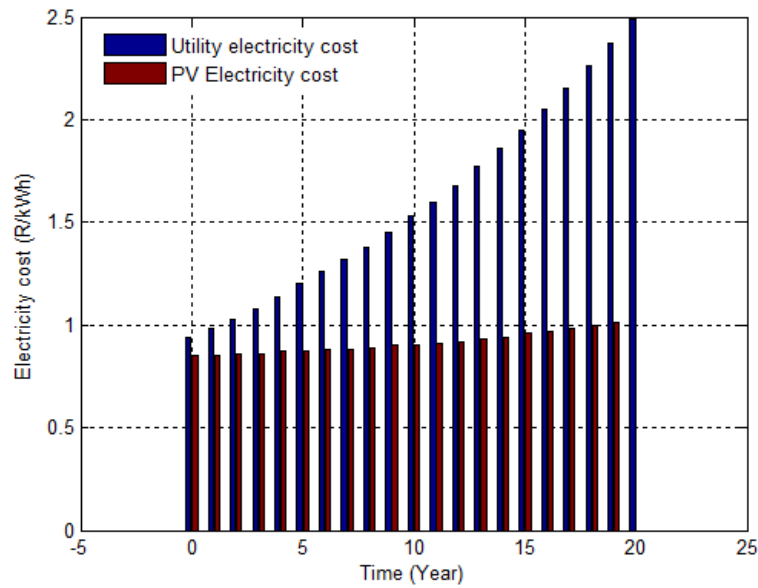


Figure 2.14: PV system variation of electricity cost over 20 years

The savings for the PV system increase linearly over 19 years from R756.70 to R11 512.70 per year. At the twentieth year, the loan balance is zero, which explains the rapid increase of savings to R21 154.71 per year for the PV system in that particularly year.

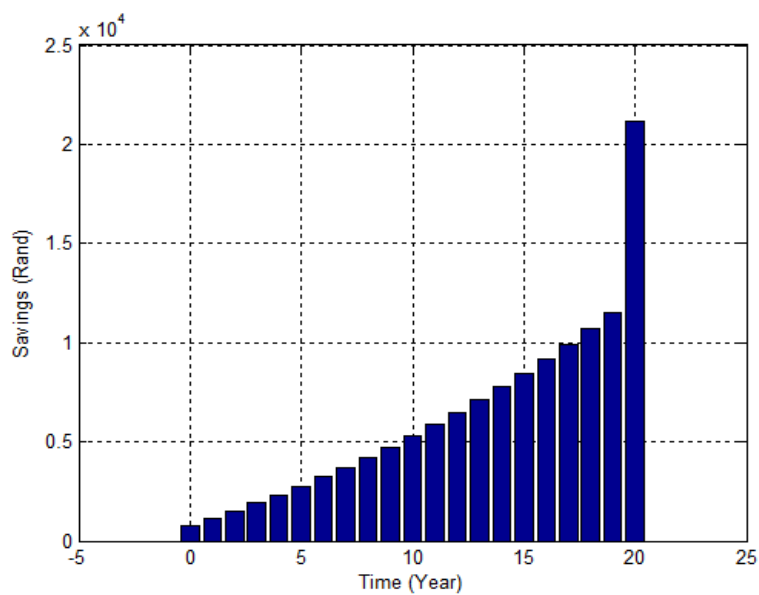


Figure 2.15: PV system tax savings over 20 years

After 20 years, R129 618.90 would be saved by using a grid connected PV system. If the same calculations are made with the 15% increase in Eskom tariffs due to start from 2014, the savings would be R792 101.36 for the PV system, as shown in Figure 2.15.

2.7 Conclusion and recommendations

From the design and simulation of a PV system for Durban household demand, it can be seen that the system is suitable to supply electricity requirements of this particular case of a modest Durban household. The array system performs better in summer due to higher irradiance than winter. To cover the lack of electricity at low sunlight, the system can be coupled with other types of renewable energy systems such as fuel cell systems or wind turbines depending on the area, to form a hybrid system. With a saving of R129 618.90 based on a 5% increase in Eskom tariffs and R792 101.36 based on the 15% increase in Eskom tariffs due to start from 2014 applied over 20 years, the system is one viable option to overcome the South African electricity blackout and greenhouse gas emissions from coal-fired power stations.

References

- Bekker B. 2007. "Irradiation and PV array energy output, cost, and optimal positioning estimation for South Africa." *Journal of Energy in South Africa*, 18 (2): 16-25.
- Bellingham C., G. Davies, and A. Human 2009. Greening Durban 2010. Durban (South Africa): eThekweni Municipality.
- Chow T-T., W. He, J. Ji, and A. L. S. Chan. 2007. "Performance evaluation of photovoltaic-thermosyphon system for subtropical climate application." *Solar Energy*, 81 (1): 123-130.
- Cristóbal J., G. Guillén-Gosálbez, J. Jiménez, and A. Irabien. 2012. "Optimization of global and local pollution control in electricity production from coal burning." *Applied Energy*, 92: 369-378.
- Davidson O., L. Tyani, and Y. Afrane-Okesse. 2002. "Climate change, sustainable development and energy: future perspectives for South Africa." Paris: OECD.
- Hammed A., A. Kafayat, and M. Ramos. 2009. "Aggregate demand for electricity in south africa: an analysis using the bounds testing approach to cointegration." *Energy Policy*, 37 (10): 4167-4175.
- Inglesi-Lotz R. 2010. "Aggregate electricity demand in South Africa: conditional forecasts to 2030." *Applied Energy*, 87 (1): 197-204.
- Inglesi-Lotz R. 2011. "The evolution of price elasticity of electricity demand in South Africa: a Kalman filter application." *Energy Policy*, 39 (6): 3690-3696.
- Ishaque, K., Z. Salam, and H. Taheri. 2011. "Simple, fast and accurate two-diode model for photovoltaic modules." *Solar Energy Materials and Solar Cells* 95: 586-595.
- Masters G. M. 2004. *Renewable and efficient electric power systems*. Hoboken, NJ: John Wiley and Sons.
- Mattei M., G. Notton, C. Cristofari, M. Muselli, and P. Poggi. 2006. "Calculation of the polycrystalline PV module temperature using a simple method of energy balance." *Renewable Energy*, 31 (4): 553-567.
- NASA. n.d. Surface meteorology and solar energy. Atmospheric Science Data Center. Accessed 02 17, 2013. <http://eosweb.larc.nasa.gov>.
- Niez A. 2010. "Comparative study on rural electrification policies in emerging economies: keys to successful policies." Information Paper. Paris: International Energy Agency (IEA).
- Pereira M. G., J. A. Sena, M. A. V. Freitas, and N. F. D. Silva. 2011. "Evaluation of the impact of access to electricity: a comparative analysis of South Africa, China, India and Brazil." *Renewable and Sustainable Energy Reviews*, 15 (3): 1427-1441.
- SA Loans. 2012. SA Home Loans Economic Update. Durban: SA Home Loans.

- Schmidt, S. n.d. "Coal deposits of South Africa - the future of coal mining in South Africa." Institute for Geology, Freiberg-Danemark. www.geo.tu-freiberg.de/oberseminar/os07_08/stephan_Schmidt.pdf; n.d.
- Sigauke C., and D. Chikobvu. 2011. "Prediction of daily peak electricity demand in South Africa using volatility forecasting models." *Energy Economics*, 33 (5): 882-888.
- Skoplaki E., and J. A. Palyvos. 2009. "On the temperature dependence of photovoltaic module electrical performance: a review of efficiency/power correlations." *Solar Energy*, 83 (5): 614-624.
- Suri M., T. Cebecauer, and A. Skoczek. 2012. "Solar electricity production from fixed-inclined and sun-tracking c-Si photovoltaic modules in South Africa." 1st Southern African Solar Energy Conference (SASEC), Stellenbosch (South Africa) May 21-23.
- Walker G. R. 2000. "Evaluating MPPT converter topologies using a MATLAB PV model." Australasian Universities Power Engineering Conference (AUPEC). Brisbane (Australia).
- Washington Post. 2012. Longterm historical data Durban South Africa. 16 07. http://www.washingtonpost.com/wp-srv/weather/longterm/historical/data/Durban_South_Africa.htm.
- Zawilska E., and M. J. Brooks. 2011. "Solar energy measurement on the Southern Africa East Coast." World Renewable Energy Congress, Linköping (Sweden), May 7-14.
- Ziramba E. 2008. "The demand for residential electricity in South Africa." *Energy Policy*, 36 (9): 3460-3466.

CHAPTER 3 : PERFORMANCE ANALYSIS OF THERMOSYPHON HYBRID PHOTOVOLTAIC THERMAL COLLECTOR

PUBLICATION 3

N. Marc-Alain Mutombo

Freddie Inambao*

Glen Bright

Discipline of Mechanical Engineering, University of KwaZulu-Natal, South Africa

Journal of Energy in Southern Africa • Vol 27 No 1 • February 2016

Performance analysis of thermosyphon hybrid photovoltaic thermal collector

N. Marc-Alain Mutombo

Freddie Inambao*

Glen Bright

Discipline of Mechanical Engineering, University of KwaZulu-Natal, South Africa

Abstract

The conversion of solar irradiance into electricity by a photovoltaic module (PV) is 6–17% of the incoming energy from the sun depending on the type of technology and the environmental parameters. More than 80% of incoming energy from the sun is reflected or absorbed by the solar module. The fraction of energy absorbed increases with solar cell temperature and the cells' efficiency drops as a consequence. The efficiency of a PV module is improved by combining a PV module and a thermal collector in one unit, resulting in a hybrid photovoltaic and thermal collector (PV/T). The purpose of this paper is to present the behavior a thermosyphon hybrid PV/T when exposed to variations of environmental parameters and to demonstrate the advantage of cooling photovoltaic modules with water using a rectangular channel profile for the thermal collector. A single glazed flat-box absorber PV/T module was designed, its behavior for different environmental parameters tested, the numerical model developed, and the simulation for particular days for Durban weather run. The simulation result showed that the overall efficiency of the PV/T module was 38.7% against 14.6% for a standard PV module while the water temperature in the storage tank reached 37.1 °C. This is a great encouragement to the marketing of the PV/T technology in South Africa particularly during summer, and specifically in areas where the average annual solar irradiance is more than 4.70 kWh/m²/day.

Key words: photovoltaic, thermal collector, storage tank, temperature, power output, efficiency, simulation.

Nomenclature

Roman

A	area (m ²)
b	height of the channel (m)
D	diffuse component of solar irradiance (kWh/m ² day)
G	global insolation on the horizontal (kWh/m ² day)
H	useful thermal energy [W]
H	convective heat transfer coefficient (W/m ² K)
I	current (A)
L	module length (m)
\dot{m}	mass flow rate [kg/s]
m	simplification coefficient ()
P	power (W)
S	direct component of solar irradiance on the horizontal (kWh/m ² day)
S	simplification coefficient ()
U	overall heat transfer coefficient (W/m ² K)
V	voltage (V)
w	channel water velocity (m/s)
x-y	coordinates axis
z	direction of water in channels

Greek symbols

A	altitude (°)
B	tilt angle (°)
Δ	difference
H	efficiency (%)
μ	dynamic viscosity (kg/ms)
ξ	dimensionless coefficient
ρ	density (kg/m ³)
τ	transmittivity (-)

Subscripts

a	ambient
c	cells
e	electrical
eff	effective
f	fluid
lcw	lower channel wall

* Corresponding author

Tel: +27 31 260 8530 E-mail: inambaof@ukzn.ac.za

i	inlet
o	outlet
oc	open voltage
r	reference
sc	short circuit
T	total
th	thermal
u	upper, useful
ucw	upper channel wall

Abbreviations

Cp	specific heat (J/kgK)
GRADRAD	greater radiometric
HMDE	highest minimum daily energy
HYE	highest year energy
NOCT	normal operating cell temperature (°C)
PV	photovoltaic
PV/T	photovoltaic and thermal

1. Introduction

High electrical output can be obtained from a PV panel receiving high incidence solar irradiance. However, with high incidence irradiance the temperature of the solar cells increases and this reduces their efficiency.

Photovoltaic cells must be cooled by removing the heat in some way for better efficiency. This has led many researchers to develop hybrid photovoltaic and thermal collectors (PV/T) which generate electric power and simultaneously produce hot water or hot air (Mattei *et al.*, 2006).

Using water in cooling systems is more efficient than using air. Photovoltaic cells are cooled by water convection with the water circulating in a closed circuit. The heat from PV cooling water is extracted into a storage tank and can be used in heating systems. The design of this technology uses rectangular profile thermal collector channels using natural convection fluid flow.

Theoretical and experimental studies of PV/T were conducted from as early as the mid-1970s (Chow, 2010). In 1976, Wolf M. analyzed the performance of a silicon solar array mounted inside a stationary flat plate collector using a lead-acid battery as the storage element (Wolf, 1976).

In 1979, Florschuetz presented a simple model for preliminary assessment of cooling system requirements for heat rejection from solar cells subjected to concentrated solar irradiation levels. Analysis of flat plate collectors from a Hottel-Whillier model for thermal collector was extended to the assessment of combined photovoltaic/thermal collectors and their efficiencies. Based on the extended model, examples of both thermal and electrical performance of a combined collector as a function of collector design parameters were pre-

sented and discussed. (Florschuetz, 1979).

In 1981, two separate one-dimensional analyses were developed for the prediction of the thermal and electrical performance of both liquid and air flat-plate photovoltaic/thermal (PVT) collectors (Raghuraman, 1981). Four years later, several potentially useful features in the design of photovoltaic/thermal (PVT) collectors were explored in order to determine their effectiveness and interaction (Cox III and Raghuraman, 1981).

In 1994, a hybrid photovoltaic thermal system based on natural convection of water in a thermal absorber fitted with circular channel tubes was studied and experiments were conducted for several days on a thermal collector alone. The finite difference method (FDM) was used to model and simulate the performance of the thermal collector (Agarwal and Garg, 1994). In order to understand and evaluate the solar hybrid systems, an experimental study was performed (Garg *et al.*, 1994).

One year later, Garg and Agarwal (1995) performed the study of a hybrid forced circulation photovoltaic and thermal system and developed a mathematical model for the system using the finite difference method. The algorithms for making quantitative predictions on the performance of the system were established by Bergene and Lovvik (1995) after proposing a detailed physical model of a hybrid photovoltaic thermal system.

In 2001, Huang *et al.* (2001) studied the performance of an integrated photovoltaic and thermal solar system (IPVTS) compared with a conventional solar water heater and demonstrated the idea of an IPVTS design.

In 2002, a hybrid PV/T unit that simultaneously produced low temperature heat and electricity was made from the combination of mono crystalline silicon photovoltaic cells with a polymer solar heat collector (Sandnes and Rekstad, 2002). Four 4 numerical models were built for the simulation of the thermal yield of a combined PV/T collector (Zondag *et al.*, 2002).

In 2003, Zondag *et al.* (2003) evaluated nine different designs of combined PV thermal collectors in order to obtain a clearer view of the projected efficiency of the different concepts. In the same year, Chow (2003) established an explicit dynamic model for a single-glazed flat plate water heating PVT collector based on the control volume finite difference approach, and Coventry and Lovegrove (2003) presented the methods used to develop a ratio between electrical and thermal output energy for a domestic style PVT system.

The rectangular channels used with PV/T collectors are more efficient due to the fact that they provide a large surface area for heat exchange between the PV module and the thermal collector. This study is a particular case in which a simulation was run with Durban meteorological conditions for two par-

ticular days with a single glazed hybrid PV/T based on thermosyphon principle for water flow.

2. Solar irradiance on tilted surface

The flux of energy produced by the solar source reaching a surface per unit surface of an area is the insolation or solar irradiance. It is expressed in units of kWh/m²/day for the average daily or monthly conditions at a given location. This quantity defines the maximum energy produced by a photovoltaic system for that particular location (Florida Solar Energy Center, 2010).

The photovoltaic panels are commonly tilted at a certain angle from the horizontal to receive the maximum amount of insolation. The insolation on the panels at the corresponding tilt angle is evaluated by separating the insolation into two components, the direct and the diffuse. Where solar irradiance data is available in the form of direct and diffuse components, the approach discussed in the next paragraph can be used to obtain the global insolation reaching the panels tilted at a certain angle β from the horizontal (Wenham *et al.*, 2007).

Firstly, it is assumed that the diffuse component of insolation D is independent of the tilt angle approximately right for tilt angles of about or less than 45 °C. Secondly, the direct component of insolation on the horizontal surface S is to be converted into the direct component S_{β} that reaches the PV module tilted at angle β to the horizontal (Wenham *et al.*, 2007), as shown in Figure 1.

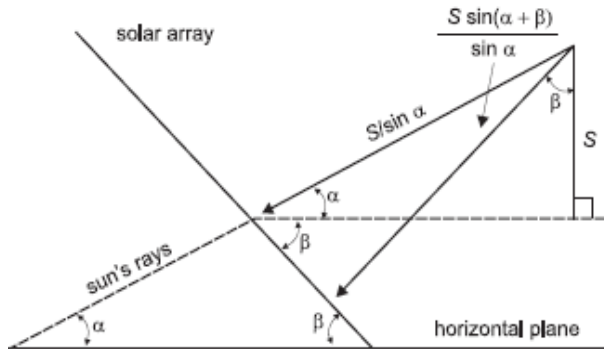


Figure 1: Light incident on a surface tilted to the horizontal

Consequently, Equation (1) is obtained:

$$S_{\beta} = \frac{S \sin(\alpha + \beta)}{\sin \alpha} \quad (1)$$

where α is the altitude of the sun and β is the tilt angle.

The global insolation on array is the sum of the direct component S_{β} incident on a plane tilted at angle β to the horizontal and the diffuse component D independent parameter of the tilt angle, given by Equation (2):

$$G = S_{\beta} + D \quad (2)$$

3. Temperature influence on PV panel

Two important parameters of the I - V curve for a PV module are short-circuit current I_{sc} and open-circuit voltage V_{oc} . I_{sc} and V_{oc} change with the incident solar irradiance G and the ambient air temperature T_a , as illustrated in Figure 2.

It is important to note that V_{oc} decreases with increasing module temperature, which leads to a noticeable decrease in the available maximum electrical power, in spite of a small increase in short-circuit current I_{sc} , as illustrated in Figures 2(a) and 2(b).

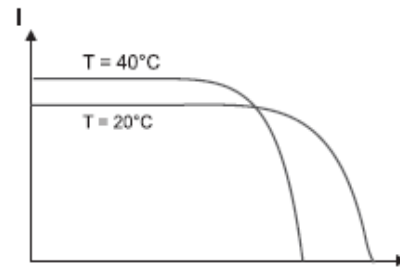


Figure 2(a): I-V characteristics of a PV cell at different temperatures

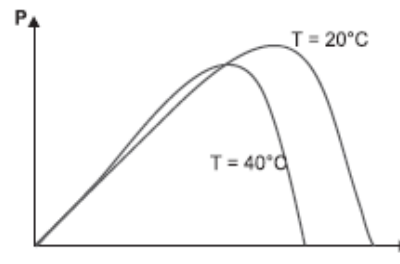


Figure 2(b): P-V characteristics of a PV cell at different temperatures

These effects must be considered in any model for photovoltaic module efficiency. By definition, the efficiency of the PV system η_e is the ratio of electrical output energy P and the solar energy on the panels $A \cdot G$ and expressed in Equation 3.

$$\eta_e = 100 \cdot \frac{P}{A \cdot G} \quad (3)$$

where G is the insolation per unit of area and A the area of the panel.

The best known model is given by the Evans-Florschuetz correlation according to Equation 4:

$$\eta_e = \eta_r [1 - \lambda(T_c - T_r)] \quad (4)$$

where η_r is the reference module efficiency at a PV cell temperature T_r of 25 °C and at a solar irradiance G on the module of 1000 Wm⁻². The T_c is the PV cell temperature, which depends on the envi-

ronmental conditions and λ is the volume expansion coefficient 1/K.

The PV module power output is given by:

$$P = \frac{\eta * A * G}{100} \quad (5)$$

4. Conventional PV module

The conventional PV module is constituted of PV encapsulation protected on top by a front glazing and at the back by the back glazing and frame as illustrated in Figure 3.

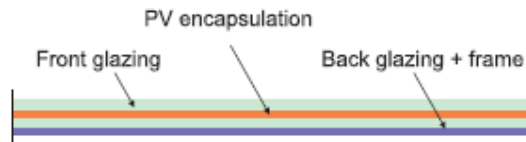


Figure 3: Cross-section view of a commercial PV module (N.T.S.)
(Chow, 2003)

The electrical energy output from the PV module increases with the irradiance. At high irradiance the temperature of the solar module increases and its efficiency decreases as we can see from Equations 4) and 5. The temperature of the PV module is given by the empirical Equation 6:

$$T_c = T_a + \frac{NOCT - 20}{0.8} G \quad (6)$$

where NOCT is the normal operating cell temperature.

Therefore to increase the efficiency, particularly at high irradiance, the PV module must be cooled.

5. The PV/T module design and temperature modelling

The cooling system is constituted with a thermal collector plate, a storage tank and inlet and outlet pipes as illustrated in Figure 4.

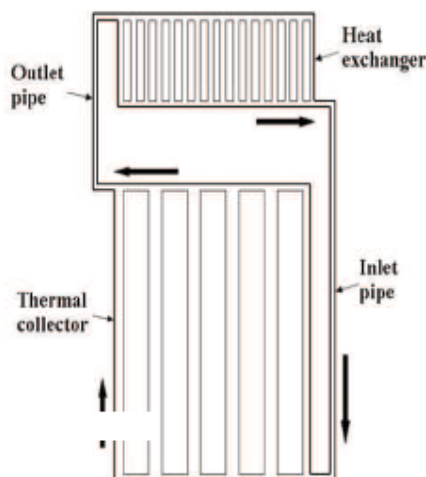


Figure 4: Water cooling PV system diagram

The heat of PV cells is removed from the module by water convection in thermal collector channels. Water is heated as the sun shines on the PV module, expands slightly, becomes lighter and is pushed through the collector outlet to the top of the tank by cold water from the tank that enters the bottom of the collector by gravity and rises again to the top of the tank by means of the thermosyphon principle as it warms up.

The collector plate comprises a front glazing PV encapsulation, a thermal absorber with rectangular flow channels, a thermal insulation and a back cover. The cross section view of the module is illustrated in Figure 5.

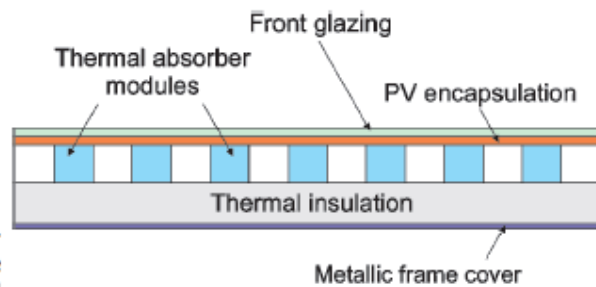


Figure 5: Cross-section view of the PV collector plate (N.T.S.)
(Chow, 2003)

The thermal absorber is relied to the storage tank by inlet and outlet pipes. The outlet pipe routes hot water from the thermal absorber to the storage tank by buoyancy. The cold water from the tank is routed back to the thermal absorber through the inlet pipe. The bottom of storage tank is at least a foot higher than the top of the collector to avoid reverse flow during the night (Arunchala, 2011).

The temperature of solar cells is defined by the rate of water flowing in the thermal absorber channels.

Applying the energy balance on the thermal absorber gives Equation 7 for fluid temperature in channels:

$$\frac{dT_f}{dz} + \frac{r}{m} T_f = \frac{s}{m} \quad (7)$$

where:

$$r = U_{f-a} + h_f(1 - \xi_{cu})$$

$$s = \xi_{fu}\xi_{cu}(\tau_{eff}G + U_{c-a}T_a - U_{c-r}T_r) + U_{f-a}T_a$$

$$m = b\rho_f w_f C_{pf}$$

The average fluid temperature is given by Equation 8:

$$\frac{dT_f}{dz} + \frac{r}{m} T_f = \frac{s}{m} \quad (8)$$

and the cell temperature is obtained from Equation 9:

$$\bar{T}_c = \frac{\tau_{eff}G + U_{c-a}T_a - U_{c-r}T_r + U_{c-ucw}\bar{T}_{ucw}}{U_{c-a} + U_{c-ucw} - U_{c-r}} \quad (9)$$

where

$$\bar{T}_{ucw} = \frac{\xi_{cu}\tau_{eff}G + \xi_{cu}(U_{c-a}T_a - U_{c-r}T_r) + h_f\bar{T}_f}{h_f + U_{c-ucw}(1 - \xi_{cu})} \quad (10)$$

is the temperature of the upper channel wall.

The velocity of water in a rectangular channel due to the thermosyphon principle is obtained from Equation 11:

$$\frac{\partial^2 w_f}{\partial x^2} + \frac{\partial^2 w_f}{\partial y^2} = -\lambda \rho_m g \cos \beta \frac{\bar{T}_{ucw} - \bar{T}_{l cw}}{\mu b} y \quad (11)$$

where g is the gravity, λ is the volume expansion coefficient, T_{ucw} is the temperature of the upper surface of the channel, T_{lcw} is the temperature of the

lower surface of the channel, μ is the dynamic viscosity, β is the tilt angle of the module and b is the height of the channel.

The total or overall efficiency of the system is the ratio of the sum of electrical energy and useful thermal energy over the solar energy and is given by Equation 12:

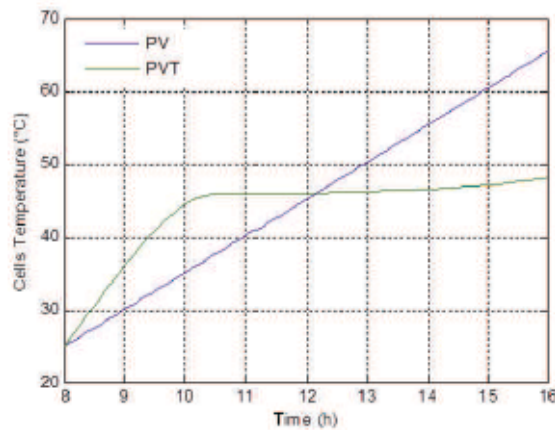
$$\eta_T = \eta_e + \eta_{th} \quad (12)$$

in which η_e is the electrical efficiency of the PV/T system that can be obtained from Equation 3 and η_{th} is the thermal efficiency of the thermal absorber given by Equation 13:

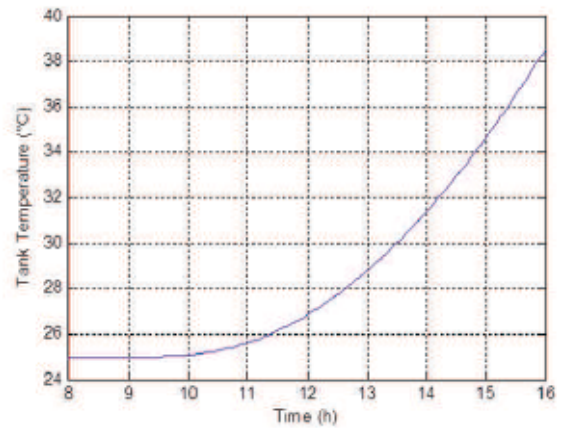
$$\eta_{th} = 100 * \frac{H_u}{AG} \quad (13)$$

where H_u is the useful thermal energy obtained from Equation 14:

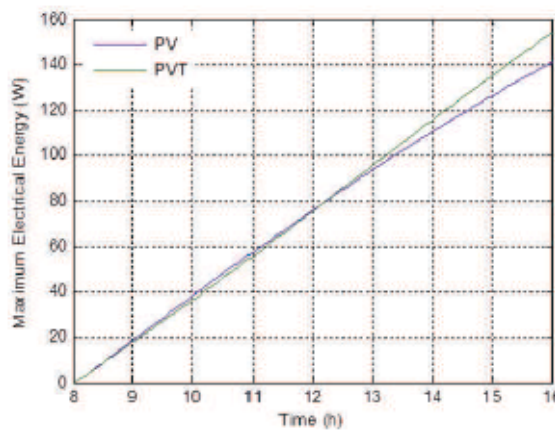
$$H_u = \dot{m} * C_{pf} * \Delta T_f \quad (14)$$



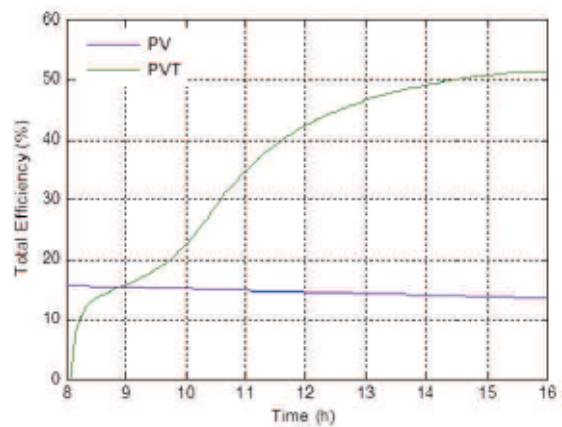
(a) PV and PVT modules temperatures variation



(b) Tank temperature variation



(c) PV and PVT modules maximum electrical energy output



(d) PV and PVT modules total efficiency

Figure 6(a)-(d): PV and PV/T modules behaviors for variation of solar irradiance at ambient temperature 25°C and wind velocity 1 m/s

6. The PV/T system behaviour against variation of environmental parameters

The important environmental parameters that influence the performance of a PV system are solar irradiance, ambient temperature and wind velocity. The most important of them is solar irradiance because of the fact that the PV panel converts the light from the sun into electrical and thermal energies.

Figure 6 shows the impact of PV module behaviour compared with that of PV/T for solar irradiance varying from 0 to 1200 W/m² at a constant ambient temperature of 25 °C and a constant wind speed of 1 m/s for eight hours. In Figure 6(a), the temperature of the cells for the PV/T module in the four first hours is observed. Temperature rises faster in the PV/T module than the PV module temperature for the first two hours, then remains nearly constant after half of total time. The tank temperature rises following a positive exponential as shown in Figure 6(b). The maximum electrical energy and the overall efficiency are represented by Figures 6(c) and 6(d). As the solar irradiance rises, the maximum power point moves to the left for the conventional PV module, while the PV/T module remains at a

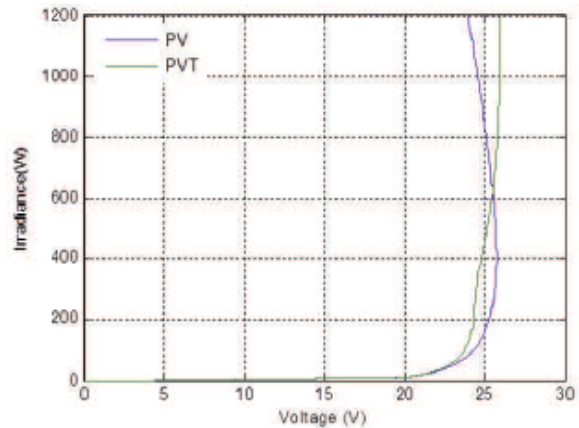
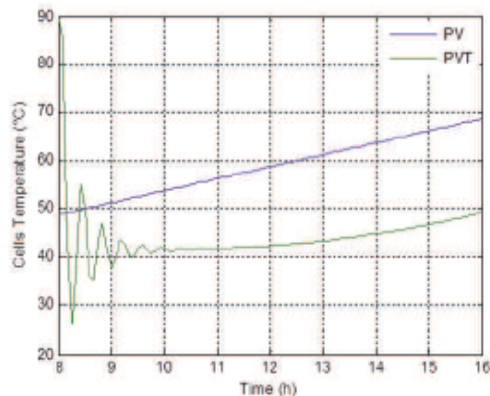


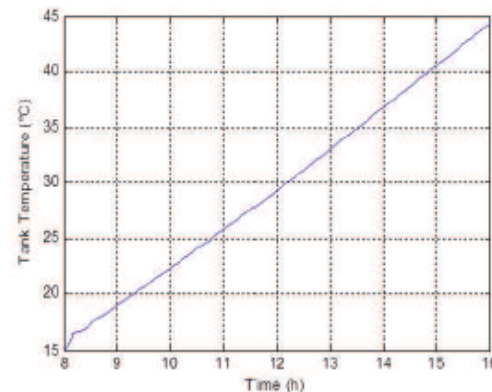
Figure 7: PV and PV/T modules MPP variation with voltage and solar irradiance

constant voltage at the right of the PV module MPP as the solar irradiance increases. This behaviour is a great advantage for the electrical output of PV/T module as shown in Figure 7.

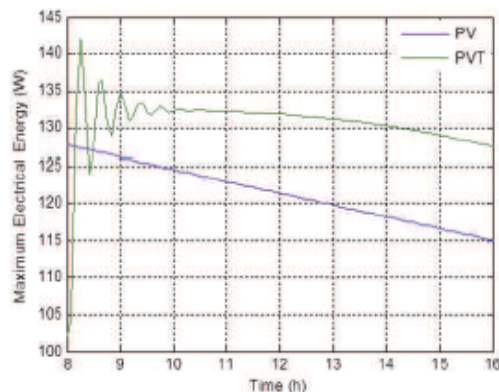
Figures 8(a)–(d) and Figures 9(a)–(d) represent the respective behaviours of PV and PV/T modules exposed to 1000 W/m² for variable ambient tem-



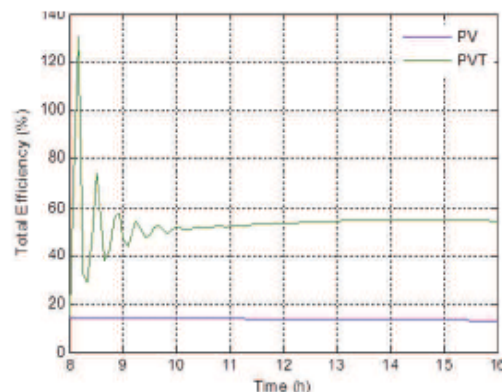
(a) PV and PVT modules temperatures variation



(b) Tank temperature variation

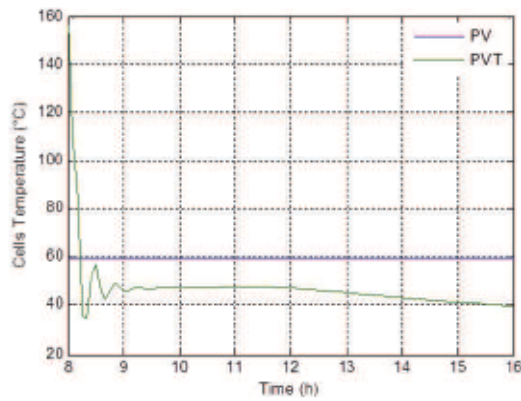


(c) PV and PVT modules maximum electrical energy output

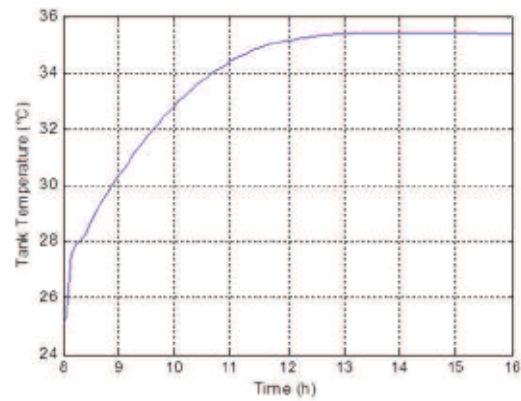


(d) PV and PVT modules total efficiency

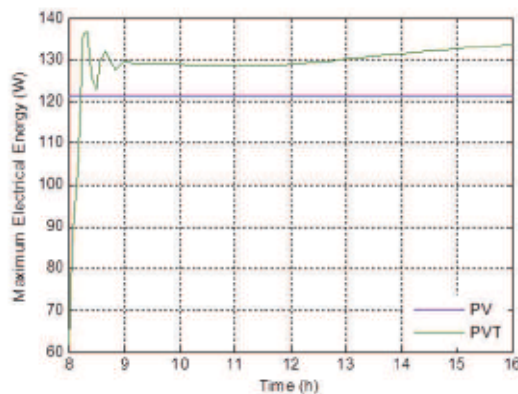
Figure 8(a)–(d): PV and PV/T modules behaviors for variation of ambient temperature at solar irradiance of 1000 W/m² and wind velocity of 1 m/s



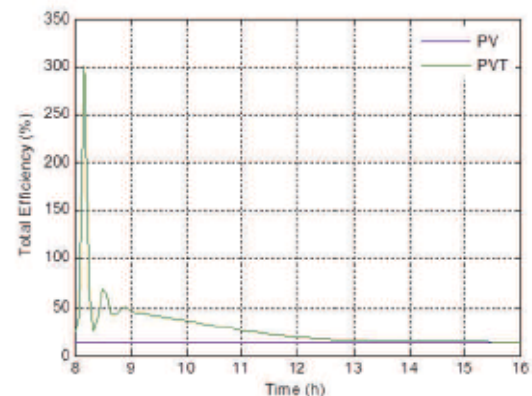
(a) PV and PVT modules temperatures variation



(b) Tank temperature variation



(c) PV and PVT modules maximum electrical energy output



(d) PV and PVT modules total efficiency

Figure 9(a)-(d): PV and PVT modules behaviours for variation of wind velocity at solar irradiance of 1000 W/m^2 and ambient temperature of 25°C

perature at wind velocity of 1 m/s and variable wind velocity at an ambient temperature of 25°C .

In both cases, due to sudden exposition of PV/T module to high solar irradiance, the solution of Equation (6) is under-damped, which explains the oscillation behaviour of temperature of the cells due to a natural response of fluid temperature in the channels to thermal shock, as seen in Figures 8(a) and 9(a).

For an ambient temperature varying from 25°C to 35°C and wind velocity of 1 m/s , both PV and PV/T module temperatures rise linearly. The gradient of cell temperature against the time curve for PV module is greater than the gradient for cell temperature against time curve for PV/T module. This leads to a rapid increase of temperature in the case of the PV module. The maximum electrical energy of both systems decrease, while the efficiency is constant as seen in Figures 8(c) and 8(d). The storage tank temperature rises linearly as shown in Figure 8(b).

For a wind velocity varying from 0 to 12 m/s at ambient temperature of 25°C . The temperature of the PV cells is constant. The temperature of the PV/T cells, which is less than that of the PV cells,

decreases after half of the total time, while the maximum electrical energy output, which is greater than the constant PV maximum electrical energy output, increases as seen in Figures 9(a) and 9(c) respectively. The PV/T total efficiency decreases and stabilizes at a constant efficiency value of the PV module as shown in Figure 9(d). The temperature of the storage tank rises following a negative exponential as seen in Figure 9(b).

7. Durban flat-plate collector tilt angle

The sun's daily position in the sky differs over the course of the year. As a result, objects looking to maximize the use of solar energy, such as building thermal mass, photovoltaic panels and solar water heaters, should be orientated at an optimum angle for intended yearly time of use (Bellingham *et al.*, 2009).

In South Africa the optimum tilt angle does not follow latitudinal gradient. It increases from about 24° in the northern part of the country towards the south-east, where it reaches values of up to 35° (Suri *et al.*, 2012).

For Durban, Chris Bellingham *et al.* (2009) proposed the best angle for overall annual solar energy harvesting to be 35° to the horizontal.

Fixed PV arrays (i.e. panels that are fixed into position for the whole year) are typically installed with one of two requirements in mind: either to deliver the highest yearly energy (HYE), e.g. grid-connected PV arrays, or to deliver the highest minimum daily energy (HMDE) through the year, e.g. for battery-charging purposes. For Durban, Bekker (2007) proposed an optimal elevation tilt angle of 30° HYE optimal elevation.

Zawilska and Brooks (2011) recorded and analyzed solar radiometry and selected meteorological parameters for Durban, South Africa, over a full one-year period from January to December 2007 and found a 13% increase in energy availability, confirming the value of tilting flat-plate collectors in Durban at an angle equal to the latitude of 29.867° south.

8. Simulation and energy output

Two monocrystalline Q.PEAK 260 PV modules were used for simulation with Durban meteorological data. The first module was used as a conventional PV module, while the second was connected to a 150 liters tank. The two collectors were tilted at 29.867° south.

Weather data for two particular days were used. The environmental parameters were obtained from the Greater Durban Radiometric network (GRADRAD) for solar irradiance, and Weather Analytics for ambient temperature and wind velocity.

For the summer period, environmental parameters for the day of 22/12/2012 are represented in Figure 10.

Simulation results for the PV and PVT modules behaviour for the particular day of 22/12/2010 with Durban weather conditions are given in Table 1.

The behaviours of both systems are represented in Figure 11(a)–(d).

For the winter period, environmental parameters for the day of 27/06/2011 are represented in Figure 12.

Simulation results for the PV and PV/T modules behaviours for the particular day of 27/06/2011 with Durban weather conditions are given in Table 2. The behaviours of both systems are represented in Figure 13.

9. Conclusions

The simulation of two monocrystalline Q.PEAK 260 PV modules was conducted with one module on top of a thermal collector and connected to a 150 liters storage tank to constitute a PV/T module and

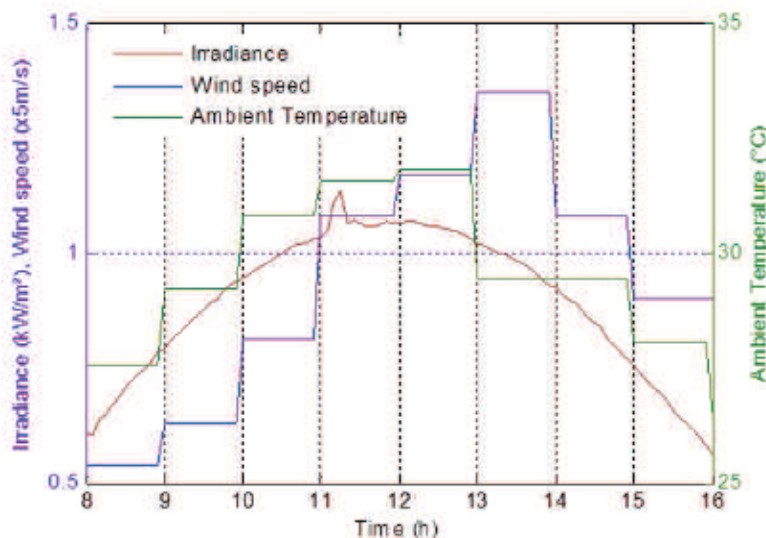
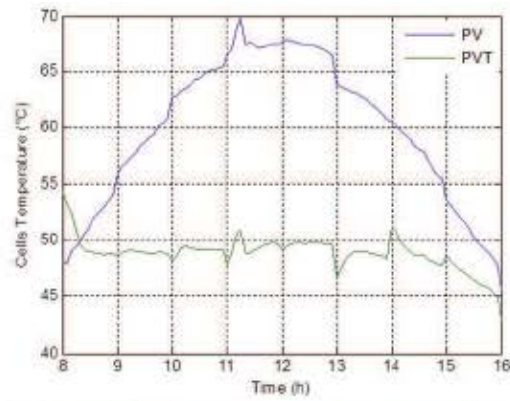


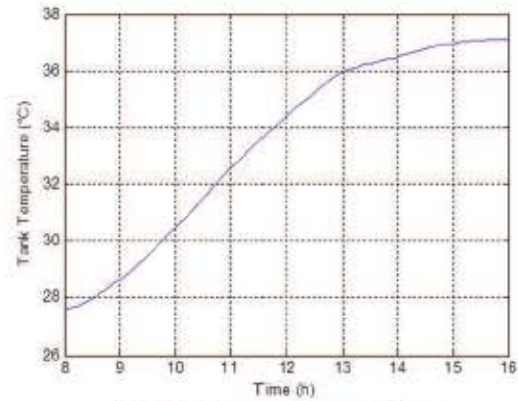
Figure 10: Environmental parameters for the date of 22/12/2010

Table 1: Comparative output values between photovoltaic module and hybrid photovoltaic module with Durban weather conditions for the particular day of 22/12/2010

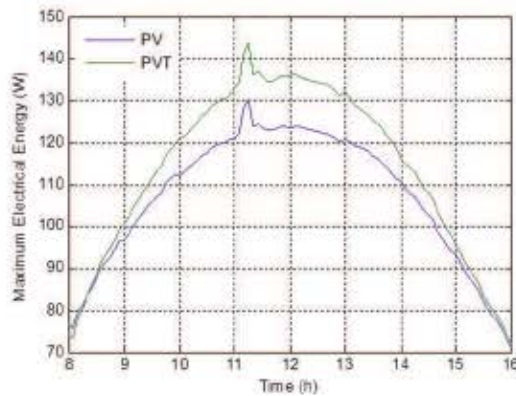
	Photovoltaic module			Hybrid photovoltaic module			
	Cell temperature (°C)	Max. electrical power output (W)	Electrical efficiency (%)	Cell temperature (°C)	Max. electrical power output (W)	Overall efficiency (%)	Tank temperature (°C)
Average	59.9	106.8	13.9	48.8	113.7	27.9	33.5
Minimum	45.4	71.0	13.4	42.8	71.9	14.6	27.6
Maximum	69.8	130.3	14.6	54.3	143.8	38.7	37.1



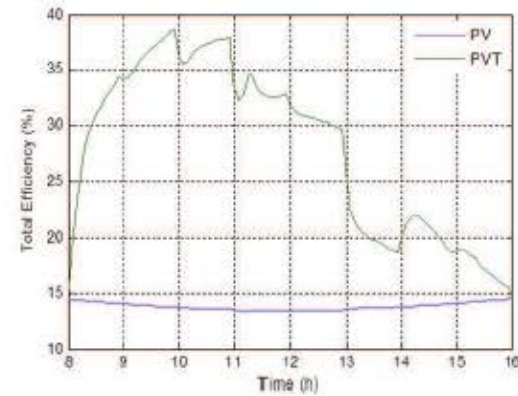
(a) PV and PVT modules temperatures variation



(b) Tank temperature variation



(c) PV and PVT modules maximum electrical energy output



(d) PV and PVT modules total efficiency

Figure 11(a)-(d): PV and PV/T modules temperature and output power with Durban weather conditions for the particular day of 22/12/2010

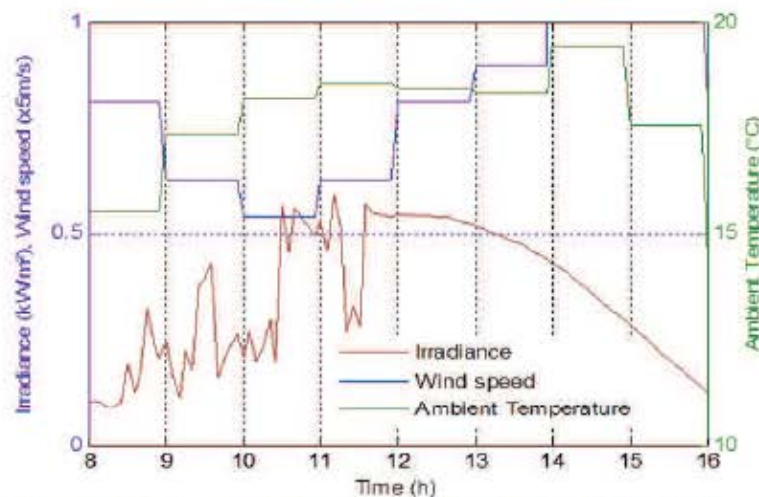


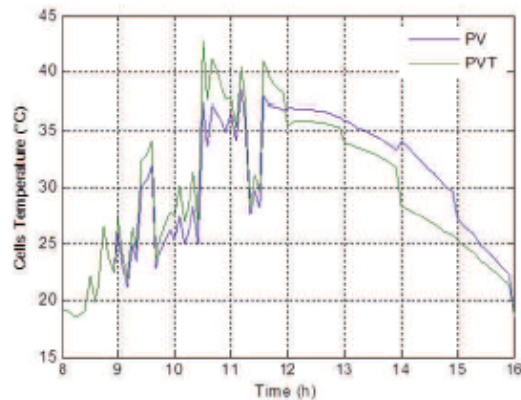
Figure 12: Environmental parameters for the date of 27/06/2011

both modules were exposed for eight hours to varying environmental conditions. It was found that no matter which environmental parameter is varied, the maximum electrical power output of PV/T module was always higher than of the PV module. The higher efficiency was obtained from the PV/T module because of cooling of the solar cells (decrease in

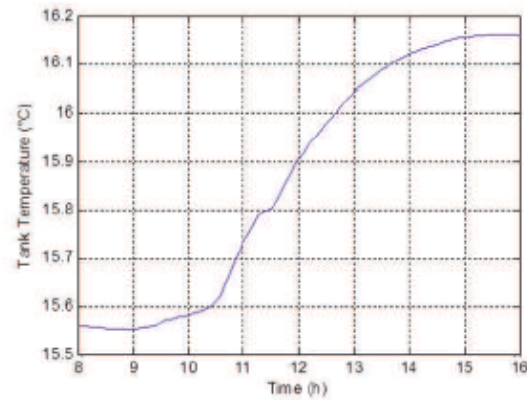
cells temperature), with the heat removed from cells being used to heat water in the storage tank. For the typical summer day of 22/12/2010, the efficiency of the PVT module was 24.1% higher than the conventional PV module for the same dimensions and characteristics and the tank water temperature reached 37.1 °C. These results are encouraging

Table 2: Comparative output values between photovoltaic module and hybrid photovoltaic module with Durban weather conditions for particular day of 27/06/2011

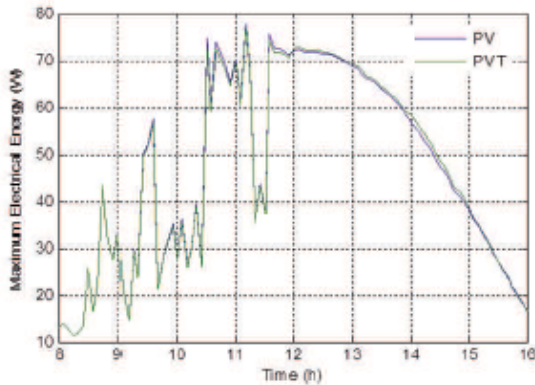
	Photovoltaic module			Hybrid photovoltaic module			
	Cell temperature (°C)	Max. electrical power output (W)	Electrical efficiency (%)	Cell temperature (°C)	Max. electrical power output (W)	Overall efficiency (%)	Tank temperature (°C)
Average	29.93	47.06	15.35	29.60	47.14	17	15.87
Minimum	18.59	11.34	14.92	18.60	11.34	13.28	15.55
Maximum	38.52	77.75	15.92	42.78	76.99	20.99	16.16



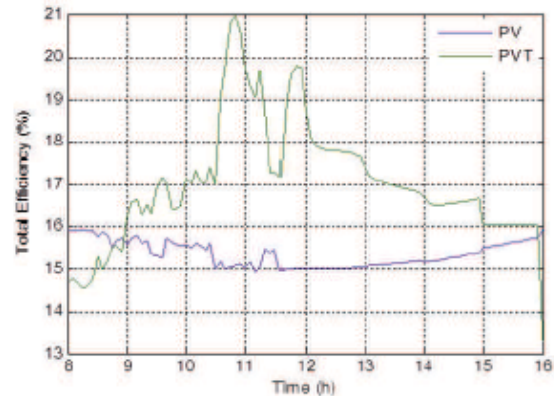
(a) PV and PVT modules temperatures variation



(b) Tank temperature variation



(c) PV and PVT modules maximum electrical energy output



(d) PV and PVT modules total efficiency

Figure 13: PV and PVT modules temperature and output power with Durban weather conditions for the particular day of 27/06/2011

regarding the use of PVT systems particularly in areas where hot water is also needed. This system provides both high electrical power output and hot water.

References

- Agarwal R.K. and Garg, H.P. (1994). Study of a photo-voltaic-thermal system thermosiphonic solar water heater combined with solar cells. *Energy Conversion and Management*, 35, 605-620.
- Arunchala U.C. (2011). Performance deterioration of thermosiphon solar flat plate water heater due to scaling. *IJUM Engineering Journal*, Special Issue, Mechanical Engineering.
- Bekker, B. (2007). Irradiation and PV array energy output, cost, and optimal positioning estimation for South Africa. *Journal of Energy in South Africa*, 18(2), 16-25.
- Bellingham, B., Davies, G. and Human, A. (2009). Greening Durban 2010. eThekweni Municipality, KwaZulu-Natal, South Africa.
- Bergene, T. and Lovvik, O.M. (1995). Model calculations on a flat-plate solar heat collector with integrated solar cells. *Solar Energy* 1995;55(6), 453-462. DOI:10.1016/0038-092X(95)00072-Y.
- Chow T.T. (2003). Performance analysis of photovoltaic-thermal collector by explicit dynamic model. *Solar Energy*, 75(2), 143-152. DOI:10.1016/j.solener.2003.07.001.

- Chow, T.T. (2010). A review on photovoltaic/thermal hybrid solar technology. *Applied Energy*, 87, 365-379. A review on photovoltaic/thermal hybrid solar technology. DOI:10.1016/j.apenergy.2009.06.037.
- Coventry J.S. and Lovegrove K. (2003). Development of an approach to compare the 'value' of electric and thermal output from a domestic PV/thermal system. *Solar Energy*, 75(1), 63-72. DOI:10.1016/S0038-092X(03)00231-7.
- Cox III, C.H. and Raghuraman P. (1985). Design considerations for flat-plate-photovoltaic/thermal collectors. *Solar Energy*, 35(3), 227-421. DOI: 10.1155/2012/957847
- Florida Solar Energy Center (FSEC). (2010). FSEC Standard 203-10: *Procedures for photovoltaic system design review and approval*. University of Central Florida, Cocoa, Florida.
- Florschuetz L.W. (1979). Extension of the Hottel-Whillier model to the analysis of combined photovoltaic/thermal flat plate collectors. *Solar Energy*, 22, 361-366. DOI:10.4028/www.scientific.net/AMM.401-403.146
- Garg H.P. and Agarwal P.K. (1995). Some aspects of a PV/T collector/forced circulation flat plate solar water heater with solar cells. *Energy Conversion and Management*, 36, 87-99.
- Garg, H.P., Agarwal, R.K. and Joshi, J.C. (1994). Experimental study on a hybrid photovoltaic-thermal solar water heater and its performance predictions. *Energy Conversion and Management*, 35, 621-633.
- Huang, B.J., Lin, T.H., Hung, W.C. and Sun F.S. (2001). Performance evaluation of solar photovoltaic/thermal systems. *Solar Energy* 70(5), 443-448. DOI:10.1016/S0038-092X(00)00153-5.
- Mattei, M. Notton, G., Cristofari, C., Muselli, M. and Poggiani P. (2006). Calculation of the polycrystalline PV module temperature using a simple method of energy balance. *Journal of Renewable Energy*, 31(4), 553-567. DOI:10.1016/j.renene.2005.03.010.
- Raghuraman P. (1981). Analytical predictions of liquid and air photovoltaic/thermal, flat-plate collector performance. *Journal of Solar Energy Engineering*, 103, 291-298. DOI:10.1115/1.3266256
- Sandnes, B. Rekestad J. (2002). A photovoltaic/thermal (PV/T) collector with a polymer absorber plate-experimental study and analytical model. *Solar Energy*, 72(1), 63-73. DOI:10.1016/S0038-092X(01)00091-3.
- Suri M., Cebecauer T., Skoczek A. and Betak, J. (2012). *Solar electricity production from fixed-inclined and sun-tracking c-Si photovoltaic modules in South Africa*. 1st Southern African Solar Energy Conference (SASEC), 21-23 May, Stellenbosch.
- Wolf M. (1976). Performance analysis of combined heating and photovoltaic power systems for residences. *Energy Conversion and Management*, 16, 79-90.
- Wenham, S.R., Green, M.A., Watt, M.E. and Corkish, R. (2007). *Applied photovoltaics*. 2nd ed. Padstow, Cornwall, UK: TJI International Ltd. pp. 22-23; 128-129.
- Zawilska E. and Brooks M.J. (2011). *Solar energy measurement on the South Africa east coast*. World Renewable Energy Congress, Linköping, Sweden.
- Zondag H.A., De Vries D.W., Van Helden W.G.J., Van Zolingen R.J.C., Van Steenhoven A.A. (2003). The yield of different combined PV-thermal collector designs. *Solar Energy*, 74, 253-269. DOI:10.1016/S0038-092X(03)00121-X.
- Zondag H.A., de Vries, D.W., van Helden, W.G.J., van Zolingen, R.J.C. and van Steenhoven, A.A. (2002). The thermal and electrical yield of a PV-thermal collector. *Solar Energy*, 72(2), 113-128. DOI:10.1016/S0038-092X(01)00094-9.

CHAPTER 4 : FUEL CELLS DEVELOPMENT, APPLICATIONS AND MARKET

PUBLICATION 4

Ntumba Marc-Alain Mutombo^a; Freddie L. Inambao^b; Remy Tiako^c

^{a,c} University of KwaZulu-Natal, School of Engineering, Discipline of Electrical Engineering, Howard College Campus, Durban, South Africa (marcntumba@yahoo.fr; Tiako@ukzn.ac.za)

^b University of KwaZulu-Natal, School of Engineering, Discipline of Mechanical Engineering, Howard College Campus, Durban, South Africa (inambaof@ukzn.ac.za)

Abstract

Climate change, energy security and air pollution have propelled the demand and the interest of renewable energies such as photovoltaics, fuel cells and wind turbines. Each of these technologies have their advantages and disadvantages.

Fuel cell technology is a prominent form of renewable energy technology as it allows not only the production of electrical energy but also the production and storage of energy in the form of hydrogen if connected to an electrolyser and a tank. Moreover, the production of electrical energy is silent, free of pollution and two to three times more efficient than combustion. If the hydrogen used was obtained from non-polluting sources, the fuel cell system can be a true zero-emission system [1].

This paper is a review of types of fuel cells, their applications and their economy. Different types of fuel cells are presented and their efficiency and operating temperature compared, the progress of the different types and applications are presented as well as the market, the economy and projections for the future.

Keywords: Fuel cell, power, efficiency, application, market, economy

4.1 Introduction

A fuel cell transforms the chemical energy of a fuel into electrical energy through a chemical reaction of positive hydrogen anions with oxygen cations or another oxidant agent [2].

A typical fuel cell produces 0.6 V to 0.7 V at full rated load. To obtain the quantity of energy needed, fuel cells can be connected in series to produce high voltage or in parallel to obtain high current; this type of connexion is called a fuel cell stack. To obtain high current from fuel cells, the surface area of fuel cells can be increased to allow high current to come from each cell. Within the stack, the reactant gases must be uniformly distributed to fuel cells to maximize the energy produced [3] [4] [5].

First references to fuel cells were mentioned in 1838 by Welsh physician and barrister William Grove, and appearing in London and Edinburg Philosophical Magazine and Journal of Science. He combined sheet iron, copper and porcelain plates with a solution of copper sulphate and diluted acid [6] [7]. Since then, different types of fuel cells were manufactured for different applications.

4.2 Types of fuel cells

Fuel cells are manufactured based on different designs; however, they operate in the same manner. They are composed of three following connected segments: the anode, the electrolyte and the cathode.

At the anode, a catalyser oxidises the fuel, often hydrogen, by transforming the fuel into a positive ion and a negative electron. The free electrons flow through electric conductors producing electricity. The ions pass across the electrolyte membrane and get to the cathode electrode where they recombine with electrons and the two react with the third chemical substance, often oxygen, to produce water and carbon dioxide. The leading fuel cell types are presented below.

4.2.1 Proton exchange membrane fuel cells

The proton exchange membrane fuel cell (PEMFC) uses a solid polymer membrane as the electrolyte. The operating temperature is generally in the range of 60 °C to 100 °C [8]. In the design architecture of hydrogen-oxide PEMFC, a proton conducting polymer membrane, generally nafion, contains an electrolyte solution separating the anode side from the cathode side [9] [10]. At the anode side, hydrogen is dissociated by the anode catalyser into protons and electrons. Protons move from the anode through the electrolyte membrane to the cathode, while electrons flow in an external circuit as the electrolyte is electrically insulated and reach the cathode. At the cathode catalyser, oxygen molecules react with protons and electrons to produce water. The membrane electrode assembly (MEA) is considered to be the heart of PEMFC and it is often made of two catalyst-coated carbon papers with a proton exchange membrane placed between them in sandwich form.

4.2.2 Phosphoric acid fuel cell

The phosphoric acid fuel cell (PAFC) uses a concentrated phosphoric acid (H_3PO_4) as the electrolyte to allow positive hydrogen ions to move from the anode to the cathode. Electrons are forced to flow from anode to cathode through an external electric circuit. This type of fuel cell operates in a temperature range of 160 °C to 250 °C [14]. The high operating temperature

introduces a loss of energy that if collected and used properly in systems that consume thermal energy could increase the efficiency of the fuel cell [11]. Using this heat in cogeneration can improve the efficiency of PAFC from 40% to 50% to about 80% [11]. Platinum is used as a catalyst in this type of fuel cells to increase the ionization rate as the quantity of hydrogen ions produced at the anode is small. The key disadvantage of those cells is that the components exposed to phosphoric acid are subject to corrosion or oxidation.

4.2.3 Solid oxide fuel cell

The solid oxide fuel cell (SOFC) use a solid non-porous metal oxide such as the dioxide of Zirconium (ZrO_2) treated with Y_2O_3 [8] or yttria-stabilised zirconia (YSZ) as the electrolyte. The YSZ is a ceramic solid material which means that SOFC does not need to be limited to flat plate configurations like other fuel cell types and can be designed as rolled tubes. Oxygen ions O^{2-} are carried from cathode to anode. The entire monoxide of carbon (CO) in the gas produced is oxidized into dioxide of oxygen (CO_2) at the anode [8]. SOFC operates at 800 °C to 1000 °C and can be fed with different types of fuels including natural gas [12]. The cell is fed with oxygen gas by the cathode, where it absorbs electrons to form oxygen ions. The oxygen ions then pass through the YSZ electrolyte to the anode, where they react with hydrogen gas to produce electricity and water. Depending on the fuel used to feed the fuel cell, CO can also be produced at the anode as product of the reaction, but SOFC have less carbon emissions than fossil fuel combustion plans [13]. The SOFC can operate with fuels other than hydrogen, although hydrogen is always necessary for reactions at the anode and the cathode. The fuel chosen to feed a SOFC must have at least hydrogen atoms which can be converted into pure hydrogen gas. The high operating temperature of SOFC is an advantage for this type of fuel cell because precious metals like platinum as a catalyst are not necessary, hence, there is a cost reduction.

4.2.4 Alkaline fuel cell

The alkaline fuel cell (AFC) uses a concentrated solution of KOH or NaOH as electrolyte. Referring to the operating temperature of the AFC, the concentration ratio is about 85% for cells operation at 250 °C and 35% to 50% for operating temperatures less than 120 °C. A highly pure hydrogen is required for this type of fuel cells due to the sensitivity of the electrolyte to CO_2 and CO that react with the KOH to form K_2CO_3 , thus altering the electrode [14]. The cell runs continuously until reactants are completely finished in the feeder or supply tank. Better efficiency of this type of fuel cell is obtained when operating at temperature range of 70 °C to 140 °C and supplies a potential of about 0.9 V [15].

4.2.5 Molten carbonate fuel cell

The molten carbonate fuel cell (MCFC) uses lithium carbonate salt as the electrolyte; this salt is melted at high temperatures allowing negatively charge carbonate ions (CO_3^{2-}) to move from cathode to anode in the cells [16]. Similar to SOFC, the cells require a high operating temperature of about 650 °C [8] in order to change fossil fuels into a rich hydrogen gas at the anode. Hydrogen from the gas reacts with carbon ions from the electrolytes to produce water, carbon dioxide, electrons and a small quantity of other chemical components. The electrons flow into the external circuit producing electricity and return to the cathode. They react with air oxygen and recycled carbon dioxide from the anode to form carbonate ions that replenish the electrolytes, completing the circuit [16].

Like SOFCs, one of the advantages of MCFCs is their slow-up time due to their operating temperature which is high. This makes these systems more interesting for stationary applications and less suitable for mobile applications. The high temperature and carbonate electrolyte contribute to anode and cathode corrosion. MCFC fuel cells have more advantages compared to other fuel cell technologies. They are not subject to carbon cooking (referring to carbon build up at anode resulting in the decrease of their performance by slowing down internal reformation process of the fuel).

4.2.6 Direct methanol fuel cell

The direct methanol fuel cell (DMFC) uses a polymer membrane (ionomer) as the electrolyte. The operating temperature for this type of fuel cell is in the range of 20 °C to 90 °C. With low output power these cells can be used supply portable electronics equipment in this particular growing area [17].

4.2.7 Summary of fuel cell types

Fuel cells can be classified based on the type of electrolyte and/or type of fuel used as enumerated at Section 3. Table 4.1 gives a list of some of those fuel cells, the type of electrode used, the range of energy produced, their operating temperature, the cell efficiency as well as system efficiency.

Table 4-1: Summary of fuel cell types

Type	Electrode	Mobile ion	Operating temperature	Efficiencies		Applications
				Cell	System	
Proton Exchange Membrane (PEMFC)	Solid polymer membrane	H^+	40 °C - 80 °C	50% - 70%	30% - 50%	- Vehicles and mobile applications - Lower power CHP systems
Phosphoric Acid Fuel Cell (PAFC)	Liquid phosphoric acid	H^+	160 °C - 250 °C	40% *Co-G: 90 %	55%	Large number of 200 kW CHP systems in use
Solid Oxide Fuel Cell (SOFC)	Solid non-porous metal oxide	O^{2-}	600 C - 1000 C	60 % - 65 %	55 % - 60 %	CHP systems, 2 kW to multi - MW
Alkaline Fuel Cell (AFC)	Aqueous alkaline solution	OH^-	65 C - 220 C	60 % - 70 %	62 %	Space vehicles
Molten Carbonate Fuel Cell (MCFC)	Molten carbonate	CO_3^{2-}	600 C - 650 C	55 %	45 % - 50 %	Medium to large scale CHP systems, up to MW capacity
Direct Methanol Fuel Cell (DMFC)	Liquid methanol	H^+	20 C - 90 C	20 % - 30 %	10 % - 25 %	Portable electronic systems of low power, running for long times

Fuel cells can be classified based on the type of electrolyte and/or type of fuel used as enumerated in Section 3. Table 4.1 gives a list of some of those fuel cells, the type of electrode used, the range of energy produced, their operating temperature, the cell efficiency as well as system efficiency.

4.3 Evolution of fuel cells

The evolution of fuel cells by cell type based on shipment and power are represented in Figure 4.1 and Figure 4.2 respectively.

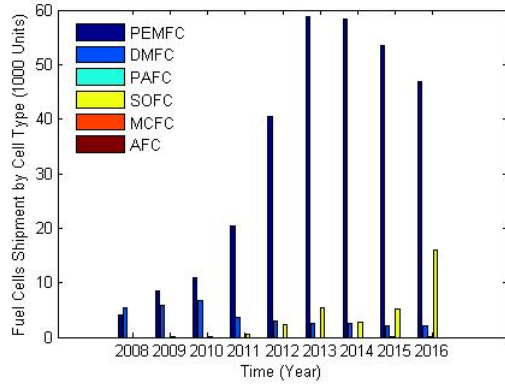


Figure 4.1a: Evolution of fuel cells shipment by cell type using bar representation

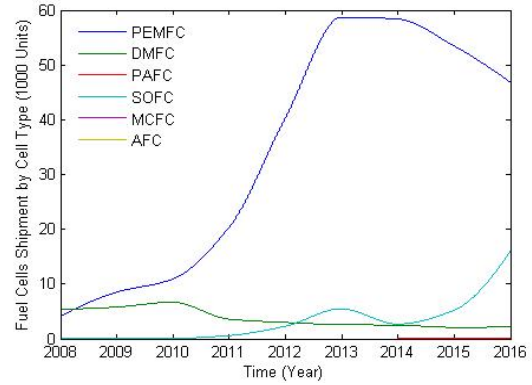


Figure 4.1b: Evolution of fuel cells shipment by cell type using piecewise cubic hermite interpolating polynomial

Figure 4.1: Evolution of fuel cells by cell type

PEMFC dominate the shipment of fuel cell equipment with 46 900 units and a power production of 311.2 MW in 2016, followed by SOFC and DMFC, with DMFC having a decrease in shipment and SOFC having an increase from 2013 to 2016 as seen in Figure 4.1a and Figure 4.1b. Concerning the energy produced, PEMFC is followed by MCFC with 66.9 MW produced as presented in Figure 4.2a and Figure 4.2b.

4.4 Efficiency of fuel cell

The energetic efficiency of a device or a system is defined as the ratio of the useful quantity of energy produced by the device or system and the total quantity of energy put into the system. In the case of a fuel cell, the useful quantity of energy is the electrical energy produced by the fuel cell while the energy to be converted by the system is the energy contained in the fuel. Referring to the US Department of Energy, the energetic efficiency of fuel cells is generally between 40% and 60% [18].

The maximum theoretical efficiency of a fuel cell is 83%, with the fuel cell operating at low energy density and using pure hydrogen and oxygen as reactants (without heat being re-captured) [19]. As those efficiencies are not close to most of applications in reality, high temperature fuel cells (SOFC and MCFC) can theoretically be combined with a gas turbine to allow stationary fuel cell systems to reach efficiencies close to the theoretical limit. Heat generated by the fuel cells is captured and use to run a gas turbine and obtain mechanical energy. The overall efficiency of the fuel cell is then improved to as much as 80% by summing the electrical energy produced by the fuel cell and the mechanical energy from the gas turbine [20].

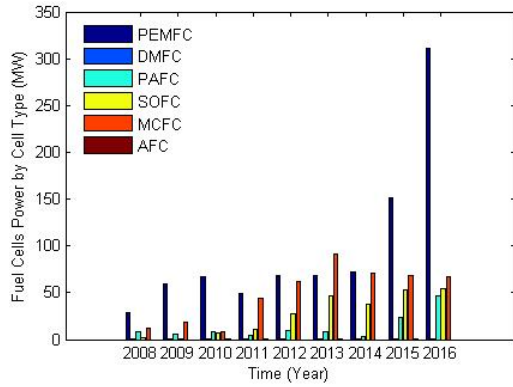


Figure 4.2a: Evolution of fuel cells power by cell type using bar representation

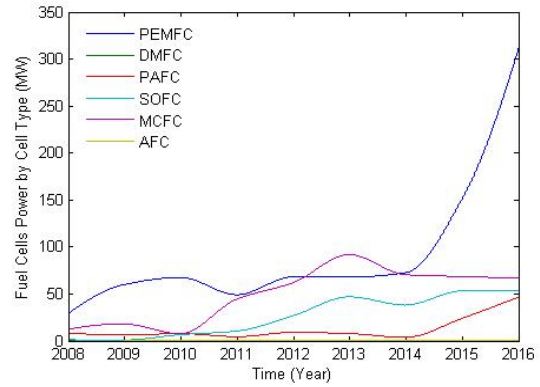


Figure 4.2b: Evolution of fuel cells power by cell type using piecewise cubic hermite interpolating polynomial

Figure 4.2: Evolution of fuel cells power by cell type

In practice, in a fuel cell vehicle, tank-to-wheels efficiency is greater than 45% at low loads [21] with an average of about 36% when the evaluation test is done based on driving cycle requirement like the New European Driving Cycle (NEDC) [22]. In 2008, Honda released the Honda FCX clarity, a fuel cell vehicle that was claimed to operate at 60% tank-to-wheels efficiency [23]. Supply with hydrogen gas stored at high pressure fuel cell vehicles can produce a power-plant-to-wheel efficiency of 22%; and 17% if liquid hydrogen is used [24]. Fuel cells do not store energy like batteries [25]; at least hydrogen can be stored. Fuel cells coupled with photovoltaic arrays and / or wind turbines as hybrid system can be connected to electrolyzers to store electrical energy in the form of pure hydrogen in storage tanks and form storage systems [26]. The global efficiency of such systems can be 35% to 50%, depending on the gas density and other conditions [27]. The SOFC produces heat from recombination of hydrogen and oxygen. Ceramic can reach 800 °C when heated. If this heat is collected and used to heat water in micro-combined heat and power (μ CHP) applications, without taking into consideration losses due to production and distribution, the total efficiency of this type of system approaches 80% to 90% at the unit.

4.5 Applications

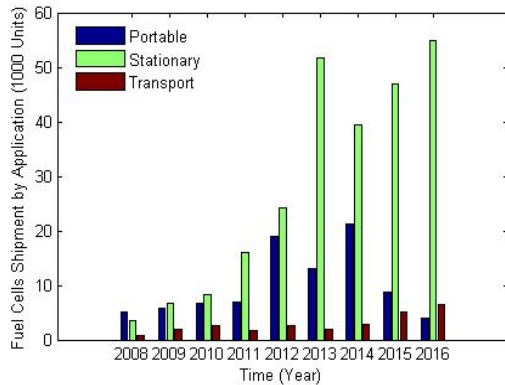


Figure 4.3a: Evolution of fuel cells shipment by application using bar representation

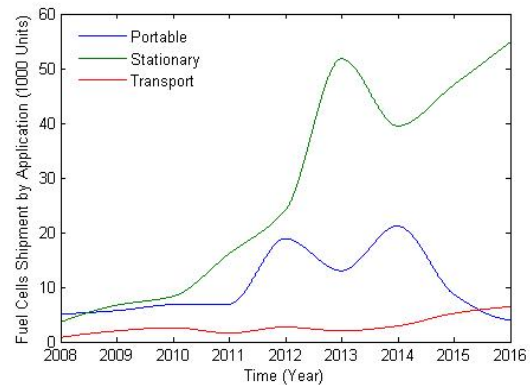


Figure 4.3b: Evolution of fuel cells shipment by application using piecewise cubic hermite interpolating polynomial

Figure 4.3: Evolution of fuel cells by application

Three categories have characterized the fuel cell technology market: stationary power, transport power and portable power [1]. Fuel cell application is led by stationary applications with a shipment of 548 000 units. In terms of power produced, transport applications lead with 277.5 MW of power produced. Stationary applications is followed by transport applications for shipment while it follows transport applications for power produced, as presented in Figure 4.3 and Figure 4.4. This explains why PEMFC is dominating or leading the fuel cell market. Portable applications reached a maximum shipment of 21 200 units in 2014 than started falling.

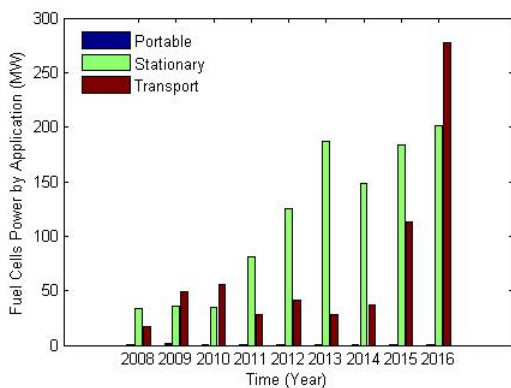


Figure 4.4a: Evolution of fuel cells power by application using bar representation

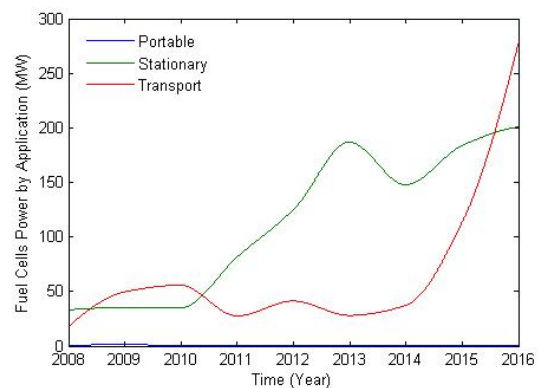


Figure 4.4b: Evolution of fuel cells power by application using piecewise cubic hermite interpolating polynomial

Figure 4.4: Evolution of fuel cells power by application

4.5.1 Power

Stationary fuel cells are used as primary and backup energy sources for commercial, industrial and residential sectors. Fuel cells are mostly useful as energy sources in remote areas such as in spacecraft, remote weather stations, large parks, communication centres, rural areas as well as in recharge stations and in certain military applications. For energy storage on a large scale,

electrolyser fuel cell systems can be used as external storage units with an efficiency of about 40% to 60% [12].

4.5.2 Cogeneration

Combined heat and power (CHP) fuel cell systems are used to produce electric energy and heat simultaneously for homes, building, offices and factories. The system produces constant electrical energy (selling extra energy to the grid if not used) while at the same time producing hot water or air by using heat rejected by the system to heat water or air. These systems save heat energy rejected by thermal systems [28]. The typical capacity of residential fuel cells is in the range of 1 kW_{el} to 3 kW_{el} / 4 kW_{el} to 8 kW_h [29]. CHP systems connected to absorption chillers use heat waste for refrigeration. Co-generation systems can reach an efficiency of 85% (40% to 60% electrical plus the remains as thermal) [12].

4.5.3 Fuel cell electric vehicles (FCEVs)

4.5.3.1 Automobiles

Until 2015, only two fuel cell vehicles were produced and sold in the Fuel Cells Electric Vehicles (FCEV) market in limited quantities: the Toyota Mirai and the Hyundai ix 35 FCEV. Others vehicles like the Honda FCV Clarity and Mercedes-Benz F-Cell have been demonstrated and could be introduced in the market by 2016.

The US Department of Energy's Fuel Cell Technology Program claimed that by 2011, vehicle fuel cell efficiency reached 53% to 59% at quarter power and 42% to 53% at total power, and durability above 120 000 km with a degradation of less than 10% [30]. After analyzing the simulation results of well-to-wheels testing realized by General Motors and their partners, they concluded that a fuel cell electric vehicle supplied with compressed hydrogen gas obtained from natural gas could use about 40% less energy and emit 45% less greenhouse gases than an internal combustion engine vehicle [31]. Some specialists think that fuel cell electric vehicles will never become economically competitive with others technologies or it will take time for sales to become benefit [32].

4.5.3.2 Buses

Fuel cell buses are operating around the world particularly at Whistler in Canada, San Francisco in United States, Hamburg in Germany, Shanghai in China, London in England and Sao Paulo in Brazil. Since August 2011, a about hundred buses operate across the world and this number seem to increase in future to come. Most of them are manufactured by Proton Motors, UTC Power, Ballard, Toyota and Hydrogenics. Fuel cell buses have a fuel economy of 39% to 41% greater than diesel and natural gas buses [33].

4.5.3.3 Aeroplanes

In 2003, the first propulsion aeroplane in the world entirely fed by fuel cell flew. In 2007, Horizon Unmanned Aerial Vehicles (UAV), whose electrical energy was supplied by fuel cells, accomplished a record flying distance for small UAVs. In 2008, Boeing researchers and their industrial partners in Europe carried experimental flying tests for a manned airplane supplied with electrical energy by fuel cells and lightweight batteries only. This plane used PEMFC and lithium-ion battery hybrid systems to supply an electric motor coupled to a conventional propeller [34]. In 2009, the Naval Research Laboratory's (NRL's) Ion Tiger used hydrogen

fuel cells to fly about 23 hours and 17 minutes. The military is interested in using fuel cells because of low thermal signature, low noise, and the ability to reach high altitudes. Fuel cells are also used as auxiliary energy sources on board aeroplanes in place of fossil fuel generators that were previously used to start reactors and supply electrical energy on board in case of need [35].

4.5.3.4 Forklifts

A fuel cell forklift or fuel cell lift truck is an industrial forklift powered by fuel cells and used for transport of materials. They are used by many companies, examples being SYSCO Foods, FedEx Freight, GENCO, HEB Grocers [36].

Most companies in Europe and United States don't use diesel integrated combustion motor forklifts because those vehicles are working inside buildings so their gas emissions must be controlled. Instead many of those companies use electric forklifts. Forklifts powered by fuel cells can be beneficial compared to ones using batteries because they can operate for one shift of 8 hours with only one hydrogen tank and can be refuelled in 3 minutes.

4.5.3.5 Boats

The world's first boat powered by fuel cells is HYDRA. The boat uses an AFC system with a net produced energy of 6.5 kW. Some European countries like Iceland are determined to convert their vast fishing fleets to fuel cell energy. Recently, Amsterdam has introduced its first tourist ferry boats powered by fuel cells [37].

4.5.3.6 Submarines

The use of fuel cells in submarines makes submarines silent gaining them the advantage of being undetectable by other submarines [38]. The German naval shipyard Howarldtswerke Deutsche Werft has developed a non-nuclear submarine U212A used by German and Italian navies. The system is constituted of nine PEMFC's producing energy in the range of 50 kW to 80 kW each allowing the 212 submarines to remain underwater for weeks without coming to the surface.

4.5.3.7 Other applications

Fuel cells are used in many other applications like portable power systems, emergency power systems, telecommunication, uninterrupted power supply (UPS), hybrid power systems, etc.

4.6 Markets and economics

The fuel cell industry is still in the process of formation. The industry remains predominantly focused on PEMFC and SOFC technologies, but others types remain strong, particularly MCFC in large power plant stations [39].

Figure 4.5a and Figure 4.5b show the net progress and dominance of stationary fuel cell applications (from 38% to 84%) over portable applications (from 54% to 6%) with an approximately constant proportion of transportation (from 8% to 10%) by comparing values obtained in 2008 to those obtained in 2016.

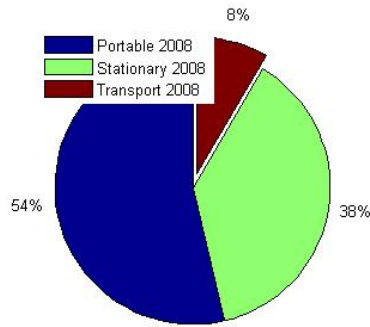


Figure 4.5a: Production ratio of fuel cells by application in 2008

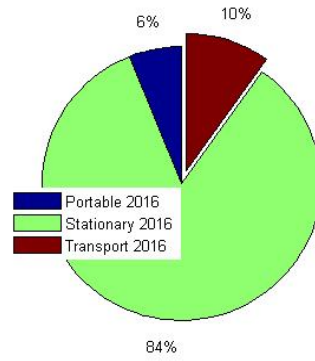


Figure 4.5b: Production ratio of fuel cells by application in 2016

Figure 4.5: Production ratio of fuel cells by application

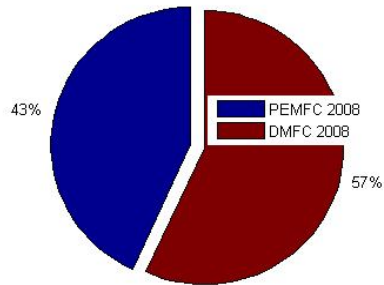


Figure 4.6a: Production ratio of fuel cells by cell type in 2008

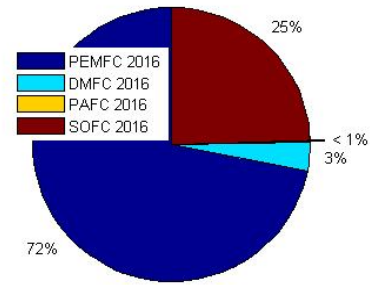


Figure 4.6b: Production ratio of fuel cells by cell type in 2016

Figure 4.6: Production ratio of fuel cells by cell type

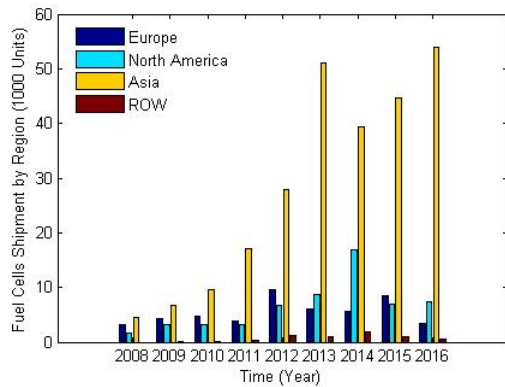


Figure 4.7: Evolution of fuel cells shipment by region using bar representation

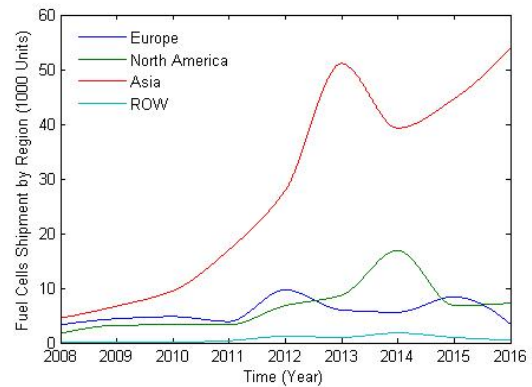


Figure 4.7: Evolution of fuel cells shipment by region using piecewise cubic hermite interpolating polynomial

Figure 4.7: Evolution of fuel cells by region

Figure 4.6a shows the dominance in 2008 of DMFC production of 57% compared to 43% for PEMFC. Figure 4.6b shows that in 2016 PEMFC dominated production with 72% followed by SOFC with 25%. The decrease of DMFC production is noticeable, from 57% in 2008 to 3% in 2016. The introduction of PAFC can also be noticed with less than 1% of production ratio in 2016.

The highest shipment and energy produced values of 53 900 units and 245.9 MW respectively are attributed to the Asia region, followed by North America with 7 300 units shipped and 209.1 MW power produced as seen in Figure 4.7 and Figure 4.8.

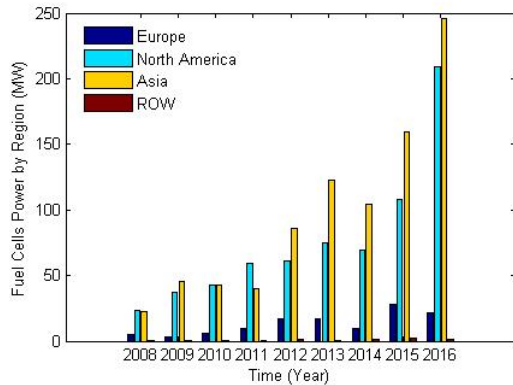


Figure 4.8a: Evolution of fuel cells power by region using bar representation

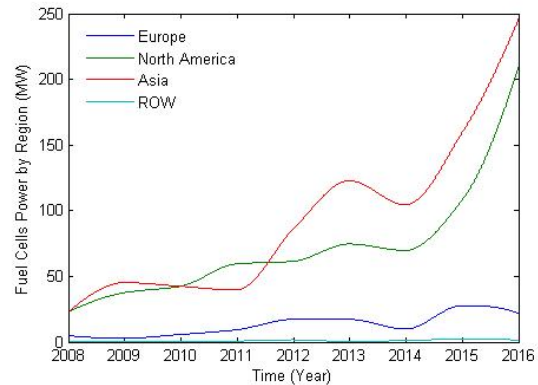


Figure 4.8b: Evolution of fuel cells power by region using piecewise cubic hermite interpolating polynomial

Figure 4.8: Evolution of fuel cells power by region

In 2012, fuel cell incomes surpassed \$1 billion of the worldwide market value, with Asia Pacific countries exporting more than three quarters of worldwide fuel cell systems. Despite this volume, in January 2014 no company in the fuel cell industry had yet made a profit [40]. Fuel cell exportation was 140 000 fuel cell stacks in 2010, higher than the 11 000 fuel cell stacks in 2007. From 2011 to 2012, throughout the world fuel cell exports increased at a rate of 85% [41]. In 2010, approximately 50% of fuel cells exported were stationary fuel cells, this figure being one third greater than 2009. The dominant producers in fuel cell industries at that time were the United States, Germany, Japan and North Korea [42]. The US Department of Energy Solid State Energy Conversion Alliance found that around January 2011, the cost of energy produced by fuel cells was about \$724 to \$775 per kilowatt installed [43]. In 2011, Bloom Energy, a major supplier of fuel cells, announced that its fuel cells produced electrical energy at 9 cents to 11 cents per kilowatt hour, fuel cell price, maintenance and hardware included [44]. Industrial groups predicted that there are enough platinum resources to cover the demand for the future and in 2007, researchers at Brookhaven National Laboratory proposed that platinum could be substituted by a gold-palladium coating that could be susceptible to less poisoning and thereby ameliorate the lifetime of the fuel cell [45]. Others materials like iron and sulphur are being developed to replace the platinum and could reduce the fuel cell price. In 2016, Samsung decided to stop projects related to fuel cells as the market outlook was not promising.

4.7 Conclusion

Fuel cell types, applications, power, efficiency as well as technical progress and market size have been covered in this paper. It has been shown that PEMFC is leading the market of fuel cells and is used in all market applications. It is followed by DMFC which is used particularly for portable and transport applications. The stationary application is dominated by SOFC and MCFC particularly for large power plants due to their higher operating temperature allowing the efficiency to be improved when used in large stationary combined heat and power systems.

The fuel cell market is controlled by the Asia and North America regions with the largest shipment and power produced by fuel cells achieved by the Asia region followed by North America.

This technology is a better candidate for hybrid systems when combined with photovoltaic arrays or wind turbines than batteries and super capacitors due to their operating mode.

Fuel cell technology is still expensive compared to other renewable technologies. Nevertheless, the use of gold-palladium instead of platinum could reduce the cost and, with less poisoning, improve the lifetime of fuel cells making this technology more affordable.

References

- [1] B. Vincent, J. Gangi, S. Curtin, and E. Delmont, "2008 fuel cell technologies market report," US Department of Energy, 2010.
- [2] R. S. Khurmi, *Material Science*. New Delhi: S. Chand & Company Ltd, 2004.
- [3] J. Y. Wang, "Pressure drop and flow distribution in parallel-channel of configurations of fuel cell stacks: U-type arrangement," *International Journal of Hydrogen Energy*, vol. 33, no. 21, p. 6339–6350, 2008.
- [4] J. Y. Wang and H. L. Wang, "Discrete approach for flow-field designs of parallel channel configurations in fuel cells," *International Journal of Hydrogen Energy*, vol. 37, no. 14, p. 10881–10897, 2012.
- [5] J. Y. Wang and H. L. Wang, "Flow field designs of bipolar plates in PEM fuel cells: theory and applications," *Fuel Cells*, vol. 12, no. 6, p. 989–1003, 2012.
- [6] W. R. Grove, "On a new voltaic combination," *The London and Edinburgh Philosophical Magazine and Journal of Science*, 1838.
- [7] W. R. Grove, "On voltaic series and the combination of gases by platinum," *Philosophical Magazine and Journal of Science*, vol. XIV, p. 127–130, 1839.
- [8] Energy Efficiency and Renewable Energy, "Fuel cell technologies program: glossary," 07 07 2011. [Online]. Available: energy.gov.
- [9] A-C. Dupuis, "Proton exchange membranes for fuel cells operated at medium temperatures: materials and experimental techniques," *Progress in Materials Science*, vol. 56, no. 3, p. 289–327, 03 2011.
- [10] Seong Kon Lee, Gento Mogi, Zhuolin Li, K. S. Hui, Sang Kon Lee, K. N. Hui, Sang Yong Park, Young Jin Ha, and Jong Wook Kim, "Measuring the relative efficiency of hydrogen energy technologies for implementing the hydrogen economy: an integrated fuzzy AHP/DEA approach," *International Journal of Hydrogen Energy*, vol. 36, pp. 12655 -12663, 2011.
- [11] "Collecting the history of phosphoric acid fuel cells," [Online]. Available: americanhistory.si.edu.
- [12] "Types of fuel cells," [Online]. Available: energy.gov.
- [13] A. Boudghene Stambouli, "Solid oxide fuel cells (SOFCs): a review of an environmentally clean and efficient source of energy," *Renewable and Sustainable Energy Reviews*, vol. 6, no. 5, pp. 433-455, 10 2002.
- [14] EG & G Technical Services Inc., *Fuel cell handbook*, 7th ed., US. Department of Energy, November 2004, p. 10.
- [15] H. C. Nootan Srivastava, *ISC Chemistry*, 12th ed., vol. 18, Meerut, Uttar Pradesh: Nageen Prakashan, 2014, pp. 458-459.

- [16] U.S. Department of Energy, "Molten carbonate fuel cell technology," accessed 9 August 2011. //energy.gov," 09 08 2011. [Online]. Available: energy.gov.
- [17] J. Larminie and A. Dicks, *Fuel cell systems explained*, 2nd ed., Hoboken, New Jersey: John Wiley & Sons Ltd, 2003.
- [18] Energy Efficiency and Fuel Cell Technologies Program, "Comparison of fuel cell technologies," 02 2011. [Online].
- [19] "Fuel cell efficiency," in World Energy Council, the Wayback Machine, 2007.
- [20] J. Milewski, A. Miller, and K. Badyda, "The control strategy for high temperature fuel cell hybrid systems," *The Online Journal on Electronics and Electrical Engineering*, vol. 2, no. 4, p. 331, 2009.
- [21] U. Eberle and R. von Helmolt, "Sustainable transportation based on electric vehicle concepts: a brief overview," *Energy & Environmental Science*, 14 05 2010.
- [22] R. Von Helmolt and U. Eberle, "Fuel cell vehicles: status 2007," *Journal of Power Sources*, vol. 165, no. 2, p. 833, 20 03 2007.
- [23] Honda, "Honda FCX Clarity- fuel cell comparison," 2009. [Online]. Available: automobiles.honda.com. [Accessed 17 02 2009].
- [24] U. Bossel, "Efficiency of Hydrogen PEFC, Diesel-SOFC-Hybrid and Battery Electric Vehicles," in *European Fuel Cell Forum*, Oberrohrdorf (Switzerland), 2003.
- [25] "Batteries, supercapacitors, and fuel cells: scope," 20 08 2007. [Online]. Available: www.loc.gov.
- [26] K. Nice, "How fuel processors work," [Online]. Available: auto.howstuffworks.com. [Accessed 03 08 2011].
- [27] C. P. Garcia, B-J. Chang, D. W. Johnson, D. J. Bents, V. J. Scullin, and I. J. Jakupca, "Round trip energy efficiency of NASA Glenn regenerative fuel cell system," in NHA Annual Hydrogen Conference, Long Beach, California (USA), 2006.
- [28] K. U. Birnbaum, J. Linssen, and P. Leifeld, "Reduction of residential carbon dioxide emissions through the use of small cogeneration fuel cell systems – combined heat and power systems," IEA Greenhouse Gas R&D Programme (IEAGHG), 2008.
- [29] "Reduction of residential carbon dioxide emissions through the use of small cogeneration fuel cell systems – scenario calculations," IEA Greenhouse Gas R&D Programme (IEAGHG), 2008.
- [30] U. S. Department of Energy, "Accomplishments and Progress," 24 06 2011. [Online]. Available: energy.gov.
- [31] N. Brinkman, M. Wang, T. Weber, and T. Darlington, "Well-to-wheels analysis of advanced fuel/vehicle systems – a North American study of energy use, greenhouse gas emissions, and criteria pollutant emissions," General Motors Corporation, 2005.
- [32] B. Warshay, "The Great Compression: the future of the hydrogen economy," Lux Research, Inc, 2013.

- [33] J. Garbak, "FY 2010 annual progress report: VIII.0 Technology Validation Sub-Program Overview," Department of Energy, Fuel cell technology program, 2010.
- [34] "Boeing successfully flies fuel cell-powered airplane," 03 04 2008. [Online]. Available: web.archive.org.
- [35] J. Ford, "Hydrogen-powered unmanned aircraft completes set of tests," 20 06 2011. [Online]. Available: www.theengineer.co.uk.
- [36] "Fact sheet: materials handling and fuel cells," 2014. [Online]. Available: archive.org.
- [37] "Lovers introduces zero-emission boat," 2011. [Online].
- [38] "U212 / U214 Attack Submarines," Germany, 2011. [Online]. Available: Naval-Technology.com.
- [39] D. Hart, F. L., R. Rose, and J. Lewis, "Fuel cell industry review 2014," E4tech, 2014.
- [40] C. Martin, "Plug, fuel cell climb as 'experiments' seen as profitable," 10 03 2014. [Online]. Available: Bloomberg.com. [Accessed 28 12 2015].
- [41] J. Bond, "Fuel cell report highlights continued growth in material handling applications," 2013.
- [42] K-A. Adamson and C. Wheelock, "Fuel cell annual report 2011," Pike Research, 2011.
- [43] "Solid state energy conversion alliance SECA cost reduction," U.S. Department of Energy, 2011.
- [44] E. Wesoff, "Bloom energy plays the subsidy game like a pro," 13 04 2011.
- [45] R. C. Johnson, "Gold is key to ending platinum dissolution in fuel cells," 22 01 2007. [Online]. Available: EETimes.com.
- [46] "Fuel cells and CHP," The Wayback Machine, 2012.
- [47] D. Hart, F. Lehner, R. Rose, and J. Lewis, "Fuel cell industry review 2016," E4tech, 2016.

CHAPTER 5 : ENERGY MANAGEMENT FOR STAND ALONE HYBRID PHOTOVOLTAIC PEM FUEL CELLS SYSTEMS

PUBLICATION 5

Ntumba Marc-Alain Mutombo^a; Freddie L. Inambao^b; Remy Tiako^c; Samuel A. O. Ilupeju^d

^{a,c} University of KwaZulu-Natal, School of Engineering, Discipline of Electrical Engineering, Howard College Campus, Durban, South Africa (marcntumba@yahoo.fr; Tiako@ukzn.ac.za)

^{b,d} University of KwaZulu-Natal, School of Engineering, Discipline of Mechanical Engineering, Howard College Campus, Durban, South Africa (inambaof@ukzn.ac.za; ilupejus@ukzn.ac.za)

Abstract

A better performance of photovoltaic (PV) generator is obtained at high insolation. But at high insolation, the temperature of the PV system increases and leads to a reduction of the performance of the system making the system unable to supply the load. The problem becomes more difficult with irregular solar insolation; the system experiences variation in its output, which is not good for the user. One way of overcoming this problem is to couple the PV generator with a proton exchange membrane fuel cell (PEMFC) system particularly for stand-alone systems for household demand. The simulation results show that with good energy management, the PV-PEMFC hybrid system can supply the load in summer as well winter. This paper presents the energy management for the control of energy flow for a PV-PEMFC system in a particular case of household demand in Durban, South Africa.

Keywords: Photovoltaic, fuel cell, hybrid system, energy management

5.1 Introduction

Diminishing fuel sources and world-wide environmental concerns regarding pollution and global warming have made renewable energy systems more interesting [1] [2]. The increase in demand for electrical energy, greenhouse gas effects and global warming, as well as the high installation costs of grids in remote areas, constitute the motivation behind renewable energy technology [3] [4].

Many sources of renewable energy are available with popular sources being solar energy, hydro-energy, wind energy, fuel cell energy, battery energy, etc. Solar energy is one of the most important due to its availability (almost everywhere) and it can be directly converted from solar energy to electrical energy [5]. The conversion of solar energy to electrical energy is made possible by the use of photovoltaic modules. This device converts the irradiance or solar insolation into electrical energy (more details on the subject can be found in [6]). Under different insolation levels PV output can experience large variances [1][6] which are not good for the user. To remedy to this problem, PV systems can be integrated with two or more sources of energy with or without storage systems [1] [8] [9] to produce a hybrid system [10] [11] [12]. In the design of a hybrid power system, the main goal is to produce as much energy as possible to supply the load by combining different renewable energy sources[13].

The fuel cell is the best candidate to be integrated with a PV system. This technology presents the advantages of being a green power source with higher efficiency than conventional power plants, has very low noise, and has a flexible modular structure [3] [2] [4]. There are different types of fuel cells used in different applications, mainly portable, stationary and transport applications. The most common type of fuel cell for small and medium stationary application is the proton exchange membrane fuel cell (PEMFC). It can be coupled with a PV array to supply electrical energy for household demand and can operate as an independent power source or as a storage system. The PEMFC as a fuel cell technology has the disadvantage of poor dynamic response to transient power demand [14] so a battery bank or super capacitors have to be incorporated to the hybrid PV-PEMFC system.

The main focus of this paper is on the energy management of the system for domestic use.

5.2 System description and size

The system studied is a hybrid photovoltaic-battery fuel cells system equipped with an electrolyser and a hydrogen storage tank.

The study is based on a hybrid PV-PEMFC system made up of a photovoltaic array of 24 Q-PEAK 250 monocrystalline solar modules with a fixed orientation collector for a DC STC rated power of 6 000 W able to provide about 8 500 kWh/year, more than the average of 8 300 kWh/year needed for Durban modest household electrical demand. The parameters for the PV array generator are given in Table 5.1. Details about the design and size of the PV generator can be found in [77].

Table 5-1: PV array parameters

Parameters	Values
Module Type	Q-PEAQK 250 Monocrystalline Silicon
Array Size	42.60 m ²
Number of Strings	24
Number of Modules per String	8
Maximum Voltage at MPP (V_{PM})	180.06V
Open Circuit Voltage (V_{OC})	222.90V
Maximum Current at MPP (I_{PM})	33.64A
Short Circuit Current (I_{SC})	A

To overcome the variance of the PV array generator output under different insolation levels, a 2000 Horizon PEMFC with characteristics in Table 5.2 is coupled to the PV array generator.

Table 5-2: Fuel cell parameters

Parameters	Values
Type of fuel cell	Horizon PEM FC
Number of cells	48
Rated power	2000 W
Performance	28.8 V @ 70 A
Max stack temperature	65 °C
H ₂ Pressure	0.45 – 0.55 bar
Hydrogen purity	≥ 99.995 % dry H ₂
Flow rate at max output	36 L/min
Startup time	≤ 30 s at ambient temperature
Efficiency of stack	40 % @ 28.8 V

This fuel cell is used with an electrolyser to produce hydrogen from water using electrical energy from the PV array generator.

The lithium-ion battery bank composed of 4 batteries connected in series is added to the system to compensate for the poor dynamic response of fuel cells to transient power demand. This type of battery has a high energy density, a long cycle life and a relatively low self-discharge rate. Table 5.3 gives more details on the battery.

Table 5-3: Battery parameters

Parameters	Values	
	12 V / 120 Ah	96 V / 120Ah
Capacity	120 Ah	120 Ah
Output voltage	9 – 13.5 V	72 – 108 V
Continuous current (0.5C)	45 A	45 A
Energy	5.4 kWh	10.5 kWh
Life cycle (0.3C, 80% DOD)	1500	1500
Maximum discharging current (2C in 10s)	90 A	90 A

All the sub-systems and the load are connected to the busbar through different power electronic interfaces together constituting the power conditioning for the hybrid system as shown in Figure 5.1.

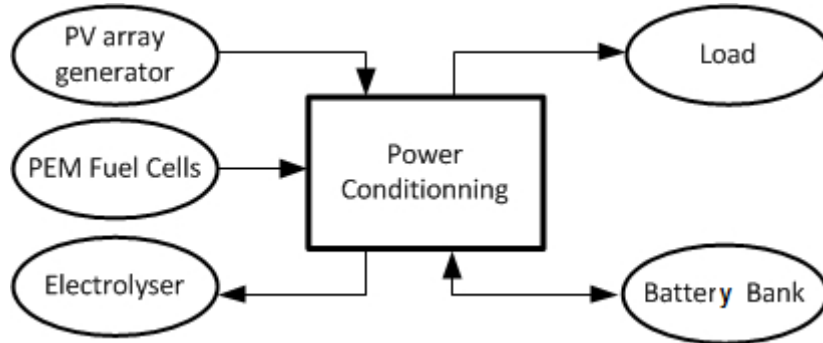


Figure 5.1: Hybrid PV-PEMFC electrolyser system equipped with a battery bank

5.3 System configuration

There are several ways to combine different alternative energies sources to form a hybrid system. Different configurations are competing for an optimal design of hybrid photovoltaic-battery fuel cells systems.

Two types of configurations, the direct current (DC) coupled system and the alternating current (AC) coupled system are used based on reference busbar [2] [15], each with its advantages and disadvantages [14]. In this paper the DC coupled system is used as both supplied sources are DC. To increase the flexibility of the system, an inverter is inserted between the busbar and the load. The topology studied is given in Figure 5.2.

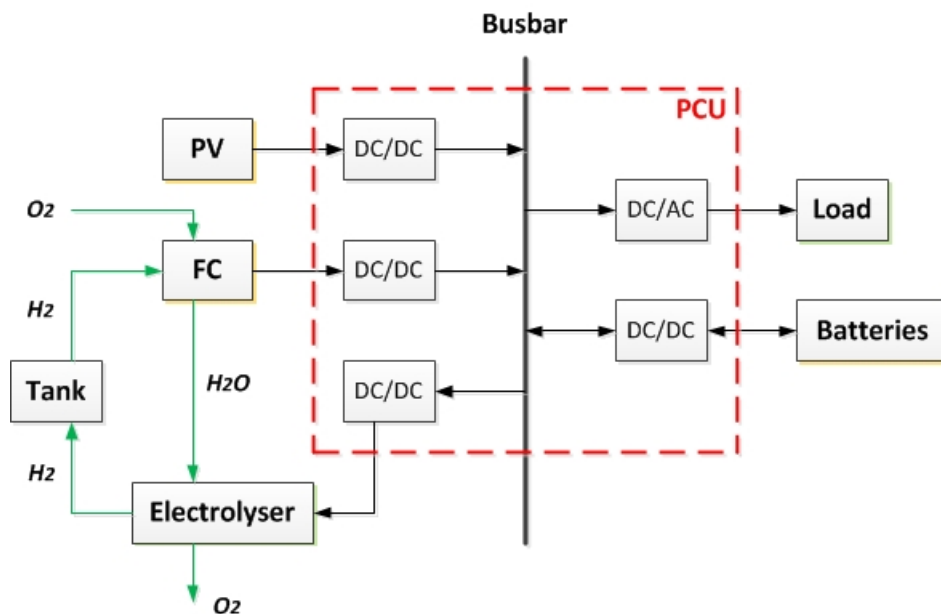


Figure 5.2: Hybrid PV-PEMFC topology

To obtain a correct coupling of different sources to the busbar, they must have equal voltage. This is realised by using electronic interface systems.

5.4 System modelling

5.4.1 Photovoltaic model

The PV model is based on the calculation of the output current as a function of the voltage. To simulate this generator coupled to PEM fuel cells stack and battery bank, the one diode-one resistance model is used. This model presents the advantage of a low number of parameters to be determined and low simulation time compared to the one diode-two resistances and two diodes-two resistances models. The two resistances models are more accurate compare to the one resistance model, but the difference between results are insignificant. More details on different models are given in [17] [80]. For simplicity and due to the short running time, the one diode one resistance model is used and mathematic the model is given in the Equation (1):

$$I = I_{sc} - I_o \left(e^{q \left(\frac{V + IR_s}{AkT} \right)} - 1 \right) \quad (1)$$

where I is cell current (A); I_{sc} is short circuit current which is equal to photocurrent (A); I_o is dark saturation current (A); q is electronic charge (1.602×10^{-19} C); k is the constant of Boltzmann (1.381×10^{-23} J/K); A is idealizing factor; T is cell temperature (K); V is cell voltage (V) and R_s is shunt resistance (Ω).

The equation for R_s is deduced by differentiating the Equation (1) and then rearranging it in terms of R_s :

$$R_s = -\frac{dV}{dI} - \frac{AkT/q}{I_o e^{q \left(\frac{V + IR_s}{AkT} \right)}} \quad (2)$$

At the open circuit, the voltage $V = V_{oc}$ and the current $I = 0$ so that Equation (2) gives the value of R_s as:

$$R_s = -\left. \frac{dV}{dI} \right|_{V_{oc}} - \frac{AkT/q}{I_o e^{\frac{qV_{oc}}{AkT}}} \quad (3)$$

where $-\left. \frac{dV}{dI} \right|_{V_{oc}}$ is slope of the I-V curve at the V_{oc} obtained from the I-V curve in the solar cell datasheet; V_{oc} is the open-circuit voltage of cell, found in the solar cell datasheet.

5.4.2 Fuel cell model

The FC model is built by establishing the relationship between the output voltage and the current. The most popular model for PEM fuel cell is the algebraic sum of Nernst voltage, the activation voltage, the ohm's voltage drop and the concentration voltage [19][20]. Its mathematic model is given in Equation (4):

$$V_{fc} = E_{oc} - NA \ln \left(\frac{i_{fc}}{i_o} \right) - i_{fc} r_{fcin} \quad (4)$$

Where E_{oc} is the open circuit voltage (V); N is the number of cells; A is the Tafel slope; i_{fc} is fuel cell output current (A); i_o is fuel cell exchange current (A) and r_{fcin} is internal resistance (Ω).

The ideal open circuit voltage for a fuel cell is obtained by the Nernst relation given in Equation (5):

$$E_{oc} = K_c E_n \quad (5)$$

where K_c is voltage constant (-) and E_n is Nernst voltage (V).

The PEM fuel cell operates at a temperature between 40 °C and 80 °C, and for fuel cells operating at temperatures below 100 °C, the Nernst equation is given by Equation (6) [32]:

$$E_n = 1.229 + (T - 298) \frac{-44.43}{2F} + \frac{RT}{2F} \ln(p_{H_2} p_{O_2}^{1/2}) \quad (6)$$

where T is temperature of operation (K); R is gas constant (8.3145 J/molK); F is Faraday constant (96485 As/mol); p_{H_2} is partial pressure of H_2 (atm) and p_{O_2} is partial pressure of O_2 (atm). More details about fuel cell model can be found in [21][22][20].

5.4.3 Battery model

The battery model depends on the operating mode of the battery in the system. Two models are defined based on the discharge mode and the charge mode of the battery and are given in Equations (7) and (8):

Discharge mode ($i^* > 0$) model:

$$V_b = E_o - K \frac{Q}{Q - it} i^* - K \frac{Q}{Q - it} it + A \exp(-Bit) - r_b i_b \quad (7)$$

Charge mode ($i^* < 0$) model:

$$V_b = E_o - K \frac{Q}{0.1Q - it} i^* - K \frac{Q}{Q - it} it + A \exp(-Bit) - r_b i_b \quad (8)$$

where E_o is constant voltage (V); K is polarization constant (V/Ah); i^* is low frequency current dynamics (A); i_b is battery current (A); Q is maximum battery capacity (Ah); A is exponential voltage (V) and B is exponential capacity (Ah).

In hybrid PV-PEMFC equipped with battery bank, the state of charge (SOC) of the batteries is the parameter used as a gauge of the electrical energy stored in the batteries. The SOC of the battery is given by Equation (9) [25]:

$$SOC(t) = \frac{\int_{t_o}^t I_b(\tau) d\tau}{Q_o} * 100 \quad (9)$$

where $I_b(t)$ is the charging current, t_o is the initial charging time, t is the final charging time, Q_o is the total charge the battery can hold.

In practice, the SOC of the batteries is kept in certain limits to improve the life span of the batteries.

5.4.4 Electrolyser model

Different V-I models for the electrolyser model have been developed [9]. The basic form of V-I curve for a known operating temperature is given by Equation (10):

$$V = V_{rev} + \frac{I}{A}r + s \log\left(\frac{I}{A}t + 1\right) \quad (10)$$

where V is operating cell voltage (V); V_{rev} is reversible cell voltage (V); r is ohmic resistance of electrolyte (Ω); s and t are coefficients for over-voltage on electrodes (Ωm^2); A is area of electrode (m^2) and I is current through cell (A).

The electrolyser operates at the inverse of the fuel cell stack; the quantity of hydrogen produced is set by the current consumed by the electrolyser. This current is obtained by the power allocated to the electrolyser by the energy management system.

5.4.5 Power conditioning

The power conditioning unit (PCU) is constituted by the electronic interfaces [14] connecting different components to the busbar [9]. The PV generator, the FC and the electrolyser are connected to the busbar via one direction DC/DC converters, while the battery bank is connected to the busbar via a bi-directional DC/DC converter. The DC/AC inverter is used to connect the load to the busbar and increase the flexibility of the system. This is related to the configuration or topology adopted and represent in Figure 5.3.

5.5 Energy management

Generally, in photovoltaic hybrid systems, the PV subsystem operates as a main source. It converts solar irradiance into electricity supplied to a DC bus. When the PV system cannot provide the full charge, especially when the load exceeds the power produced by the PV generator, the PEM fuel cell then supplies the electrical energy to overcome the load demand by sharing the load with the PV generator. In case of worst scenario, during the night for example, the load is then supplied with the energy produced exclusively by the fuel cell

subsystem which produces electrical energy using hydrogen to supply the DC bus. As the fuel cell subsystem needs more time to supply the power needed and the output should only be increased slowly after start up, batteries are used to assist the fuel cell subsystem. The batteries are also used to back up the fuel cell subsystem at peak load or transient load.

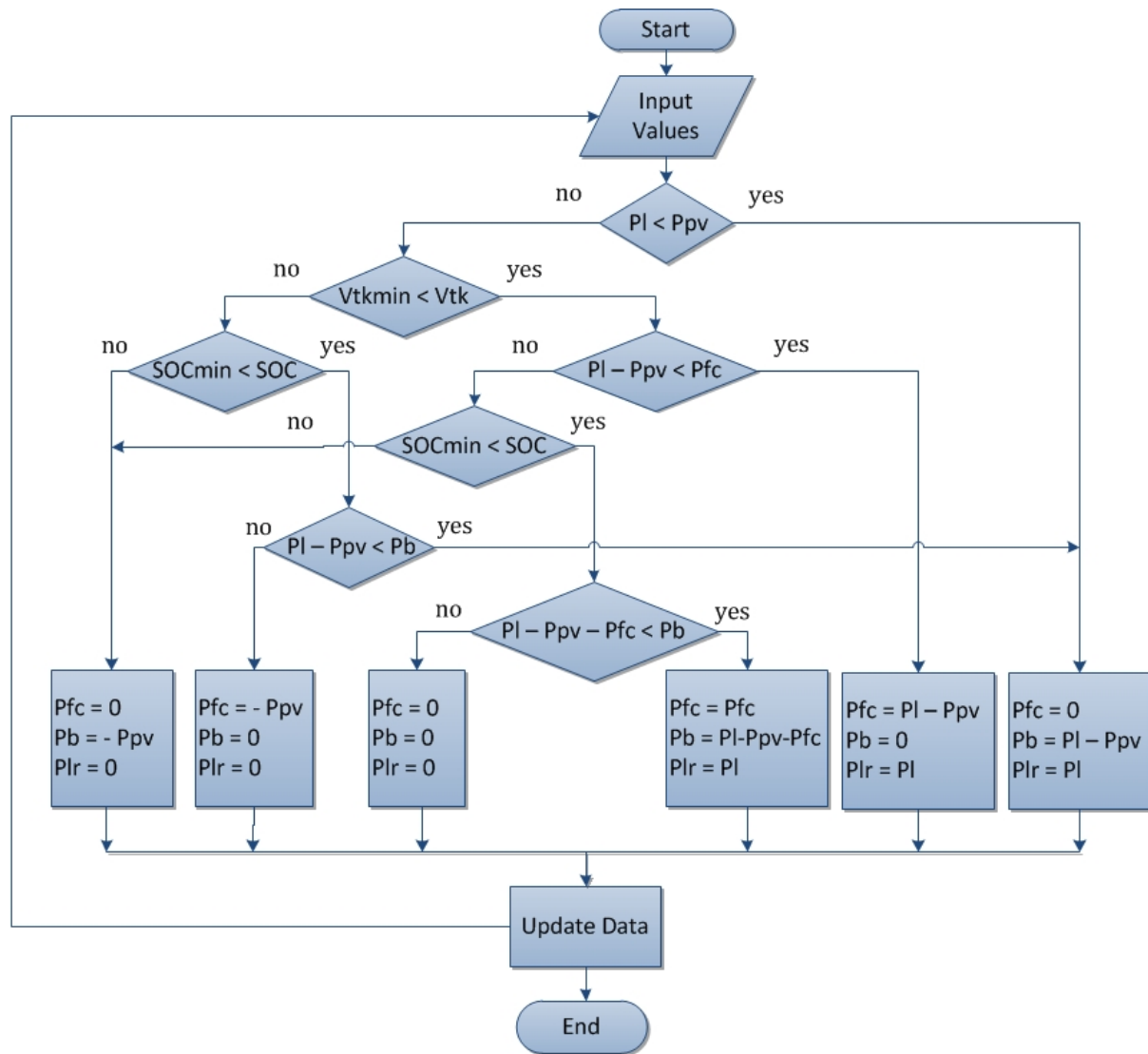


Figure 5.3: Flowsheet diagram of the PV-PEMFC hybrid system energy management

Over a short period of time, if the PV-FC cannot cover the full load, or neither the PV nor the FC subsystems can deliver energy to the load, the battery bank automatically starts feeding the load with energy stored and disconnects if the SOC reaches the minimum. In the case of high insolation with a low load connected to the system, the PV generator supplies electrical energy to the load. The extra energy produced by this subsystem is used to charge batteries until the maximum SOC of batteries is reached then to produce hydrogen from water by the electrolyser. The hydrogen produced is stored in a tank and can be used by the fuel cell to produce electricity in case of need.

5.6 Simulations and analysis of results

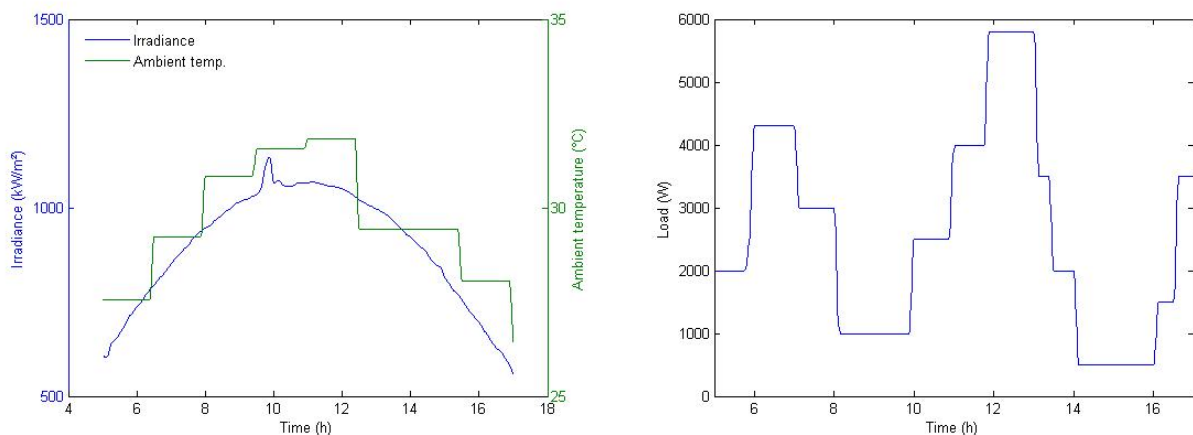
The simulation of the system is done using the Matlab package. Four different days are used, two winter days and two summer days. The same load is used for simulation for four particular days, two summer days and two winter days. For each season, one day corresponds to regular insolation and the other to irregular insolation. Results for the simulation are given in Figure 5.4 to Figure 5.7.

The PV generator supplied the load during interruptions in summer regular insolation day. The power supplied to the load is higher compared to winter days as seen in Figure 5.4A, with a mean power supplied relative error of 38.4% and rms value of 32.0%. While in summer irregular insolation, the load is supplied by intermittence with a power supplied main relative error of 45.7% and rms value of 32.0% as seen in Figure 5.5A.

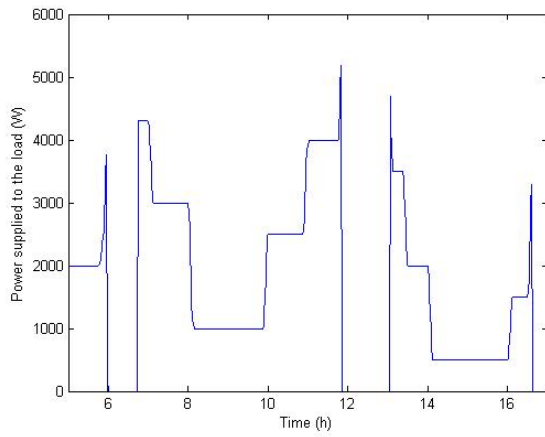
In winter irregular insolation day, the load is supplied during interruption by the PV generator, due to variations of insolation reaching very low values that can't provide enough power as seen in Figure 5.6A. The power supplied mean value is 89.5% and the rms value is 81.5%. The PV generator supplies during interruptions in the winter regular insolation day. The power supplied error mean value is 77.7% and the rms value of 67.8% as seen in Figure 5.7A.

Compared to the PV generator, the PV-PEMFC hybrid system supplies the load almost continuously in summer regular insolation day with interruption between 11:45 and 12:30 due to the load peak before the storage system could produce sufficient energy to compensate the PV generator as seen in Figures 5.4B. The power relative error mean value is 16.6% and the rms value is 12.2%. In the summer irregular insolation day the PV-PEMFC supplies the load during intermittence with high output energy. The power supplied relative error mean value is 14.3% and the rms value is 7.6%. Those values are low compared to the summer regular insolation day because of high insolation reaching sometimes $1\ 300\text{W/m}^2$ as seen in Figure 5.5B.

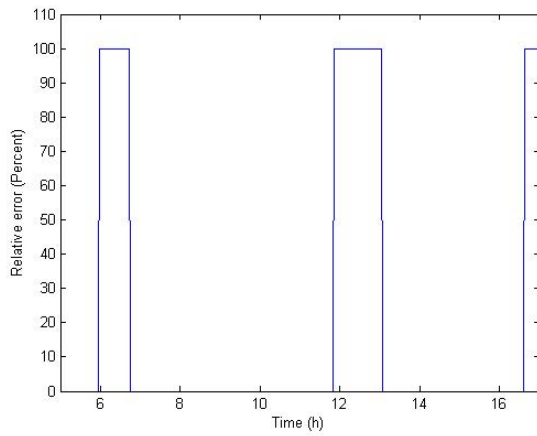
The performance of the PV-PEMFC hybrid system in the winter irregular insolation day is shown in Figure 5.6B. The load is supplied by intermittence with good performance obtained before 11:00. The power supplied relative error mean error is 45.3% and the rms value is 34.9%. The winter regular insolation day is characterised by a better performance of the system providing almost the total energy needed by the load as seen in Figure 5.7B. This is justified by the regularity of the insolation, the low operating temperature and the impact of storage systems. The power supplied relative error mean value is 13.6% and the rms value is 6.2%.



A1) Environmental data

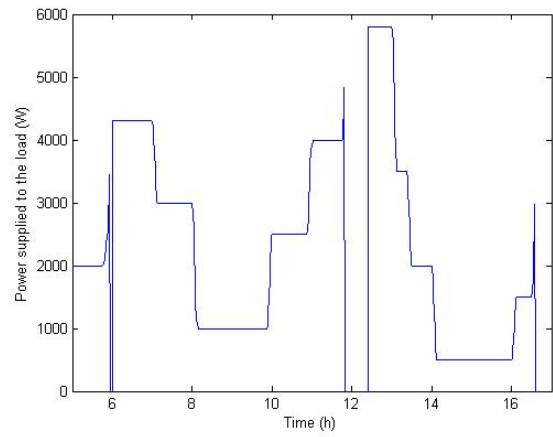


A2) Stand-alone PV generator power supplied to the load

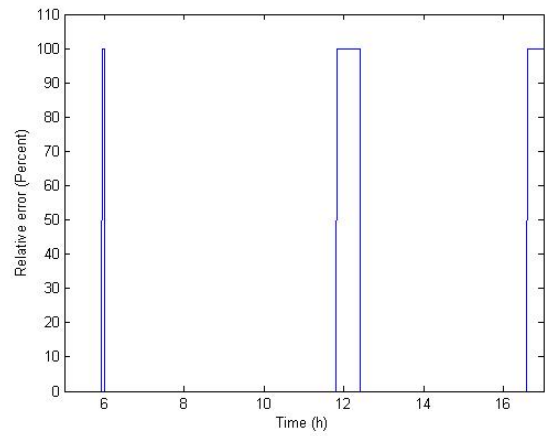


A3) Stand-alone PV generator power relative error

B1) Load profile for simulation

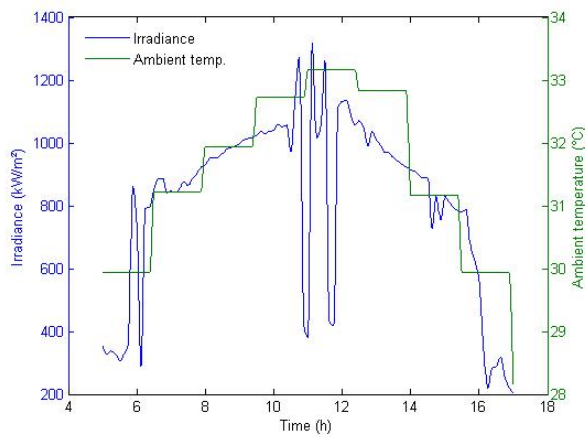


B2) Stand-alone hybrid PV-PEMFC generator power supplied to the load

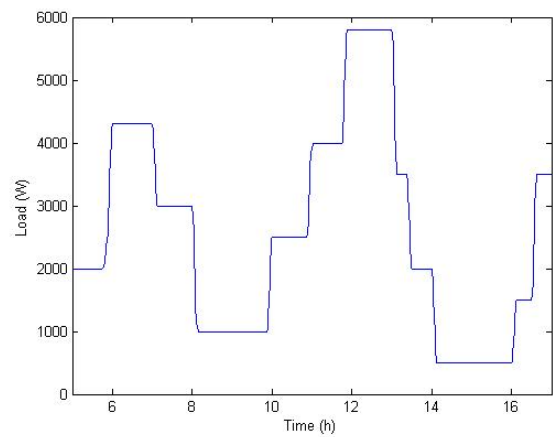


B3) Stand-alone hybrid PV-PEMFC generator power relative error

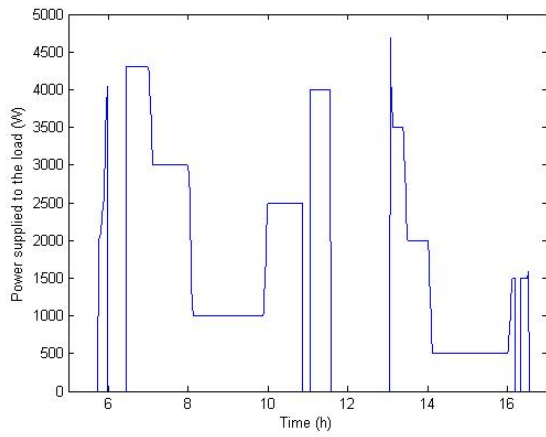
Figure 5.4: Simulation results for summer day of 2010/12/22



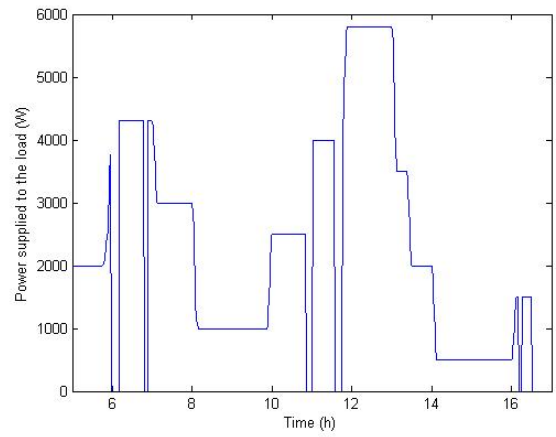
A1) Environmental data



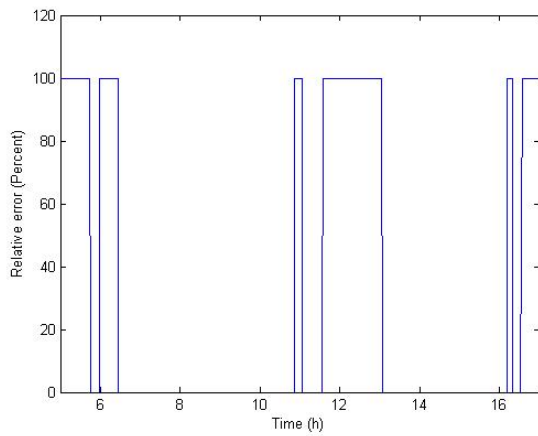
B1) Load profile for simulation



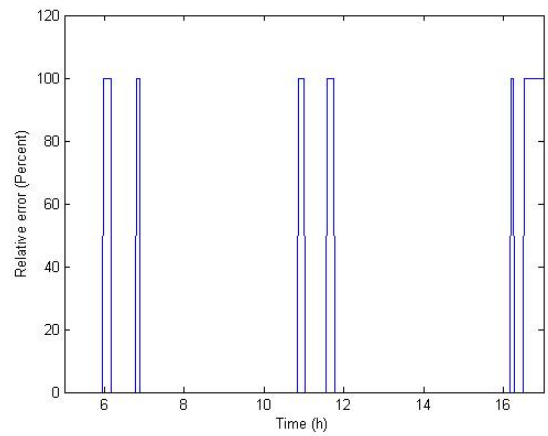
A2) Stand-alone PV generator power supplied to the load



B2) Stand-alone hybrid PV-PEMFC generator power supplied to the load

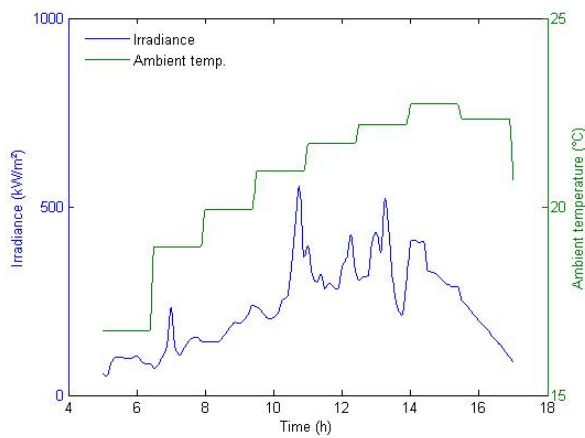


A3) Stand-alone PV generator power relative error

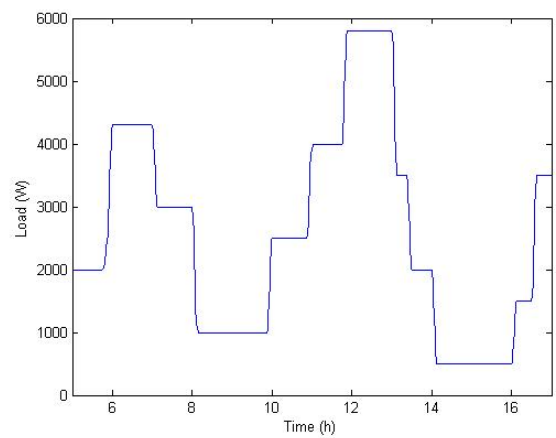


B3) Stand-alone hybrid PV-PEMFC generator power relative error

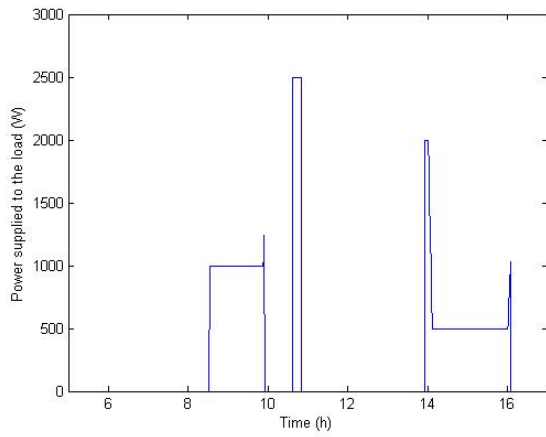
Figure 5.5: Simulation results for summer day of 2010/12/29



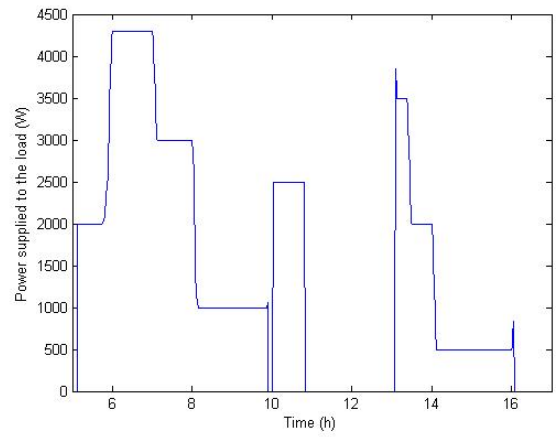
A1) Environmental data



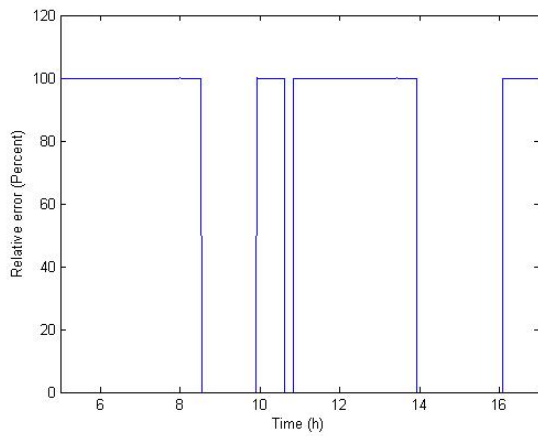
B1) Load profile for simulation



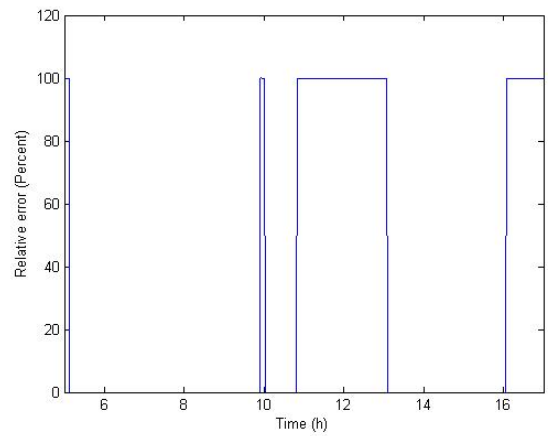
A2) Stand-alone PV generator power supplied to the load



B2) Stand-alone hybrid PV-PEMFC generator power supplied to the load

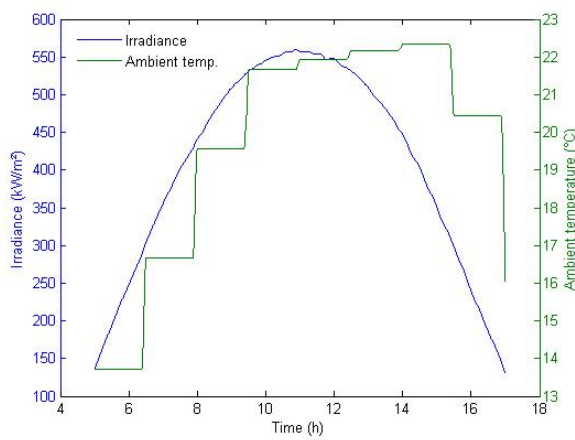


A3) Stand-alone PV generator power relative error

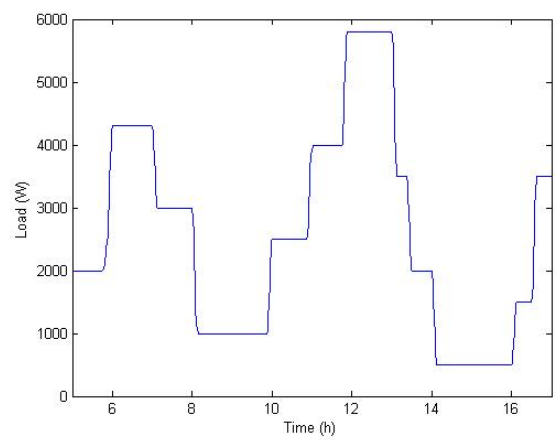


B3) Stand-alone hybrid PV-PEMFC generator power relative error

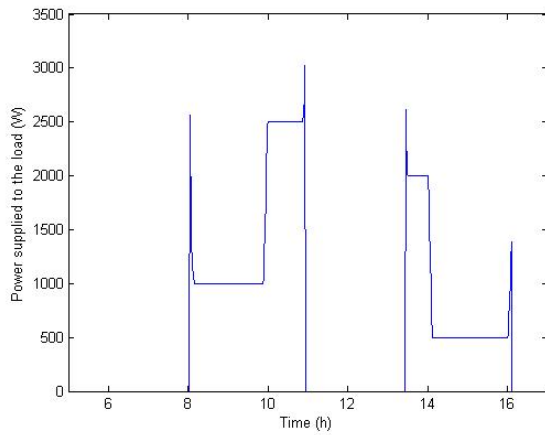
Figure 5.6: Simulation results for winter day of 2011/06/07



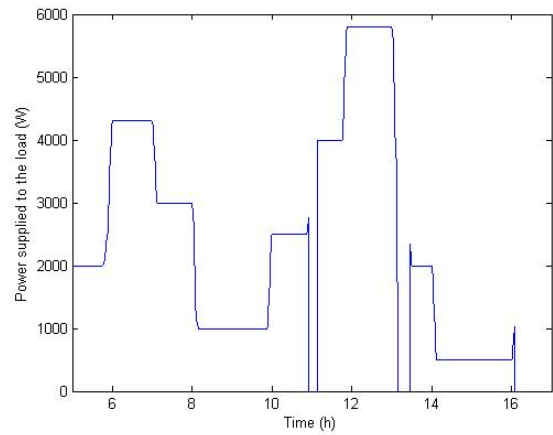
A1) Environmental data



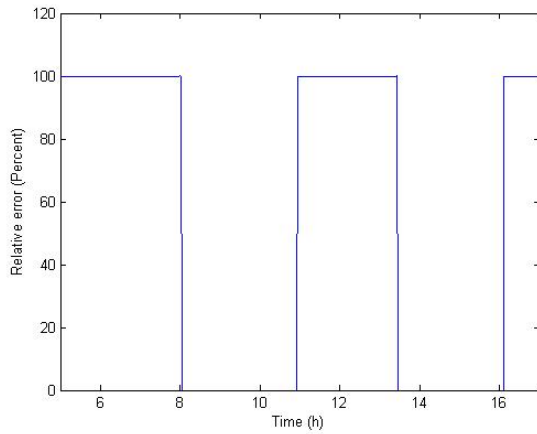
B1) Load profile for simulation



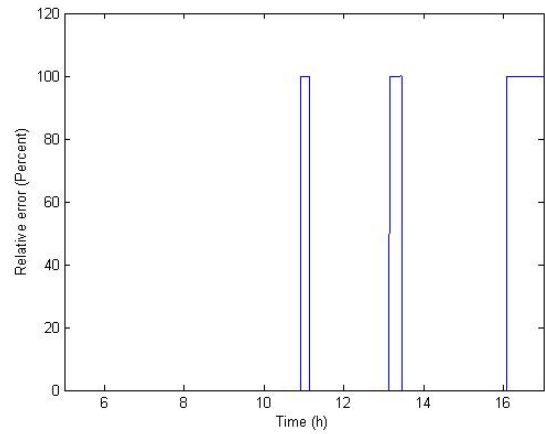
A2) Stand-alone PV generator power supplied to the load



B2) Stand-alone hybrid PV-PEMFC generator power supplied to the load



A3) Stand-alone PV generator power relative error



B3) Stand-alone hybrid PV-PEMFC generator power relative error

Figure 5.7: Simulation results for winter day of 2011/06/28

Simulation results are summarised in Tables 5.4 and 5.5. It can be noticed that the PV-PEMFC hybrid system presents a better performance compared to the conventional stand-alone PV system.

Table 5-4: Simulation results for stand-alone PV generator

Date	Day type	Power supplied to the load (W)		Relative error (%)	
		Mean value	Rms value	Mean value	Rms value
2010/12/22	Regular summer insolation	1579.2	2072.9	38.4%	32.0%
2010/12/29	Irregular summer insolation	1390.6	1972.7	45.7%	35.3%
2011/06/07	Irregular winter insolation	269.61	563.17	89.5%	81.5%
2011/06/28	Regular winter insolation	570.14	982.05	77.7%	67.8%

The performance of the PV-PEMFC system is observed in the winter regular insolation day followed by the summer irregular insolation day and then by the summer regular insolation day. This is justified by the regular insolation and the low temperature below 25 °C in the regular winter insolation, while the summer irregular insolation day presents higher insolation than the summer regular insolation day with peaks of about 1 300 W/m², the system operating at temperatures sometimes above 32 °C on both summer days.

Table 5-5: Simulation results for stand-alone hybrid PV-PEMFC generator

Date	Day type	Power supplied to the load (W)		Relative error (%)	
		Mean value	Rms value	Mean value	Rms value
2010/12/22	Regular summer insolation	2137.8	2676.1	16.6%	12.2%
2010/12/29	Irregular summer insolation	2196.4	2818.8	14.3%	7.6%
2011/06/07	Irregular winter insolation	1402.8	1984.8	45.3%	34.9%
2011/06/28	Regular winter insolation	2213	2861	13.6%	6.2%

5.7 Conclusion

There is a lot of disturbances in power supplied to the load in summer as well as in winter with irregular insulations, but the PV-PEMFC performs much better in this situation than the conventional stand-alone PV generator as shown. The better performance of the system in handling the load with variations in solar insolation is observed more particularly in the summer as expressed by power supplied relative errors as the PV generator produced enough power to supply the load and was more efficient at storing energy. This achieves better energy management as demonstrated in this paper.

References

- [1] M. Y. El-Sharkh, A. Rahman, M. S. Alam, P. C. Byrne, A. A. Sakla, and T. Thomas, "A dynamic model for a stand-alone PEM fuel cell power plant for residential application," *Journal of Power Sources*, vol. 138, pp. 199-204, 2004.
- [2] D. Rekioua, S. Bensmail, and N. Bettar, "Development of hybrid photovoltaic-fuel cell system for stand-alone application," *International Journal of Hydrogen Energy*, vol. 39, pp. 1604-1611, 2014.
- [3] T. El-Shatter, M. Eskandar, and M. El-Hagry, "Hybrid PV/Fuel system design and simulation," *Renewable Energy*, vol. 27, pp. 479-485, 2002.
- [4] S. B. Silva, M. M. Severino, and M. A. G. de Oliveira, "A stand-alone hybrid photovoltaic, fuel cell and battery system: A case study of Tocantins, Brazil," *Renewable Energy*, vol. 57, pp. 384-389, 2013.
- [5] Z. Jiang, "Power management of hybrid photovoltaic-fuel cell power systems," *IEEE*, pp. 1-6, 2006.
- [6] A. L. Laura, "Compact hybrid power source using fuel cell and PV array," *International Journal of Science and Research Publications*, vol. 4, no. 11, 2014.
- [7] S. Rahman, and K. Tam, "A Feasibility Study of Photovoltaic-Fuel Cell Hybrid Energy System," *Transactions on Energy Conversion*, vol. 3, no. 1, pp. 50-55, March 1988.
- [8] K. Tam and S. Rahman, "System performance improvement provided by a power conditioning system for central station photovoltaic-fuel cell power plant," *IEEE Transactions on Energy Conversion*, vol. 3, no. 1, pp. 64-70, March 1988.
- [9] L. Wei, Z. Xin-jian, and C. Guang-yi, "Modelling and control of a small solar fuel cell hybrid energy system," *Journal of Zhejiang University SCIENCE A*, vol. 8, no. 5, pp. 734-740, 2007.
- [10] S. G. McGowan and S. F. Manwell, "Hybrid/PV/diesel system experiences," *Revue Renewable Energy*, vol. 16, pp. 928-933, 1999.
- [11] M. Belhamel, S. Moussa, and Kaabeche A., "Production of electricity of a hybrid system (Wind-Photovoltaic-Diesel)," *Review of Renewable Energy*, pp. 49-54, 2002.
- [12] A. El Khadimi, L. Bachir, and A. Zerowel, "Sizing optimization and techno-economic energy system hybrid photovoltaic-wind with storage system," *Renewable Energy Journal*, vol. 7, pp. 73-83, 2004.
- [13] M. Mwinga, B. Groenewald, and M. McPherson, "Design, modelling and simulation of a fuel cell power conditioning system," *Journal of Thermal Engineering*, vol. 1, no. special Issue 3, No.6, pp. 408-419, 2015.
- [14] C. Wang and M. Hashem Nehrir, "Power management of a stand-alone wind/photovoltaic/fuel cell energy system," *IEEE Transactions on Power Systems*, vol. 23, no. 3, 2008.

- [15] El-Maaty Abou, Metwally Aly Metwally, El-Aal Abd, "Modelling and simulation of a photovoltaic fuel cell hybrid system," University of Kassel, Kassel, 2005.
- [16] N. M.-A. Mutombo, "Design and performance analysis of hybrid photovoltaic-thermal grid connected system for residential application," Master's dissertation, University of KwaZulu-Natal, Durban, SA, 2012.
- [17] K. Ishaque, Z. Salam, and H. Taheri, "Simple, fast and accurate two diode model for photovoltaic modules," *Solar Energy Materials & Solar Cells*, vol. 95, pp. 586-594, 2011.
- [18] F. M. Gonzalez-Longatt, "Model of photovoltaic module in Matlab," in 2Do Congreso Iberoamericano De Estudiantes De Ingenieria Electrica, Electronica Y Computacion, 2005.
- [19] N. M. Souleman, T. Olivier, and L. A. Dessaint, "A generic fuel cell model for the simulation of fuel cell vehicles," in *Proceedings of the IEEE Power & Energy Society General Meeting*, AB Canada, 2009.
- [20] SimPowerSystems, Natick, M. A.: MathWorks Inc., 2010.
- [21] F. Khan, A. Nawaz, M. A. Muhammad, and M. Ali Khadim, "Review and analysis of MATLAB Simulink Model of PEM fuel cell stack," *International Journal of Engineering & Computer Science*, vol. 13, no. 03, 03 June 2013.
- [22] J. Han, J-F.c Charpentier, and T. Tang, "An energy management system of a fuel cell/battery hybrid boat," *Energies*, vol. 7, pp. 2799-2820, 2014.
- [23] B. Lindermark and G. Oberg, "Solar power for radio base station (RBS) sites applications including system dimensioning, cell planning and operation," in *Proceedings of 23rd International Telecommunications Energy Conference*, 2001.
- [24] A Chaurey and S. Dembi, "Battery storage for PV Power systems: an overview," *Renewable Energy*, vol. 2, no. 3, pp. 227-235, 1992.
- [25] B. H. Chowdhurg and S. Rahman, "Analysis of interrelationships between photovoltaic power and battery storage for electric utility load management," *IEEE Transactions on Power Systems*, vol. 3, no. 3, pp. 900-907, August 1998.
- [26] K. Ro and S. Rahman, "Two-loop controller for maximizing performance of a grid connected photovoltaic-fuel cell hybrid power plan," *IEEE Transactions on Power Systems*, vol. 13, no. 3, pp. 276-281, 1998.
- [27] K. Agbossou, M. Kolhe, J. Hamelin, and T. K. Bose, "Performance of stand-alone renewable energy system based on energy storage as hydrogen," *IEEE Transactions on Energy Conversion*, vol. 19, no. 3, pp. 633-640, September 2004.
- [28] US Department of Energy, Office of Fossil Energy, National Energy Technology Laboratory, *Fuel Cell Handbook*, 7th ed., Morgantown, WV: E.G. & G. Technical Services, Inc., 2004.
- [29] G. M. Masters, *Renewable and Efficient Electric Power Systems*, Hoboken, New Jersey: John Wiley & Sons, Inc., 2004.

- [30] O. Ulleberg, "Modelling of advanced alkaline electrolyzers: a system simulation approach," *International Journal of Hydrogen Energy*, vol. 28, no. 1, pp. 21-33, 2003.
- [31] J. Chiasson, B.Vairamohan, "Estimating the state of charge of a battery," Knoxville, TN 37996.

CHAPTER 6 : NEURO-FUZZY STRATEGIES FOR PREDICTION AND MANAGEMENT OF HYBRID PV-PEMFC-BATTERIES SYSTEMS

PUBLICATION 6

Ntumba Marc-Alain Mutombo^a; Freddie L. Inambao^b; Remy Tiako^c; Samuel A. O. Ilupeju^d

^{a,c} University of KwaZulu-Natal, School of Engineering, Discipline of Electrical Engineering, Howard College Campus, Durban, South Africa (marcntumba@yahoo.fr; Tiako@ukzn.ac.za)

^{b,d} University of KwaZulu-Natal, School of Engineering, Discipline of Mechanical Engineering, Howard College Campus, Durban, South Africa (inambaof@ukzn.ac.za; ilupejus@ukzn.ac.za)

Abstract

Advances in knowledge, research and development of hybrid systems in the field of renewable energy and their non-linear behaviour have led to the application of artificial intelligence techniques to deal with modelling, prediction, management and control of the flow of energy from different components of those systems.

In this paper, an adaptive neuro-fuzzy interference system (ANFIS) for the management and control of energy flow of a hybrid photovoltaic-battery fuel cells system is developed. The ANFIS structure obtained was compared to an artificial neural network (ANN). This study found that ANN gives good prediction in the management of energy flow of the hybrid system, but better results are obtained with ANFIS.

Key words: Photovoltaic, fuel cell, batteries, energy management, artificial neural network, adaptive neuro-fuzzy interference

6.1 Introduction

Due to different factors enumerated in many publications [1] [2] [3] [4] such as the expense of access to the electricity grid for remote area communities, the increase in world electric energy demand, the negative impact of carbon dioxide (CO₂) and other greenhouse related gases on the ozone layer and the resulting ecosystem deterioration, researchers have developed new techniques of production of electricity. These techniques seek to generate ‘renewable energy’ to solve problems brought about by conventional techniques. These techniques convert natural forms of energy such as solar irradiance, kinetic wind energy etc. into electrical energy that can be stored in batteries, super-capacitors or hydrogen tanks (by conversion of electrical energy into hydrogen via an electrolyser).

Of all the available natural sources, solar energy has the greatest potential due to its availability, it is free to harvest, and it can be transformed directly into electric energy by photovoltaic (PV) generators. However, changes or variations of solar irradiation, ambient temperature, and load, cause instability to the photovoltaic generators output with negative impact upon users. To overcome this situation, other renewable energy systems and storage units can be integrated to the PV generators to form a hybrid system. The most popular hybrid system is photovoltaic-proton exchange membrane fuel cells-batteries. This system uses the PV generator as a primary energy source and fuel cells and batteries as auxiliary or back up sources [5].

In order to keep the state of charge (SOC) of the battery in a certain range to improve its life time on the one hand and in order to optimize hydrogen consumption on the other hand, good energy management and control between the different sources and the load is necessary.

In this work, an intelligent energy flow control based on neuro-fuzzy method is developed so as to ensure the appropriate energy management between different sources and the load for a better load supply and optimum operation of the hybrid photovoltaic-battery fuel cells system.

6.2 Review of artificial intelligence applied to photovoltaic and fuel cell systems

The use of artificial intelligence techniques in the engineering field has opened a new window to the control of non-linear systems and optimization calculations. The most popular of these techniques are fuzzy-logic (FL) and artificial neural network (ANN).

Fuzzy-logic and ANN were applied to PV systems for modeling, simulation and control as well for the prediction and control of maximum power point tracking (MPPT) [6] [7]. Related to the application of FL and ANN to the PV systems control, Ohsawa et al. [8] applied an ANN for the operation and the control of a PV-diesel system. Moreno et al. [9] proposed an algorithm based on FL technique to control a stand-alone PV system. A new parameter called weighted loss of load probability (WLLP), which is a weighted sum loss of load probability of individual loads, was introduced. In that study, a comparison of the results provided by the fuzzy controller system compared to the conventional system in terms of performance showed significant ameliorations of WLLP. Mellit et al. [10] used a FL controller to control the MPPT of a stand-alone PV system. Patcharaprakiti et al. [11] proposed a MPPT method using adaptive FL controller for grid-connected PV systems. Bahgat et al. [12] used a neural network to estimate the maximum power and the operating power of a PV module. The proposed neural network detected with accuracy the power produced in the case of direct coupling or maximum power output. The accuracy of the neural network was the same for all the operating conditions. El-Shafy et al. [13] used FL to evaluate the proper performance of the MPPT controller of a stand-alone PV system. The results obtained were compared to a proportional integral (PI)

controller. Experimental results showed that the system implemented with the FL controller or the PI controller provided a better operating power of the PV array compared to the direct coupling of the PV.

Later, Teken et al. [16] proposed a management strategy for embedded fuel cells based on a FL controller. Hatti [17] developed a neural network based on a PI controller used for neural network system training. Bhoopal et al. [18] investigated the performance and the prediction for a PEMFC system using a back propagation (BP) network. By using the fuel cells' stack current and hydrogen pressure as model input, the authors succeeded in predicting PEMFC voltage and current. In the same way, Ghaderi et al. [19] proposed a neural network model to control stack terminal voltage and improve system performance by using air pressure as a control signal. Simulation results proved that the applied feed forward neural network control can track the fuel cells terminals' voltage and improve the overall system performance. Other intelligent techniques like genetic algorithm have also been used, more details can be found in [6] [7].

Two or more artificial intelligence techniques can be combined to use the advantages of one or many techniques to overcome the weaknesses of others and vice versa producing a hybrid intelligent system. Each of those techniques is chosen and used based on the type of data to be processed or the type of problem to be solved.

Until 2008, only a few applications of neuro-fuzzy for PV modeling were realized. The first model was proposed by Mellit and Kalogirou [14] in which the authors used a neuro-fuzzy system to model and simulate stand-alone PV systems. For PV systems modeling, it is recommended to find suitable adaptive neuro-fuzzy interface system (ANFIS) models for different components of the system in variable climate conditions. The overall block diagram of the developed model is given in Figure 6.1.

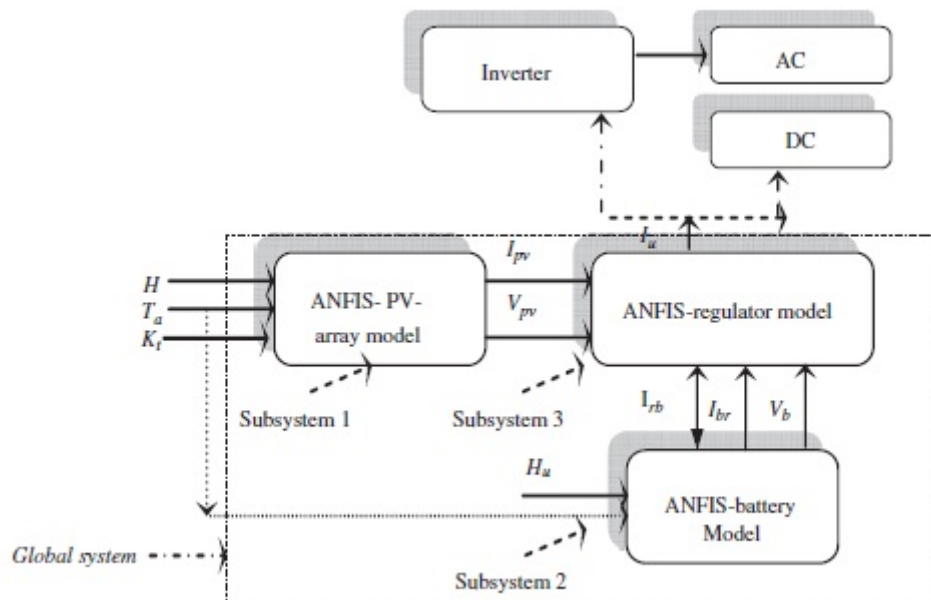


Figure 6.1: Block diagram of developed global model [14]

The correlation coefficient between measured values and values estimated by the ANFIS give a good prediction with precision of 98%. A second application was proposed by Abdulhadi et al. [15] who described a hybrid modeling technique-based computer program that facilitated PV cells modeling with previous measured data for different given operating conditions. The technique used neuro-fuzzy models to predict short-circuit current and open-circuit voltage of the PV cell, followed by the coordinated translation of the current-voltage measured response.

6.3 Description and operation of the system

For a better performance, different renewable energy sources and storage systems are combined into one hybrid system for the production of electric energy, each source as a sub-system compensating for the weaknesses of the others or vice versa in this integrated system. Advantages and weaknesses of the principal energy sources can be found in [20] [21] [22] [23] [24] [25] [26].

This study is based on a hybrid PV-PEMFC system constitute of photovoltaic array of 24 Q-PEAK 250 monocrystalline solar modules with fixed orientation collector for a Direct Current Standard Test Conditions (DC STC) rated power of 6 000 W able to provide about 8 500 kWh/year, more than the average of 8 300 kWh/year needed for Durban modest household electrical demand. Details about the design and size of the PV generator can be found in [27]. To overcome the variance of the PV array generator output under different insolation levels, a 2000 Horizon PEMFC is coupled to the PV array generator. This fuel cell is used with an electrolyser to produce hydrogen from water using electrical energy from the PV array generator.

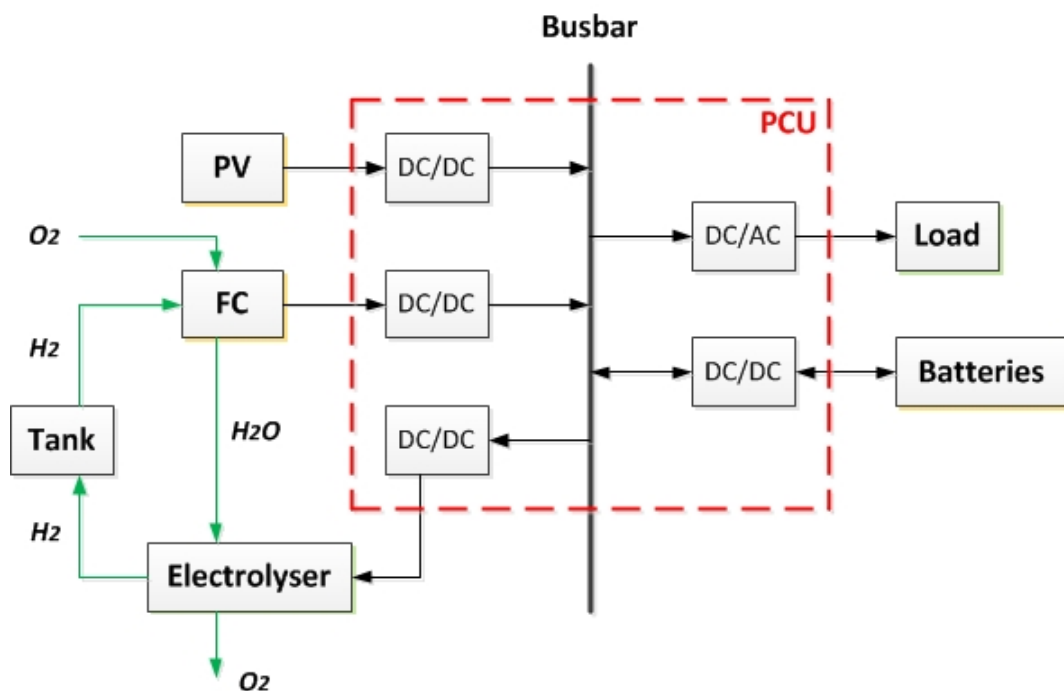


Figure 6.2: Hybrid PV PEMFC topology [5]

A lithium-ion battery bank composed of 4 batteries connected in series is added to the system to compensate for the poor dynamic response of fuel cells to transient power demand. This type

of battery has a high energy density, a long cycle life and a relatively low self-discharge rate. All the sub-systems and the load are connected to the busbar through different power electronic interfaces together constituting the power conditioning for the hybrid system. Details about system components and their functions are given in [5] [27]. The schematic diagram is given in Figure 6.2.

In this hybrid system, the photovoltaic generator supplies the load with electrical energy as the main energy source, and the PEMFC stack and battery bank operate as auxiliary energy sources and supply the load in case of low solar irradiance or failure of the PV generator to supply the energy need to the load. The large amount of energy demand is supplied by the PV generator primarily and then by the fuel cells secondarily followed by the battery bank.

6.4 Control strategies

The main challenge met by combining different energy sources in an integrated system is control of the energy flow from different sub-systems to meet the load demand. This is difficult to be accomplished using classic control tools due to the variable nature of the output energy from sources like photovoltaic systems, but also the variable nature of the connected load leading to the development of non-linear models of the system.

System control is recommended to assure an efficient and robust power transfer from different sources to the load without damaging the components. In order to assure a continuous power supply to the load, the controller manages the energy supply to the load by regulating the DC bus and balancing the energy flow from all sources to satisfy the connected load demand and other constraints.

Different control strategies can be used to reach the energy management goal. Some of these can be in conflict with others as expected. Therefore, balance and compromise are necessary. For example one can look to reach a maximum utilisation of fuel cells as a secondary energy source and minimise battery use to improve battery life or vice versa to consume less hydrogen. The control strategy proposed in [5] seeks to increase battery lifetime primarily and then provides low or optimum hydrogen consumption assuring continuous supply of electric energy to the load based on the overall system capability. The flowchart for control and energy flow management is given in Figure 6.3.

Due to the nature of data set used, only ANN and ANFIS are used for energy management and control in this work and the simulation results obtained from these two techniques are compared to the expected values.

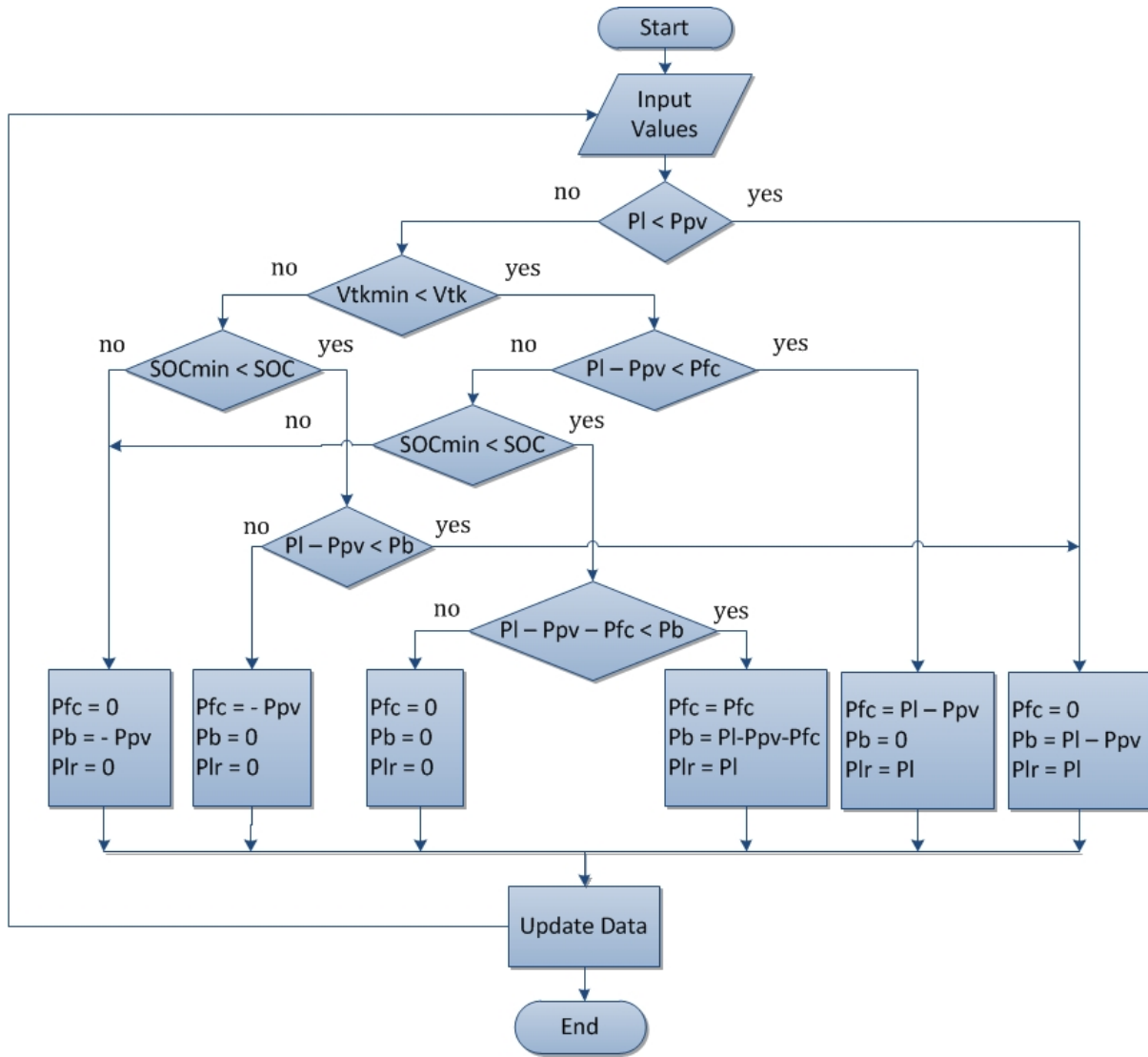


Figure 6.3: Flow chart energy management [5]

6.5 Artificial neural networks

6.5.1 Algorithm and structure

ANN models are computer programs conceived to imitate human ways of treating data for predict, classify and control [28]. ANN is largely recognized as an application offering an alternative way to solve complex problems. The ANN ability to learn spontaneously from examples, “reason”, from imprecise data sets and produce adequate and accurate results from new information that has never been stored in memory before, has increased the application of this technology in many engineering fields [28]. In recent years, the use of ANN models in various fields has increased due to the fact that ANN models operate like a black box, with no need for detailed system information to obtain results. The major element in the construction of any ANN is a neuron. These neurons are linked together by communication lines [29] in a the configuration of a communication network. This topology has an important effect in the performance of the network.

ANN determines relationships between input variables and outputs by learning previously recorded data. After being trained, these ANN can be used to approximate an arbitrary map of an input-output data set [30]. Among training algorithms available, the back propagation algorithm [31] [32] is frequently used because it is stable, robust and easy to implement. In back propagation architecture, each element or neuron receives input from the external environment (real world) or from other neurons, and produces a specific output. The back propagation uses the supervised training technique, more details about this technique can be found in [28]. To be sure of the network precision and its capability of generalisation, the network is tested continuously and is followed during training and testing operations. To be sure that the ANN model provides a right prediction or classification, predicted results produced by the ANN models are compared with expert predictions results for the same case or they are compared with results from another computer program.

6.5.2 Simulation and validation of ANN model

Based on the nature of the problem being time series prediction, a dynamic time series neural network is used. Before simulation, the first step is to define the problem by selecting a data set. Then the network is trained to fit that time series data set using a nonlinear input-output prediction with the number of hidden neurons of 5 and the number of delays of 2. Many algorithms exist for this purpose such as Levenberg-Marquardt, Bayesian Regularisation, Scaled Conjugate Gradient, Jacobien calculations, etc. for the training of the network. The field of application of each algorithm is determined by its advantages and inconveniences [33].

A total of 720 target time-steps were selected for validation and testing. Seventy percent of the data were allocated to train the network, 15% for validation and the remaining 15% for testing. During the training process, data were presented to the network and the network was adjusted according to its error. To validate the network, 15% of data allocated to the validation were used to measure the network generalization, and to stop the training when the generalization was reached. The network performance during and after training was measured by using the 15% remaining set of data, those do not have an impact on training.

The Levenberg-Marquardt algorithm was used for training the network. In this algorithm, the training stops when generalization stops improving. This can be seen in Figure 6.4 by an increase in the mean square error (mse) which is the average square difference between outputs and targets for the validation samples.

The best validation performance is obtained at epoch 22 after training the network multiple times to improve its performance.

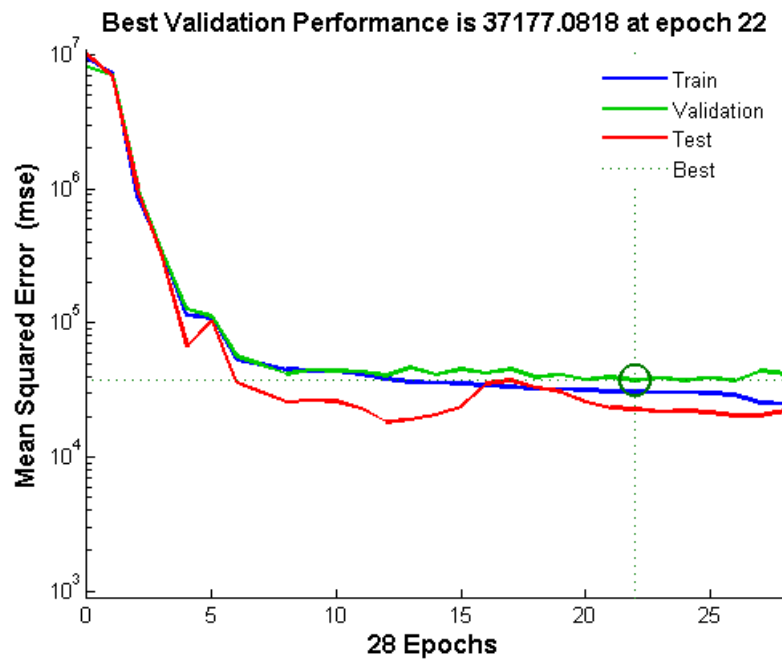


Figure 6.4: ANN performance

This network provides good results as can be confirmed in Figure 6.5 and Figure 6.6 related to the correlations.

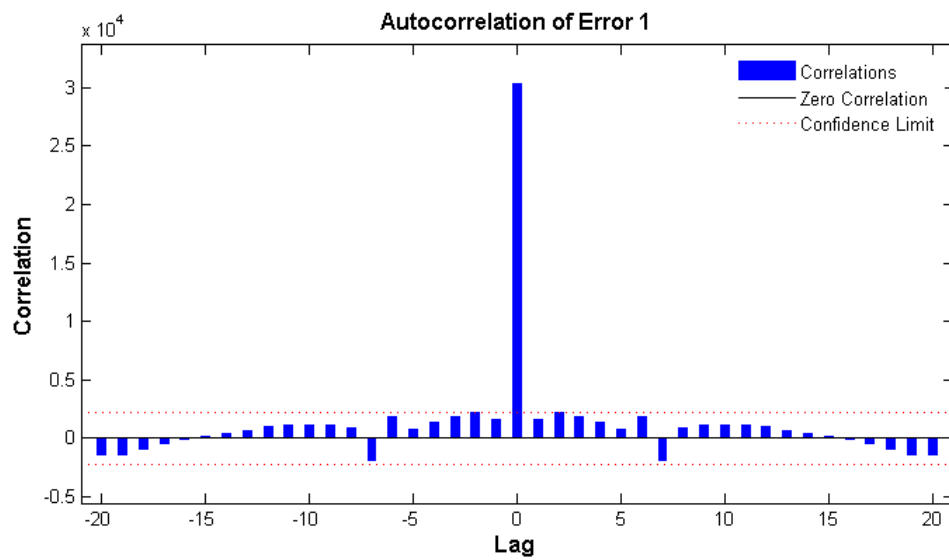


Figure 6.5: ANN error autocorrelation

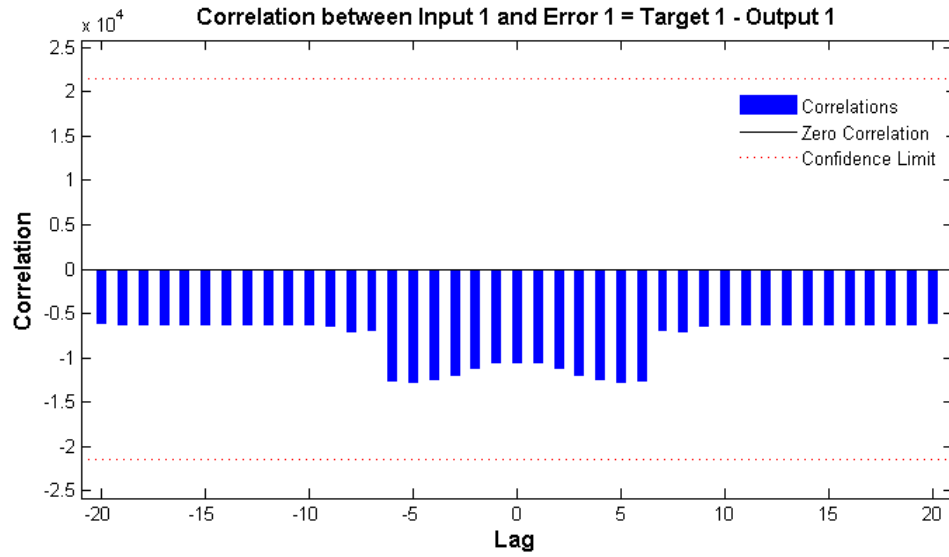


Figure 6.6: ANN input-error cross-correlation

For an accurate prediction of the model, only one non-zero value of the autocorrelation function is allowed, and it must be at zero lag which correspond to the mean square error. The present model presents important correlation to the prediction errors. It can be noticed that for this case, after multiple trainings, all of the correlations fall inside the confidence boundaries close to zero, making the model suitable to manage the energy flow of the hybrid system. The time-series response of the model and error is given in Figure 6.7.

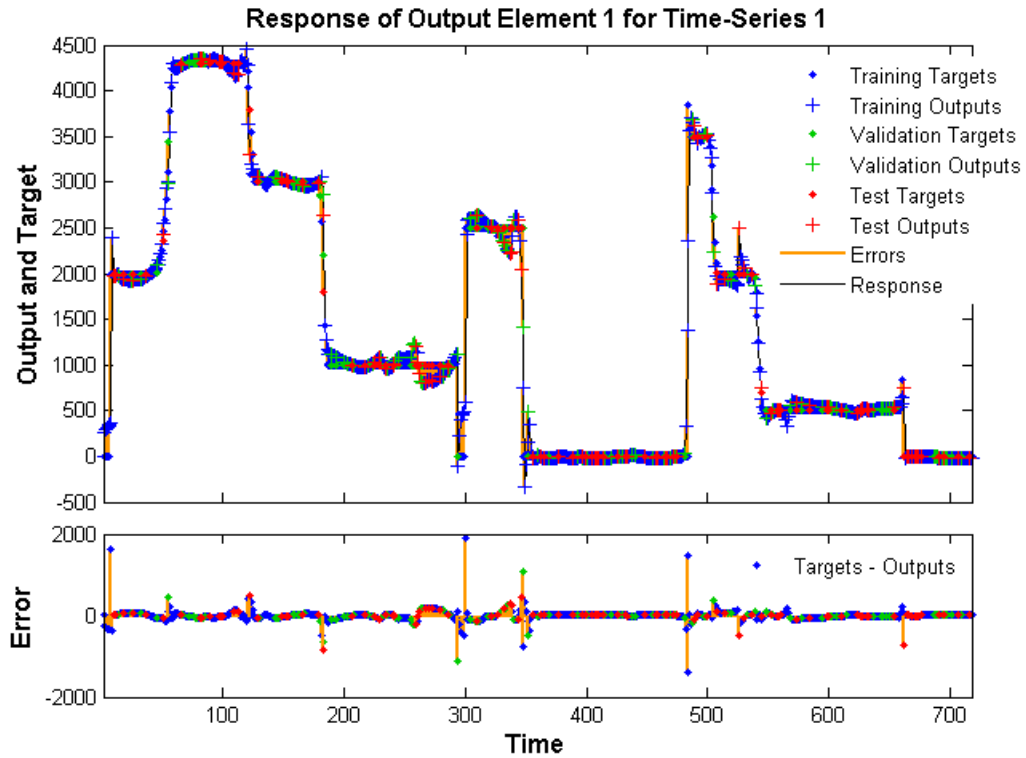


Figure 6.7: ANN time-series response

The correlation between outputs and targets are measured by the regression R values and are given in Figure 6.8. The value of 99% is obtained for the regression which confirms the accuracy of the network to manage the energy flow of different components of the PV-PEMFC-batteries system and the load.

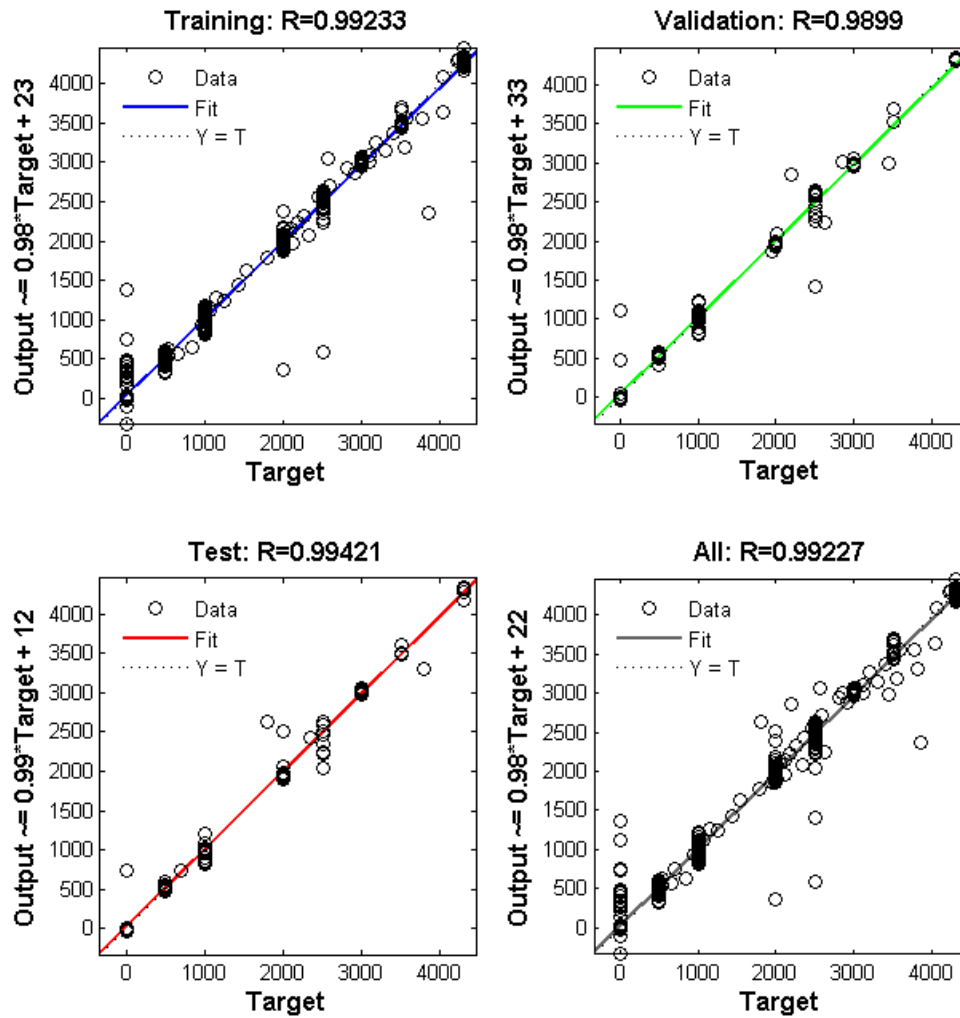


Figure 6.8: ANN regression

Figure 6.9 shows the structure of the network.

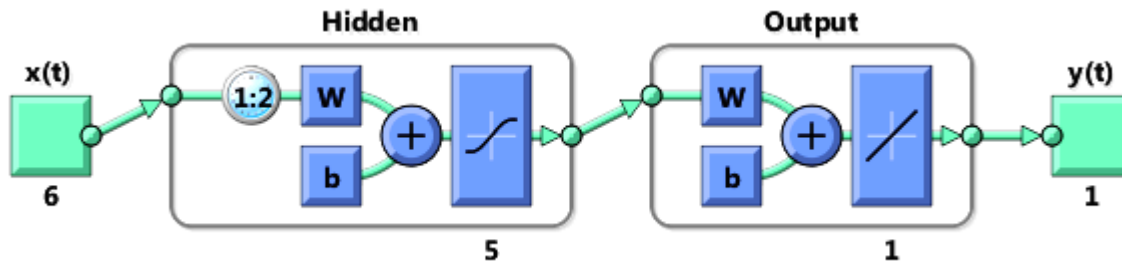


Figure 6.9: ANN structure

This network is constituted of 6 inputs related to the load, the PV power, the FC power, the batteries power, the tank hydrogen volume and the battery state of charge (SOC) respectively, with five hidden layers with delays of two and one output layer.

6.6 Neuro-fuzzy control strategies

6.6.1 Neuro-fuzzy algorithm and structure

Because ANNs do not consider statistical distribution presuppositions and characteristic data, they are much more efficient than statistical techniques often used. They use a linear approach to produce the model, meaning that when dealing with nonlinear and complex informations these methods can generate a highly accurate model similar to the original or defined model from that data. The high learning ability of ANN has made this method a good choice when combined with a fuzzy system [34]. The combination of the ANN with the fuzzy method generates a hybrid technique called neuro-fuzzy technique in which each one of these systems can cover the weaknesses of the other and improve the neuro-fuzzy system efficiency [7]. A neuro-fuzzy system uses the learning method derived from the ANN to find the fuzzy system parameters that are appropriate membership functions and fuzzy rules. As mentioned before, the reason to represent a fuzzy system in terms of a neural network is to use the learning ability of a neural network to improve the performance through adaptation.

Based on researchers' objectives, different types of ANN can be used. One of the best known is the multilayer feed forward neural network that uses a neural network instructed by a supervisor. This neural network is used to solve problems related to the study of input-output sets' relationship. In reality, it is a method of instruction by the supervisor to determine the relationship between data by training a series of data sets. The back propagation algorithm mostly used in fuzzy logic system has a negative gradient of the error function, the correction of the inputs decreases the mean square error gradually [35] [36].

Many structures suggest establishing a fuzzy system by the neural networks [34]. From different versions developed of neuro-fuzzy methods, the adaptive neuro fuzzy interface system (ANFIS) developed by Jang [37] is the most powerful and popular. In this neuro-fuzzy system, the learning algorithm coincides with the integrated learning approaches. The principal approach of the instruction in this structure is the back propagation that scatters the error value toward inputs by the steepest descent gradient algorithm and corrects the last parameters [37]. These structures are used in control systems and many other applications. Many investigations have been conducted to apply the ANFIS system in engineering process modelling [34].

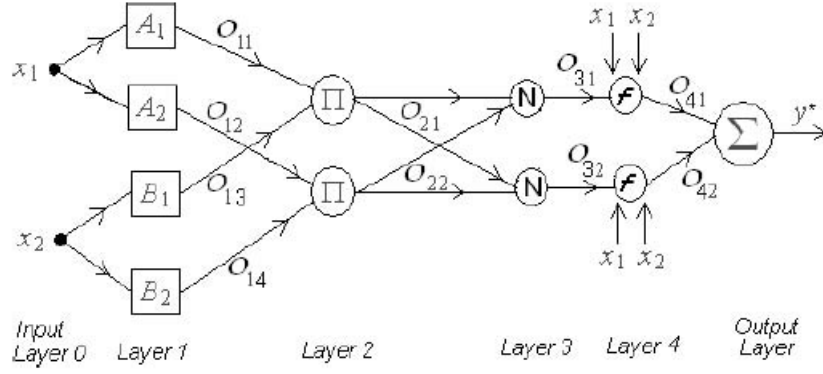


Figure 6.10: First-order Sugeno fuzzy model with two rules [38]

Like other fuzzy systems, the ANFIS structure is organised in two parts, the introductory and concluding parts related by a series of rules. The representation of the preceding section of the neural network is a graphic display of the computation steps in Sugeno-Takagi process shown in Figure 6.10. In order to make this representation more useful in implementing control laws, it is necessary to equip this representation with an efficient learning algorithm. In the conventional neural network, the back propagation algorithm is used for learning or adjusting weights in the connecting arrows between input-output neurons of training samples [38]. The ANFIS uses the back propagation or the combination of least squares estimation and back propagation for the membership function parameter estimation [33]. In order to train a fuzzy-neural network, a series of training data in form of input-output is needed, and a specification of rules, as well as a preliminary definition of correspondent membership functions [33].

6.6.2 Simulation and validation of ANFIS model

The data set of 720×7 array was used for training ANFIS and a 360×7 array for checking. The 6 first colons represent the input of the ANFIS model and the last colon is related to the output. The fuzzy inference system (FIS) is generated by using a grid partition assigning 2 membership functions to each input and using the generalized bell-shaped membership function (gbellmf) type for the inputs and a linear membership function for the output.

The initial FIS model is generated by applying grid partition techniques which generate a single-output Sugeno-type FIS by using grid partitioning on the data set ANFIS properties as shown in Figure 6.11.

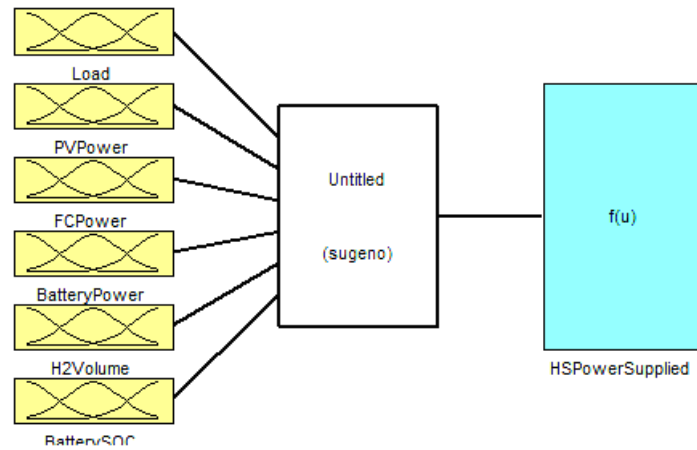


Figure 6.11: ANFIS properties

ANFIS membership functions are represented in Figure 6.12.

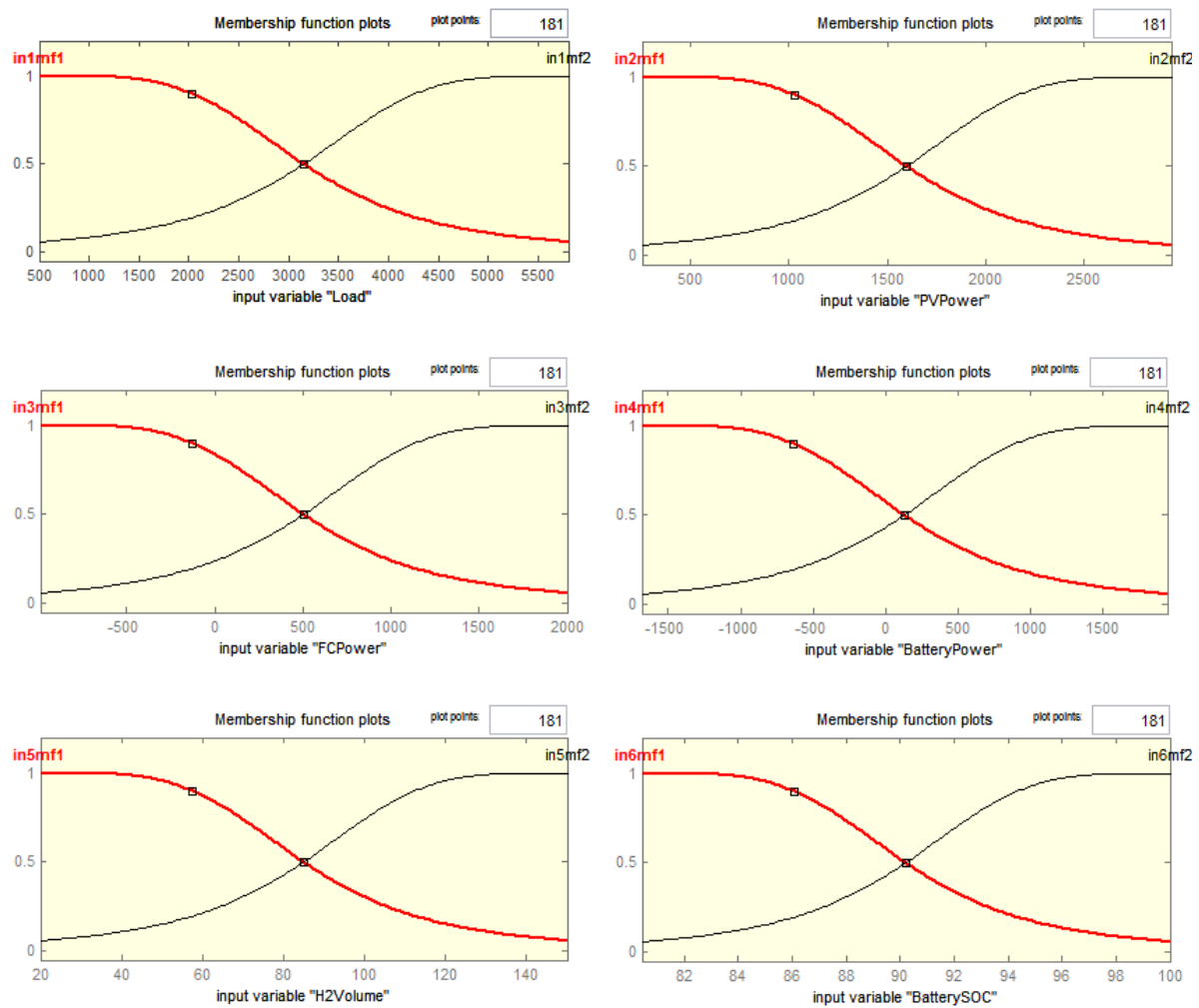


Figure 6.12: ANFIS membership functions

The combination of least-squares and back-propagation gradient descent method with an error tolerance of 0.01 and 50 epochs is used to train the FIS. This trains the fuzzy system by correcting membership function parameters that best model this data by emulating the training data. The training error in Figure 6.13 is obtained.

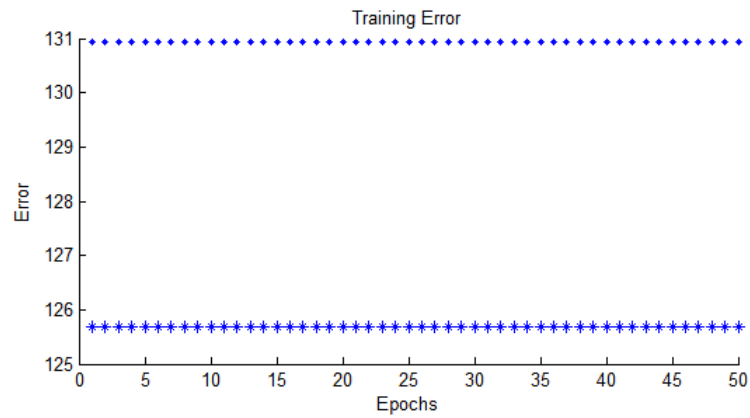


Figure 6.13: ANFIS training error

It can be noticed that the checking error of 130.941 is higher than the training error of 125.678. The ANFIS training is completed at epoch 2 with an error of 155.661. The time-series response of training data and checking data are shown in Figure 6.14 and Figure 6.15 respectively.

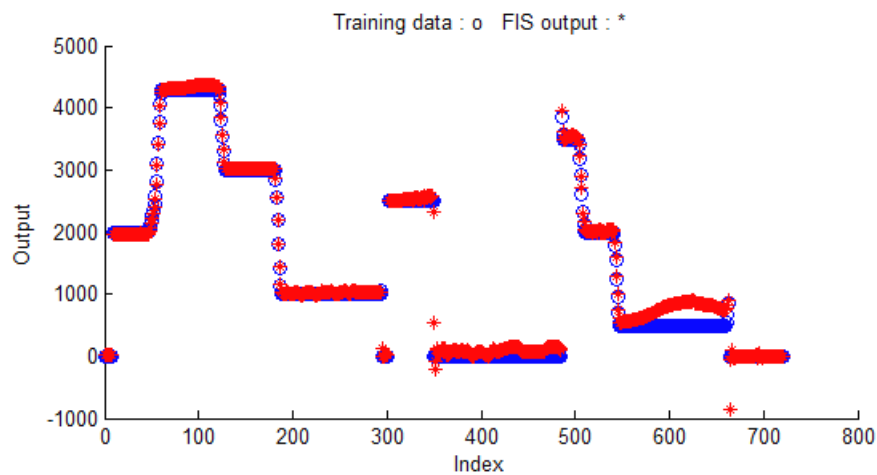


Figure 6.14: ANFIS training data time-series

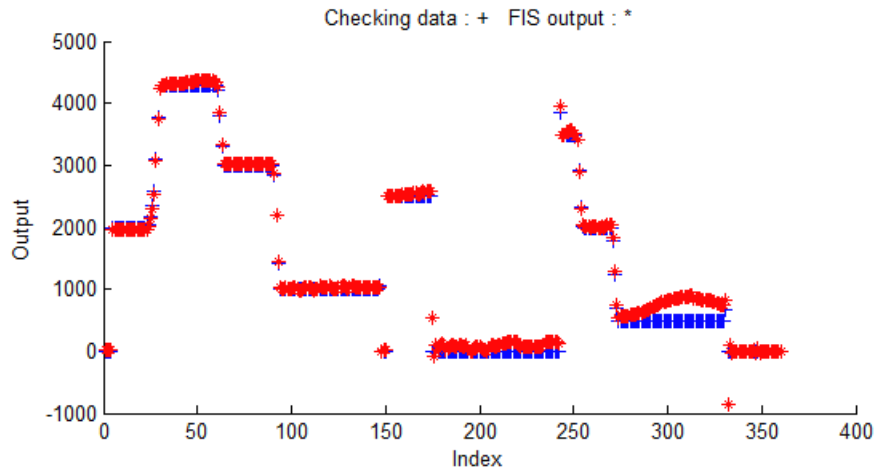


Figure 6.15: ANFIS checking data time-series

It can be seen that the time-series obtained using ANFIS for training data and checking data are the same with differences in indexes that are related to the number of data sets used [33]. The ANFIS information is given in Table 6.1.

Table 6-1: ANFIS information

PARAMETERS	VALUES
Number of nodes	161
Number of linear parameters	448
Total number of parameters	484
Number of training data pairs	720
Number of checking data pairs	360
Number of fuzzy rules	64

The structure of the network is given in Figure 6.16. This structure represents the ANFIS structure of the model. This structure contains 64 fuzzy rules and 484 parameters. We can recognize three different layers in the ANFIS network structure that make it a multilayer network. This type of network is a SUGENO type fuzzy system with six inputs and one output.

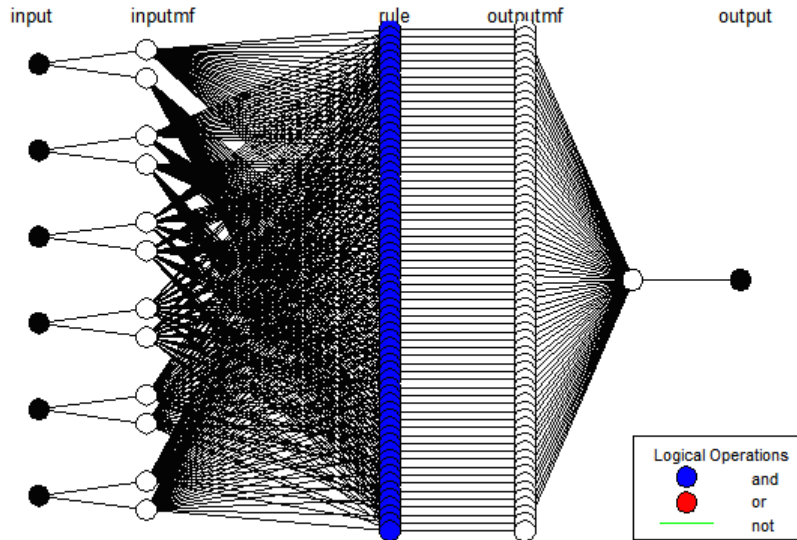


Figure 6.16: ANFIS structure

6.7 Comparison of ANN model and ANFIS model obtained

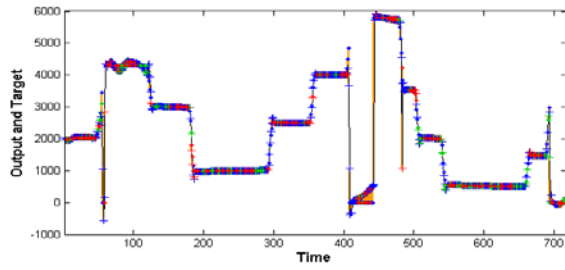
With new data set load to ANN and ANFIS structures obtained, time-series responses in Figure 6.17 and Figure 6.18 were respectively obtained for different days.

The rmse values of the ANN and ANFIS networks are given in Table 6.2.

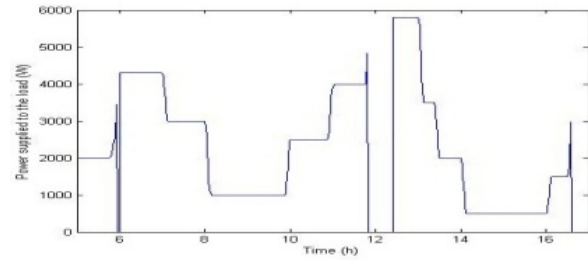
Table 6-2: The rmse values of the ANN and ANFIS networks

DAYS	ANN RMSE	ANFIS RMSE
Summer day of 2010/12/22	152.60	147.16
Summer day of 2010/12/29	225.25	181.55
Winter day of 2011/06/07	192.81	120.18
Winter day of 2011/06/28	157.35	12.33

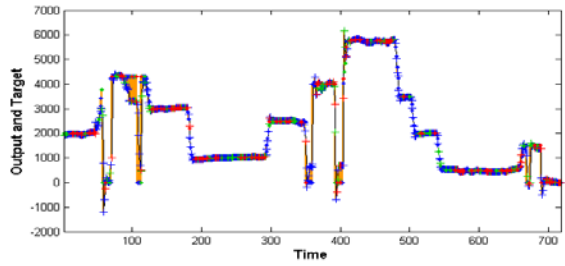
From Table 6.2, it can be seen that the values of ANFIS are small compare to the ANN values but the differences between the two are not big – both networks give good results. The ANFIS results are obtained at epoch 2 while ANN results are obtained after epoch 15 after much training of the network. This make ANFIS network better and faster compare to ANN for the prediction and management of hybrid PV-PEMFC-batteries systems.



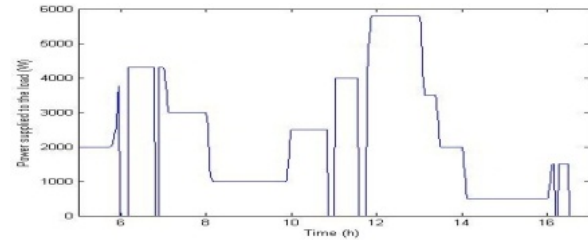
ANN Time – series response for summer day of 2010/12/22



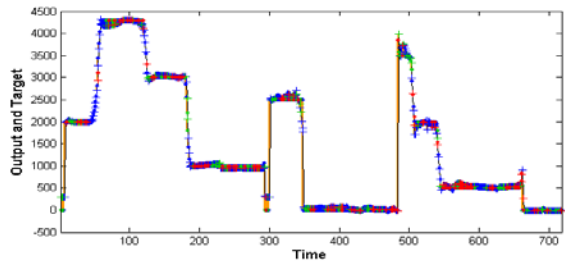
PV-FC batteries response for summer day of 2010/12/22



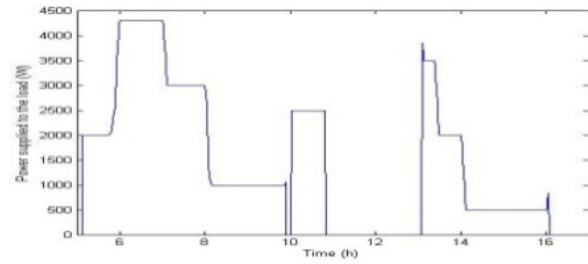
ANN Time – series response for summer day of 2010/12/29



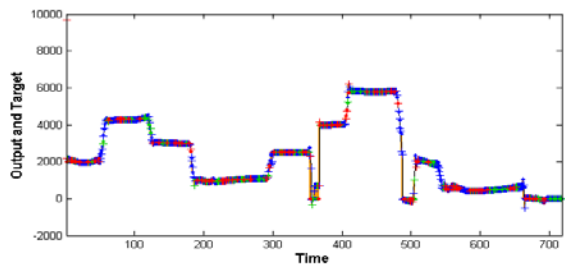
PV-FC batteries response for summer day of 2010/12/29



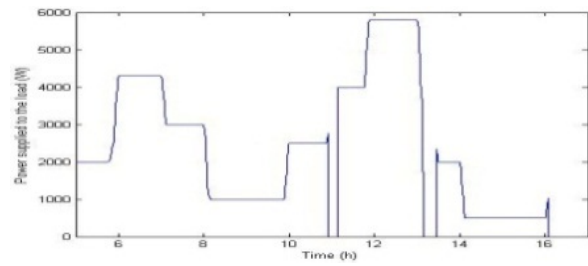
ANN Time – series response for winter day of 2011/06/07



PV-FC batteries response for winter day of 2011/06/07

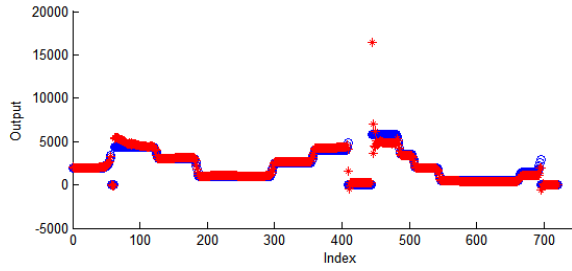


ANN Time – series response for winter day of 2011/06/28

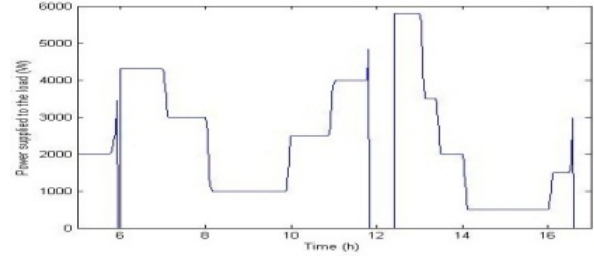


PV-FC batteries response for winter day of 2011/06/28

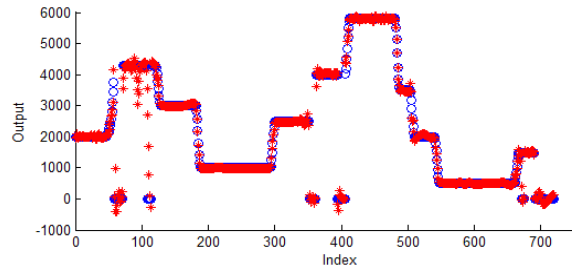
Figure 6.17: Time-series response of ANN for different weather conditions



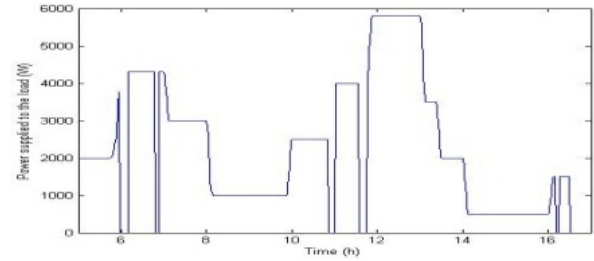
ANFIS Time – series response for summer day of 2010/12/22



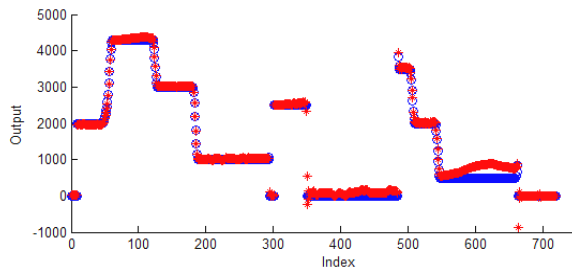
PV-FC batteries response for summer day of 2010/12/22



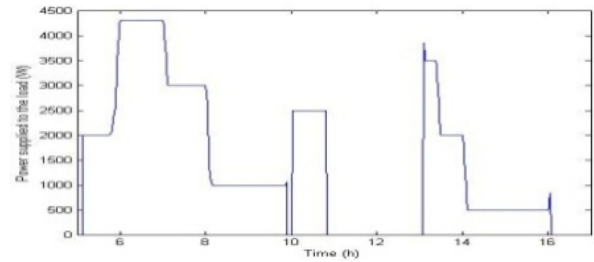
ANFIS Time – series response for summer day of 2010/12/29



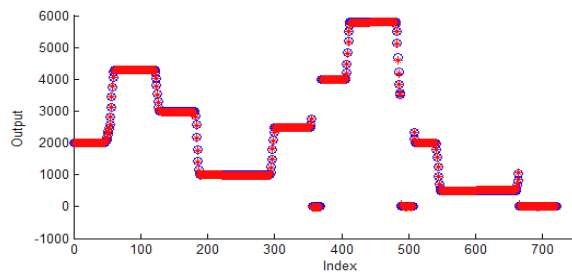
PV-FC batteries response for summer day of 2010/12/29



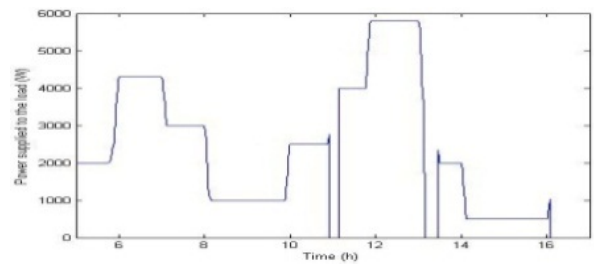
ANFIS Time – series response for winter day of 2011/06/07



PV-FC batteries response for winter day of 2011/06/07



ANFIS Time – series response for winter day of 2011/06/28



PV-FC batteries response for winter day of 2011/06/28

Figure 6.18: Time-series response of ANFIS for different weather conditions

6.8 Conclusion

Artificial network and the adaptive neuro-fuzzy interference system networks were developed for prediction and energy management of a hybrid photovoltaic-battery fuel cells system. The two systems were simulated and analysis conducted for four different weather conditions for the same variable load. The simulation results show that both systems give good results for a typical non-linear system which cannot easily be modeled by the use of classic control techniques. However, the ANFIS gives better results than the ANN as it is combining both ANN and fuzzy logic features.

References

- [1] M. Y. El-Sharkh, A. Rahman, M. S. Alam, P. C. Byrne, A. A. Sakla, and T. Thomas, "A dynamic model for a stand-alone PEM fuel cell power plant for residential application," *Journal of Power Sources*, vol. 138, pp. 199-204, 2004.
- [2] D. Rekioua, S. Bensmail, and N. Bettar, "Development of hybrid photovoltaic-fuel cell system for stand-alone application," *International Journal of Hydrogen Energy*, vol. 39, pp. 1604-1611, 2014.
- [3] T. El-Shatter, M. Eskandar, and M. El-Hagry, "Hybrid PV/Fuel system design and simulation," *Renewable Energy*, vol. 27, pp. 479-485, 2002.
- [4] S. B. Silva, M. M. Severino, and M. A. G. de Oliveira, "A stand-alone hybrid photovoltaic, fuel cell and battery system: a case study of Tocantins, Brazil," *Renewable Energy*, vol. 57, pp. 384-389, 2013.
- [5] N. M-A. Mutombo, F. L. Inambao, R. Tiako, and S. A. O. Ilupeju, "Energy management for stand-alone hybrid photovoltaic-PEM fuel cells systems," *International Journal of Applied Engineering Research*, 2017.
- [6] A. Mellit and S. A. Kalogirou, "Artificial intelligence techniques for photovoltaic applications: a review," *Progress in Energy and Combustion Science*, vol. 34, p. 574-632, 2008.
- [7] A. Mellit, S. A. Kalogirou, L. Hontoria, and S. Shaar, "Artificial intelligence techniques for sizing photovoltaic systems: a review," *Renewable and Sustainable Energy Reviews*, vol. 13, pp. 406-419, 2009.
- [8] Y. Ohsawa, S. Emura, and K. Arai, "Optimal operation of photovoltaic / diesel power generation system by neural network," in *Proceedings of the second international forum on applications of neural networks to power systems*, 1993.
- [9] A. Moreno, J. Julve, S. Silvestre, and L. Castaer, "A fuzzy logic controller for stand-alone PV systems," *IEEE*, p. 1618-1621, 2000.
- [10] A. Mellit, M. Benghanem, A. Hadj Arab, and A. Guessoum, "Use a fuzzy logic controller for control of stand-alone photovoltaic systems," in *Proceedings of IEEE 12th Mediterranean conference on control and automation*, Kusadaci, Turkey, 2004.
- [11] N. Patcharaprakiti, S. Premrudeepreechacharn, and Y. Sriuthaisiriwong, "Maximum power point tracking using adaptive fuzzy logic control for grid-connected photovoltaic system," *Renewable Energy*, vol. 30, p. 1771-1788, 2005.
- [12] A. B. G. Bahgat, N. H. Helwa, G. E. Ahamd, and E. T. El Shenawy, "Estimation of the maximum power and normal operating power of a photovoltaic module by neural networks," *Renewable Energy*, vol. 29, p. 443-457, 2004.
- [13] A. Abd El-Shafy, F. H. Nafeha, E. M. Fahmya, and D. Abou El-Zahabb, "Evaluation of a proper controller performance for maximum-power-point tracking of a stand-alone PV system," *Solar Energy Material Solar Cell*, vol. 75, p. 723-728, 2003.

- [14] A. Mellit and S. A. Kalogirou, "Neuro-fuzzy based modeling for photovoltaic power supply (PVPS) system," in Proceedings of the first international power and energy conference, IEEE, 28 and 29 November 2006, Else, Malaysia, 2006.
- [15] M. Abdulhadi, A. M. Al-Ibrahim, and G. S. Wirk, "Neuro-fuzzy based solar cell models," *IEEE Transaction Energy Conversion*, vol. 19, no. 3, p. 619-629, 2004.
- [16] M. Tekin, D. Hissel, M-C. Pera, and J. M. Kauffmann, "Energy-management strategy for embedded fuel-cell systems using fuzzy logic," *IEEE Transactions on Energy Conversion Industrial Electronics*, vol. 54, no. 1, pp. 595-603, 2007.
- [17] M. Hatti, "Neural network controller for P E M fuel cells," in *IEEE International Symposium on Industrial Electronics*, 2007.
- [18] N. Bhoopal, G. Venu Madhav, P. R. Pathapati, and J. Amarnath, "Modeling of polymer electrolyte membrane fuel cell using artificial neural networks," *International Journal of Recent Trends in Engineering*, vol. 2, p. 75, 2009.
- [19] S. M. Rakhtala, R. Ghaderi, A. Ranjbar, T. Fadaeian, and A. N. Niaki , "PEM fuel cell voltage-tracking using artificial neural network," in *IEEE Electrical Power & Energy Conference (EPEC)*, 2009.
- [20] A. L. Laura, "Compact hybrid power source using fuel cell and PV array," *International Journal of Science and Research Publications*, vol. 4, no. 11, 2014.
- [21] S. Rahman and K. Tam, "A feasibility study of photovoltaic-fuel cell hybrid energy system," *Transactions on Energy Conversion*, vol. 3, no. 1, pp. 50-55, 1988.
- [22] K. Tam and S. Rahman, "System performance improvement provided by a power conditioning system for central station photovoltaic-fuel cell power plant," *IEEE Transactions on Energy Conversion*, vol. 3, no. 1, pp. 64-70, 1988.
- [23] "L. Wei, Z. Xin-jian, and C. A. O. Guang-yi, "Modelling and control of a small solar fuel cell hybrid energy system," *Journal of Zheijiang University SCIENCE A*, vol. 8, no. 5, pp. 734-740, 2007.
- [24] S. G. McGowan and S. F. Manwell SF, "Hybrid/PV/diesel system experiences," *Revue Renewable Energy*, vol. 16, pp. 928-933, 1999.
- [25] M. Belhamel, S. Moussa, and A. Kaabeche "Production of electricity of a hybrid system (wind-photovoltaic-diesel)," *Review of Renewable Energy*, pp. 49-54, 2002.
- [26] A. El Khadimi, L. Bachir, and A. Zerowel, "Sizing optimization and techno-economic energy system hybrid photovoltaic-wind with storage system," *Renewable Energy Journal*, vol. 7, pp. 73-83, 2004.
- [27] N. M.-A. Mutombo, "Design and performance analysis of hybrid photovoltaic-thermal grid connected system for residential application," Master's dissertation, University of KwaZulu-Natal, Durban, SA, 2012.
- [28] A. Al-Alawi, S. M. Al-Alawi, and S. M. Islam, "Predictive control of an integrated PVdiesel water and power supply system using an artificial neural network," *Renewable Energy*, vol. 32, pp. 1426-1439, 2007.

- [29] A. A. Alawi, "An integrated PV-diesel hybrid water and power supply system for remote arid regions," Curtin University of Technology, Perth, 2004.
- [30] M. Veerachary, T. Senjyu, and K. Uezato, "Neural network based maximum power-point tracking of coupled inductor interleaved boost converter supplied PV system using fuzzy controller," *IEE Transactions on Industrial Electronics*, vol. 50, no. 4, 2003.
- [31] M. Veerachary, T. Senjyu, and K. Uezato, "Voltage-based maximum power point tracking control of PV systems," *IEEE Transactions on Aerospace Electronic Systems*, vol. 38, pp. 262-270, 2002.
- [32] W. B, "Control of photovoltaic-diesel hybrid energy system," Curtin University of Technology, Perth, 2000.
- [33] MathWorks, 2014, Fuzzy logic toolbox, getting start guide, MathWorks, 2013.
- [34] S. Rezazadeh, M. Mehrabi, T. Pashaei, and I. Mirzaei, "Using adaptive neuro-fuzzy interference system (ANFIS) for proton exchange membrane fuel cell (PEMFC) performance modelling," *Journal of Mechanical Science and Technology*, vol. 26, no. 11, pp. 3701-3709, 2012.
- [35] R. P. Lippmann, "Introduction to computing with neural nets," *IEE ASSP Magazine*, vol. 4, no. 2, pp. 4-22, 1987.
- [36] R. M. Tong, "A control engineering review of fuzzy systems," *Automatic*, vol. 13, no. 6, pp. 559-569, 1997.
- [37] J. S. R. Jang, "ANFIS: adaptive-network-based fuzzy interference system," *IEEE Transaction on Man and Cybernetic Systems*, vol. 23, no. 3, pp. 665-685, 1993.
- [38] H. T. Nguyen, N. R. Prasad, C. L. Walker, and E. A. Walker, *A First Course in Fuzzy and Neural Control*, Boca Raton, Florida: Chapman & Hall / CRC, 2003, p. 296.

CHAPTER 7 : CONCLUSION

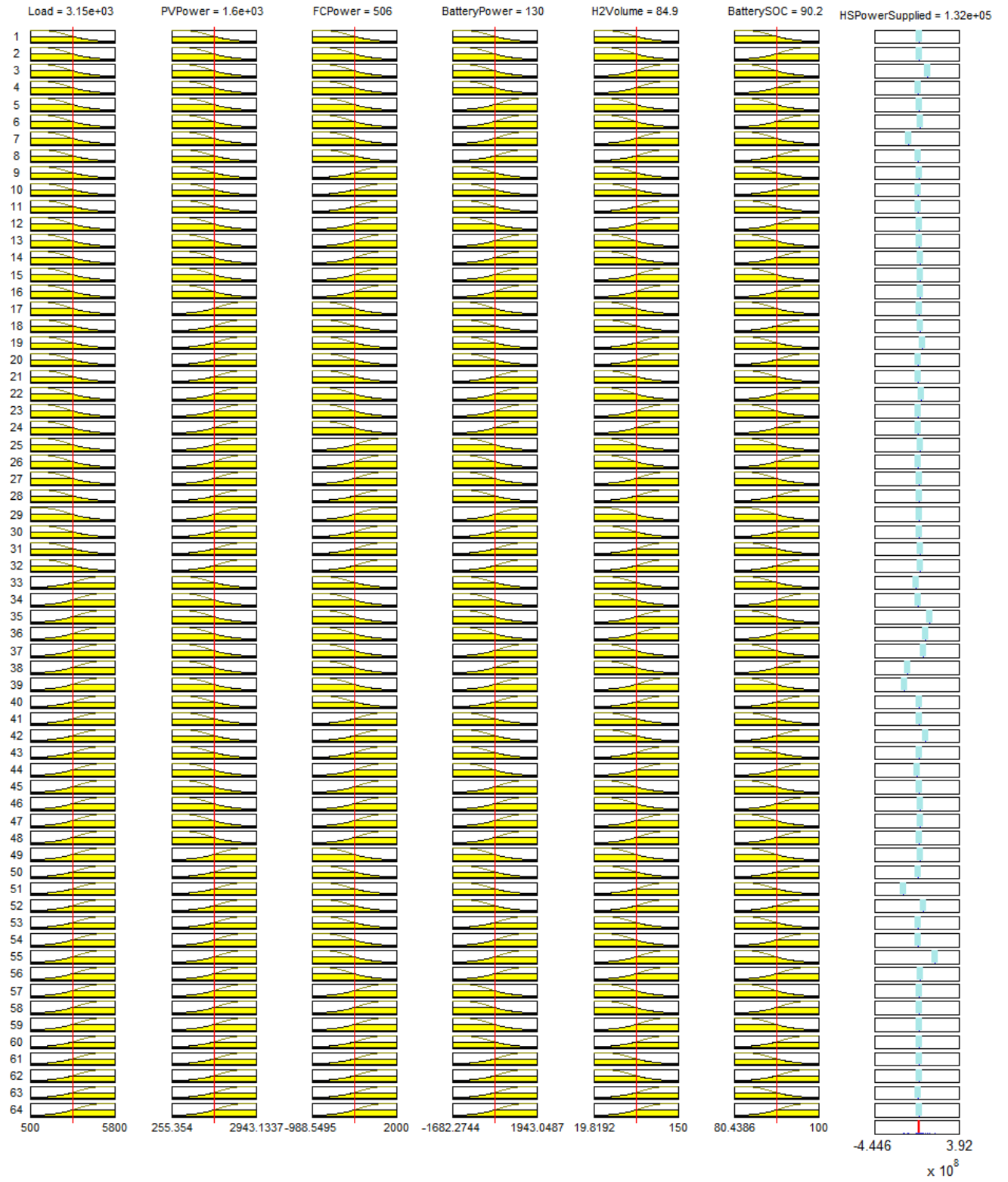
Hybrid system technology in the field of renewable energy is and continues to be explored. Different techniques have been developed for design, prediction, etc. for those technologies. Nevertheless, the management and control of flow of energy from different components remains an interesting and potential research field particularly with the growing use of artificial intelligence tools.

In this work, an adaptive neuro-fuzzy interference system for prediction and management of a hybrid renewable energy system consisted of a photovoltaic generator, a proton exchange membrane-fuel cells stack and a battery bank was developed using particular data for electric energy demand of a modest household in Durban, South Africa. Based on simulation results obtained, the system has succeeded to predict and assure the management of the energy flow of different components of the system accurately.

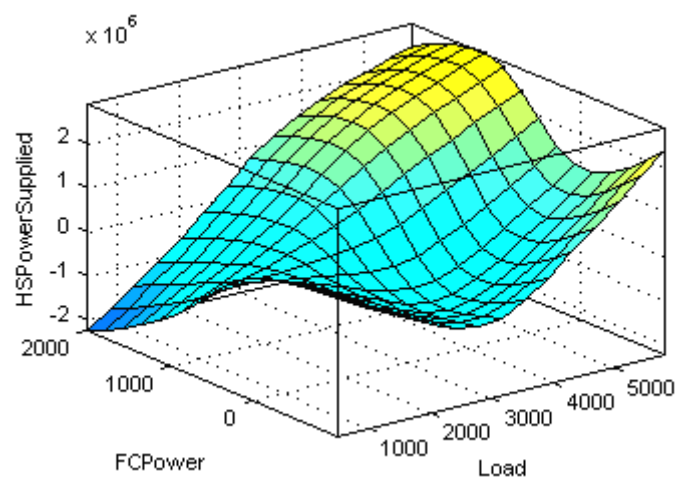
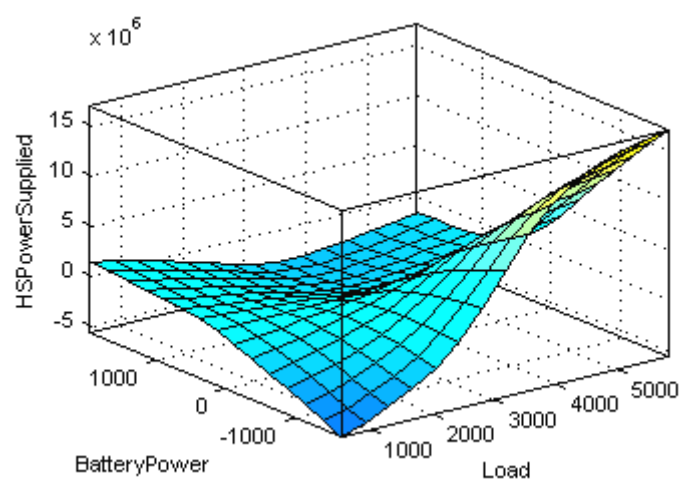
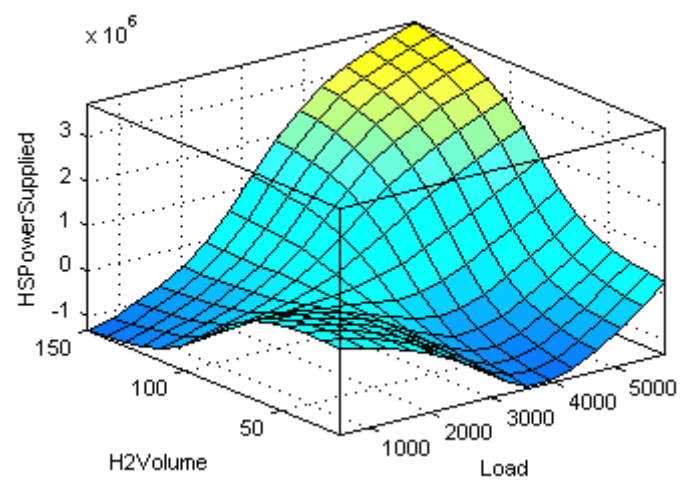
However, for a better performance of the system, the development and construction of a controller equipped with advanced supervisor techniques from results of this present work could have a great impact and would be an advance in the improvement of the energy flow management and control of this type of system.

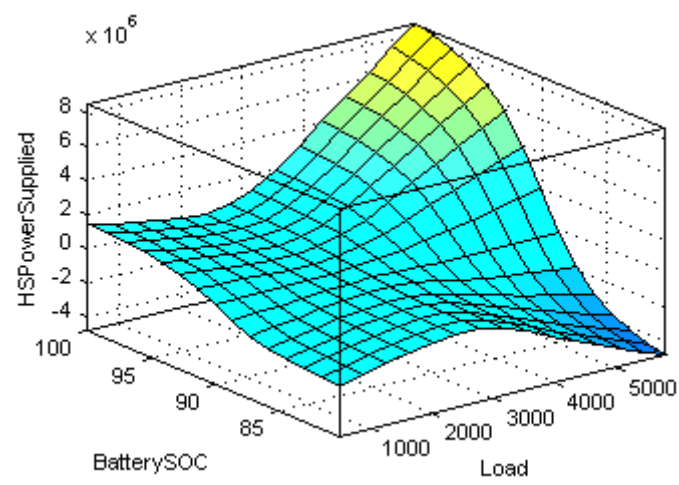
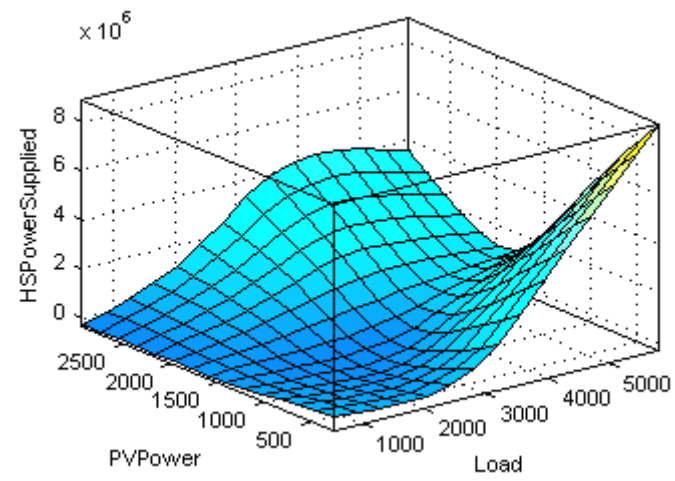
APPENDICES

Appendix A: ANFIS membership functions



Appendix B: ANFIS inputs – output surfaces





Appendix C: Design and Analysis of Grid-Connected Photovoltaic System for Residential Applications Case Studied of Durban, South Africa

African Journal of Science, Technology, Innovation and Development DESIGN AND ANALYSIS OF GRID-CONNECTED PHOTOVOLTAIC SYSTEM FOR RESIDENTIAL APPLICATION - CASE STUDY, DURBAN, SOUTH AFRICA --Manuscript Draft--

Full Title:	DESIGN AND ANALYSIS OF GRID-CONNECTED PHOTOVOLTAIC SYSTEM FOR RESIDENTIAL APPLICATION - CASE STUDY, DURBAN, SOUTH AFRICA
Manuscript Number:	RAJS-2016-0216
Article Type:	Original Article
Keywords:	design, analysis, photovoltaic, array, economy
Abstract:	<p>With its economic growth and increase in population, South Africa needs more electrical energy than ever before. The supply of electrical energy for mining companies has been prioritised over domestic use, penalising families with blackouts and neglecting remote areas. Nevertheless, the surface of the country is irradiated by large amounts of sunlight, therefore photovoltaic systems are one option among other renewable energy technologies to remediate this situation, particularly for remote areas and for household electricity demand. Solar power is considered to be one of the most reliable sources of renewable energy available today.</p> <p>This paper presents the design and simulation of a photovoltaic system for household demand for South Africa. The design is based on a particular case of Durban weather conditions and simulated with the Matlab package. After an economic analysis, it was found that the system could meet the need for electrical energy in summer time based on sunlight received, but in winter time the performance was low. To compensate for low irradiance, the system could be coupled with other renewable energy technologies such as a fuel cell system to make a hybrid system.</p>
Order of Authors:	Ntumba Marc-Alain Mutombo, MSc. Freddie L. Inambao, PhD Remy Tiako, PhD
Section/Category:	Quantative

Appendix D: Fuel cells development, applications and market

Mardi 21 mars 2017 13h52

RECEIPT OF NEW MANUSCRIPT

De: "ARPN Journal of Engineering and Applied Sciences" arpn@arnpjournals.com

A: marcntumba@yahoo.fr

Dear Sir / Madam,

We would like to inform you that we have received a manuscript titled " Fuel Cells Development, Applications and Market " for publication in the ARPN Journal of Engineering and Applied Sciences. Shortly we will send your submitted manuscript to the reviewers. After approval from referees, your paper will be published in the next available Issue of the Journal. Please quote the title of your research paper while making correspondance with us. Please do not send frequent e-mails asking recent status of your paper. We will contact you as and when required. Please note that we are charging a fee for processing of your research article (Article Processing Charge-APC). If you are willing to pay Article Processing Charge, then please visit our website and browse on the **Publication Fee** button for getting detailed information regarding our payment procedure. Now we are accepting your payments through PayPal, Credit Cards and Debit Cards also. These payments are made to ARPN through the secured PayPal Payment System (PayPal, USA) and through the Fast Spring online store (a USA based company). **Please note that we do not process any paper before receipt of the payment.** Please pay APC just after sending your paper (before reviewing process). Do not wait for the approval of your paper. We charge only APC. There is no other charges (No hidden charges). If you do not want to pay, send an e-mail to us. We will not process your research paper. Thank you very much for your interest in ARPN Journals.

Sincerely yours

Publishing
ARPN
URL:
arpn@arnpjournals.com (21/03/2017)

Editor
Journals
<http://www.arnpjournals.com>

Appendix E: Energy management for stand-alone hybrid photovoltaic-PEM fuel cells systems

From: Research India Publications <ripjournal@gmail.com>

Sent: 08 February 2017 12:06 PM

To: Samuel A Ilupeju

Subject: Paper Accepted for IJAER Paper Code: 51327

Paper Accepted for IJAER Paper Code: 51327

Dear **Dr. Samuel A. O. Ilupeju,**

Paper Code: 51327

We are very pleased to inform you that your paper "**ENERGY MANAGEMENT FOR STAND ALONE HYBRID PHOTOVOLTAIC – PEM FUEL CELLS SYSTEMS**" is accepted by our Editor-in-chief for our journal **International Journal of Applied Engineering Research (IJAER)**. Please find attached copyright transfer form.

Publication Charges is \$ 580.00 (US \$ Five Hundred Eighty only)

Publication Charges include One Print Journal copy, PDF Copy and free online access to journal issue. Please send us signed copy of copyright form along with **CHEQUE/DRAFT in US\$ PAYABLE TO "RESEARCH INDIA PUBLICATIONS"**. You can also send payment by Credit Card.

If pay by bank transfer, please add extra US\$ 30.00 for bank charges. Our bank information is given below :

SWIFT CODE -----CITIINBX

Credit to -----RESEARCH INDIA PUBLICATIONS

Account No.-----0031384222

Name of Bank-----CITIBANK N. A

Address -----27, Central Market, West Punjabi Bagh, NEW DELHI-110026, INDIA

Last date of submission of forms and payment is 24th February 2017

Please inform us when you transfer payment to our account so that we can track your payment.

Thanking you and hope to hear from you soon,

With kind regards,

Viveka Nand

Publication Department

=====

Research India Publications

B-2/84, Ground Floor, Rohini Sec-16

Delhi-110089 INDIA

Website: www.ripublication.com

Appendix F: Neuro-fuzzy strategies for prediction and management of hybrid PV PEMFC batteries systems

From: authors@scientific.net <authors@scientific.net>

Sent: 19 March 2017 07:11 PM

To: Samuel A Ilupeju

Subject: Copyright Transfer Confirmation for Article: Neuro-Fuzzy Strategies for Prediction and Management of Hybrid Pv-PEMFC Batteries Systems

Copyright Transfer Confirmation Receipt:

=====

Publication Title: JERA

Article Title: Neuro-Fuzzy Strategies for Prediction and Management of Hybrid Pv-PEMFC Batteries Systems

Congratulations!

Dear Colleague

Congratulations! You have successfully completed the Scientific.Net Electronic Copyright Form. A copy of the fully executed Form is attached here for your records. Please save this e-mail for any future reference.

Best regards,
Team Scientific.Net

Appendix G: Matlab code to load data set for simulation

```
function [t, G, T_pv, P_l, deltat] = DataforSim
%
% This matlab function import data from excel file for simulation
% written by Ntumba Marc - Alain Mutombo
% 02/February/2016
%
% IMPORT DATA
filename = 'DataforSim.xlsx';
% Import data for simulation from excel format with:
% sheet 2: Summer day of 2010/12/22
% sheet 3: Summer day of 2010/12/29
% sheet 4: Winter day of 2011/06/07
% sheet 5: Winter day of 2011/06/28
%
sheet = 4;
data = xlsread(filename, sheet);
td = data(:,1)'; % Read time data (second)
Gd = data(:,2)'; % Read irradiance data (kW/m2)
T_pvd = data(:,3)'; % Read load data (W)
P_ld = data(:,4)'; % Read load data (W)
% deltat = 1/8;
% //////////////////////////////////////
n = 60*(max(td)-min(td)); % points linearly spaced between t min and tmax
deltat = (max(td)-min(td))/(n-1); % Time increment
%
t = linspace(min(td),max(td),n); % Set points for interpolation
G = interp1(td,Gd,t,'PCHIP'); % Do PCHIP interpolation
T_pv = interp1(td,T_pvd,t,'PCHIP'); % Do PCHIP interpolation
P_l = interp1(td,P_ld,t,'PCHIP'); % Do PCHIP interpolation
%
```

Appendix H: Matlab code to calculate module current under given voltage, irradiance and temperature

```
function I_pv = PV_Current(G,T_pv,V_pv)
% function PV_Current.m models the Q 250 PV module
% calculates module current under given voltage, irradiance and temperature
% I_pv = PV_Current(G,T_pv,V_pv)
%
% Out: I_pv = Module operating current (A), vector or scalar
% In: V_pv = Module operating voltage (V), vector or scalar
% G = Irradiance (1G = 1000 W/m^2), scalar
% T_pc = Module temperature in deg C, scalar
%
% Written by Akihiro Oi 7/01/2005
% Revised by Ntumba Marc-Alain Mutombo
% 02/February/2016
%
%//////////////////////////////////////
/
% Values for the code test
% G = [400 600 1200 800];
% T_pv = [25 35 50 40];
% V_pv = 24;
%
%%
% Define constants
k = 1.381e-23; % Boltzmann's constant
q = 1.602e-19; % Electron charge
% Following constants are taken from the datasheet of PV module and
% curve fitting of I-V character (Use data for 1000W/m^2)
n = 1.62; % Diode ideality factor (n),
% 1 (ideal diode) < n < 2
Eg = 1.12; % Band gap energy; 1.12eV (Si), 1.42 (GaAs),
% 1.5 (CdTe), 1.75 (amorphous Si)
Ns = 60; % # of series connected cells (BP SX150s, 72 cells)
TrK = 298; % Reference temperature (25C) in Kelvin
Voc_TrK = 37.15 /Ns; % Voc (open circuit voltage per cell) @ temp TrK
Isc_TrK = 9.07; % Isc (short circuit current per cell) @ temp TrK
a = 0.65e-3; % Temperature coefficient of Isc (0.065%/C)
% Define variables
TaK = 273*ones(size(T_pv)) + T_pv; % Module temperature in Kelvin
Vc = V_pv / Ns; % Cell voltage
% Calculate short-circuit current for TaK
Isc = Isc_TrK * (1 + (a * (TaK - TrK)));
% Calculate photon generated current @ given irradiance
Iph = Isc .* G ./1000;
% Define thermal potential (Vt) at temp TrK
Vt_TrK = n * k * TrK / q;
% Define b = Eg * q/(n*k);
b = Eg * q /(n * k);
% Calculate reverse saturation current for given temperature
Ir_TrK = Isc_TrK / (exp(Voc_TrK / Vt_TrK) -1);
Ir = Ir_TrK .* (TaK ./ TrK).^(3/n) .* exp(-b .* (1 ./ TaK -ones(size(T_pv))
./ TrK));
% Calculate series resistance per cell (Rs = 5.1mOhm)
dVdI_Voc = -1.0/Ns; % Take dV/dI @ Voc from I-V curve of datasheet
Xv = Ir_TrK / Vt_TrK * exp(Voc_TrK / Vt_TrK);
Rs = - dVdI_Voc - 1/Xv;
% Define thermal potential (Vt) at temp Ta
```



```

Vt_Ta = n * k * TaK / q;
% Ia = Iph - Ir * (exp((Vc + Ia * Rs) / Vt_Ta) - 1)
% f(Ia) = Iph - Ia - Ir * ( exp((Vc + Ia * Rs) / Vt_Ta) - 1) = 0
% Solve for Ia by Newton's method: Ia2 = Ia1 - f(Ia1)/f'(Ia1)
I_pv = zeros(size(Vc)); % Initialize Ia with zeros
% Perform 5 iterations
for j = 1:5;
I_pv = I_pv - (Iph - I_pv - Ir .* ( exp((Vc + I_pv .* Rs) ./ Vt_Ta) - 1))...
./ (-1 - Ir .* (Rs ./ Vt_Ta) .* exp((Vc + I_pv .* Rs) ./ Vt_Ta));
end
%
```

Appendix I: Matlab code to determine the maximum power point of the PV module

```
function [Pa_max, Imp, Vmp] = find_mpp(G,T_pv)
% find_mpp: function to find a maximum power point of pv module
% [Pa_max, Imp, Vmp] = find_mpp(G, TaC)
% in: G (irradiance, KW/m^2), TaC (temp, deg C)
% out: Pa_max (maximum power), Imp, Vmp
%
% Written by Akihiro Oi July 27, 2005
% Revised by Ntumba Marc-Alain Mutombo
% 02/February/2016
%

%%%%%%%%%%%%%%%%%%%%%%%%%%%%%%%%%%%%%%%%%%%%%%%%%%%%%%%%%%%%%%%%%%%%%%%%%%%%%%
% Define variables and initialize
% T_pv = 25;
Va = 12;
Pa_max = 0;
% Start process
while Va < 48-T_pv/8
Ia = PV_Current(G,T_pv,Va);
Pa_new = Ia * Va;
if Pa_new > Pa_max
Pa_max = Pa_new;
Imp = Ia;
Vmp = Va;
end
Va = Va + .005;
end
%
```

Appendix J: Matlab function calculates the output power of the PV module or array

```
function [P_pv, V_pv, I_pv] = PV_Power
%
% This matlab function calculate the output power of the PV module or array
% Written by Ntumba Marc-Alain Mutombo
% 17/May/2016
%
%% Values for code test
[t, G, T_pv, P_l, deltat] = DataforSim;
%
%%
Npvs = 8;
Npvp = 3;
%
for s = 1:length(G)
    Gi = G(s);
    T_pvi = T_pv(s);
    V_pvi = linspace (0, 37.15, 200);
    I_pvi = PV_Current(Gi,T_pvi,V_pvi);
    [Pa_max, Imp, Vmp] = find_mpp(Gi, T_pvi);
    I_pv(s) = Npvp*Imp;
    V_pv(s) = Npvs*Vmp;
    P_pv(s) = V_pv(s)*I_pv(s);
end
%
```

Appendix K: Matlab code to determine the energy management of the hybrid photovoltaic fuel cells system equipped with batteries bank

```
% Function EnergyMgmt.m determine the energy management of the hybrid
% of the hybrid photovoltaic fuel cells system equipped with batteries bank.
% written by Ntumba Marc-Alain Mutombo
% September 17, 2016
% //////////////////////////////////////////////////
%%
clear
% Input values
[t, G, T_pv, P_l, deltat] = DataforSim;
[P_pv, V_pv, I_pv] = PV_Power;
%
% Initial values
P_fc(1) = 1e-5;
P_b(1) = 1500;
V_tk(1) = 150;
SOC(1) = 90;
Q_b(1) = 120;
%
% //////////////////////////////////////////////////
% Constants
R = 8.3145; % Gas constant (J/molK)
F = 96485; % Faraday constant (As/mol)
k = 1.38e-23; % Boltzmann's constant(J/K)
h = 6.626e-34; % Planck's constant(J.s)
m_H2 = 0.037605; % Hydrogen produced per a current of 1 kA in one hour
[kg/kAh]
rho_H2 = 0.083; % Hydrogen gas density at 1 atm and 21.1C [l/min]
%
% //////////////////////////////////////////////////
% Battery bank specifications
V_b_single = 24;
Q_b_max = 120;
SOC_min = 40;
Nbs = 4;
Q_b_maxx = 0.95*Q_b_max;
V_b = Nbs*V_b_single;
P_b_max = V_b*Q_b_maxx/deltat;
%
% Hydrogen system informations
% Electrolyser specifications
P_el_max = 3500;
V_el = 48;
% Fuel cell specifications
V_fc_perf = 28.8;
i_fc_perf = 70;
V_fc_SD = 24;
i_fc_SD = 90;
P_fc_RP = 2000;
T_fc = 65;
N = 48; % Number of series cells in stack
r_fc = 0.0217 ; % Internal resistance of fuel cell
Kc = 0.946; % Voltage constant (Kc<=1)
x = 99.9999; % Percentage of hydrogen in the fuel (%)
y = 21; % Percentage of oxygen in the oxidant (%)
Z = 2; % Number of moving electrons
alpha = 1; % Charge transfer coefficient
```

```

dG = 0.049; % Gibbs(V)
v_H2 = 26; % Flow rates of hydrogen (L/min)
v_O2 = 60; % Flow rates of air (L/min)
p_H2 = 0.49344; % Supply pressure of hydrogen (atm Nota:1 atm = 1.0133 bar)
p_O2 = 1; % Supply pressure of air (atm)
%
V_fc_max = 2*V_fc_perf - V_fc_SD; % Maximum fuel cell voltage
i_fc_min = (V_fc_max - V_fc_SD)*(i_fc_perf - i_fc_SD)/(V_fc_perf - V_fc_SD)
+ i_fc_SD; % Minimum fuel cell current calculation
%
% Hydrogen tank
V_tk_min = 20;
v_tk_out = v_H2;
P_el_max = 3500;
P_el_min = 500;
%
% //////////////////////////////////////
%%
for s = 1:length(t)
    if P_l(s) < P_pv(s)
        P_fc(s) = 0;
        P_b(s) = P_l(s) - P_pv(s);
        P_lr(s) = P_l(s);
    else
        if V_tk_min < V_tk(s)
            if P_l(s) - P_pv(s) < P_fc(s)
                P_fc(s) = P_l(s) - P_pv(s);
                P_b(s) = 0;
                P_lr(s) = P_l(s);
            else
                if SOC_min < SOC(s)
                    if P_l(s) - P_pv(s) - P_fc(s) < P_b(s)
                        P_fc(s) = P_fc(s);
                        P_b(s) = P_l(s) - P_pv(s) - P_fc(s);
                        P_lr(s) = P_l(s);
                    else P_fc(s) = 0;
                        P_b(s) = 0;
                        P_lr(s) = 0;
                    end
                else P_fc(s) = 0;
                    P_b(s) = - P_pv(s);
                    P_lr(s) = 0;
                end
            end
        else
            if SOC_min < SOC(s)
                if P_l(s) - P_pv(s) < P_b(s)
                    P_fc(s) = 0;
                    P_b(s) = P_l(s) - P_pv(s);
                    P_lr(s) = P_l(s);
                else P_fc(s) = - P_pv(s);
                    P_b(s) = 0;
                    P_lr(s) = 0;
                end
            else P_fc(s) = 0;
                P_b(s) = - P_pv(s);
                P_lr(s) = 0;
            end
        end
    end
end
end

```

```

%
%
%%%%%%%%%%%%%%%%%%%%%%%%%%%%%%%%%%%%%%%%%%%%%%%%%%%%%%%%%%%%%%%%%%%%%%%%
% Hydrogen production and storage calculation
% Electrolyser power and current calculation
if P_fc(s) > 0
    P_el_new = 0;
elseif P_fc(s) <= 0
    if abs(P_fc(s)) >= P_el_max
        P_el_new = P_el_max;
    else P_el_new = P_fc(s);
    end
end
P_el(s) = - P_el_new;
P_el_new = abs(P_el(s));
if P_el_new >= P_el_max
    P_el(s) = P_el_max;
else P_el(s) = P_el_new;
end
i_el(s) = P_el(s)/V_el;
%
% Volume of hydrogen in the tank
if P_fc(s) <= 0
    if P_el(s) > 0
        v_tk_in(s) = (m_H2/(60*rho_H2))*i_el(s);
        v_tk_out(s) = 0;
    else v_tk_in(s) = 0;
        v_tk_out(s) = 0;
    end
else v_tk_in(s) = 0;
    v_tk_out(s) = v_H2;
end
V_tk(s+1) = V_tk(s)+(v_tk_in(s)-v_tk_out(s))*deltat;
%
%
%%%%%%%%%%%%%%%%%%%%%%%%%%%%%%%%%%%%%%%%%%%%%%%%%%%%%%%%%%%%%%%%%%%%%%%%
% Fuel cell parameters calculation
% Fuel cell power calculation
P_fc_new = P_l(s) - P_pv(s);
if P_fc_new <= 0
    P_fc(s+1) = 1e-5;
elseif P_fc_new > P_fc_RP
    P_fc(s+1) = P_fc_RP;
else P_fc(s+1) = P_fc_new;
end
i_fc(s+1) = P_fc(s+1)/V_fc_perf;
% FC voltage calculation
% Temperature of operation (K)
T_fc = 273 + T_fc;
% Tafel slope
A= R*T_fc/(alpha*Z*F);
% Fuel and oxydant conversion rate ( )
U_H2 = 60000*R*T_fc*N*i_fc(s+1)/(Z*F*p_H2*v_H2*x);
U_O2 = 60000*R*T_fc*N*i_fc(s+1)/(2*Z*F*p_O2*v_O2*y);
% Partial pressures calculation (atm)
p_H2 = (1-U_H2)*(x)*p_H2;
p_O2 = (1-U_O2)*(y)*p_O2;
%

```

```

En = 1.229+(T_fc-298)*(-
44.43)/(Z*F)+(R*T_fc/(Z*F))*log(p_H2.*(p_O2).^(1/2));
Eoc = Kc*En;
% Current calculation (A)
io = (Z*F*k*(p_H2+p_O2)*exp(dG/(R*T_fc)))/(R*h);
% Fuel cell stack voltage calculation (V)
V_fc(s+1) = Eoc-N*A*log(i_fc(s+1)/io)-i_fc(s+1)*r_fc;
V_fc(s+1) = real(V_fc(s+1));
i_fc(s+1) = P_fc(s+1)/V_fc(s+1);
%
%
%%%%%%%%%%%%%%%%%%%%%%%%%%%%%%%%%%%%%%%%%%%%%%%%%%%%%%%%%%%%%%%%%%%%%%%%%%%%%%
% Battery bank parameters calculation
% calculation of the state of charge of the battery bank
I_b(s) = P_b(s) / V_b;
Q_b_new = Q_b(s)-I_b(s)*deltat;
if Q_b_new <= 0
    Q_b(s+1) = 0;
elseif Q_b_new >= Q_b_max
    Q_b(s+1) = Q_b_max;
else Q_b(s+1) = Q_b_new;
end
P_b(s+1) = P_lr(s) - P_pv(s);
SOC(s+1) = 100*Q_b(s+1)/Q_b_max;
P_bs(s+1) = V_b * Q_b(s+1)*deltat;
%
end
%
% a = [1,2,3,4,5] than a = a([1:2, 4:end]) = [1,2,4,5]
P_fc = P_fc([1:720]);
V_fc = V_fc([1:720]);
i_fc = i_fc([1:720]);
%
V_tk = V_tk([1:720]);
%
P_b = P_b([1:720]);
P_bs = P_b([1:720]);
SOC = SOC([1:720]);
Q_b = Q_b([1:720]);
%
%% Display results
X = [P_l' P_lr' P_pv' P_fc' P_b' P_el' V_tk' SOC'];
disp('P_l P_lr P_pv P_fc P_b P_el V_tk SOC')
disp(X)
%
P_l_mean = mean(P_l)
P_l_rms = rms(P_l)
P_lr_mean = mean(P_lr)
P_lr_rms = rms(P_lr)
error_Pl = 100*(P_l-P_lr)./P_l
%
Y = [P_l_mean P_lr_mean P_l_rms P_lr_rms error_Pl];
disp('P_l_mean P_lr_mean P_l_rms P_lr_rms error_Pl')
disp(Y)
%
XX = [P_l' P_pv' P_fc' P_b' V_tk' SOC'];
XX_trn = XX(1:2:end,:);
XX_chk = XX(2:2:end,:);
XX_tst = XX(1:3:end,:);

```

```

YY = [P_lr'];
YY_trn = YY(1:2:end,:);
YY_chk = YY(2:2:end,:);
YY_tst = YY(1:3:end,:);

ZZ = [P_l' P_pv' P_fc' P_b' V_tk' SOC' P_lr'];
ZZ_chk = ZZ(1:2:end,:);
ZZ_tst = ZZ(1:3:end,:);
%
%% Plot figures
figure; % Display figure 1
[AX,H1,H2] = plotyy(t,G,t,T_pv,'plot');
set(get(AX(1),'Ylabel'),'String','Irradiance (kW/m²)')
set(get(AX(2),'Ylabel'),'String','Ambient temperature (°C)')
xlabel('Time (h)');
set(H1,'LineStyle','-')
set(H2,'LineStyle','-')
h = legend('Irradiance','Ambient temp.',2);
grid off;
%
figure % Plot figure 2
plot(t,P_l)
xlabel('Time (h)');
ylabel('Load (W)');
xlim([5 17])
%
figure % Plot figure 3
plot(t,P_lr)
xlabel('Time (h)');
ylabel('Power supplied to the load (W)');
xlim([5 17])
%
figure % Plot figure 4
plot(t,error_Pl)
xlabel('Time (h)');
ylabel('Relative error (Percent)');
xlim([5 17])
%
figure % Plot figure 5
plot(t,P_pv)
xlabel('Time (h)');
ylabel('PV power (W)');
xlim([5 17])
%
figure % Plot figure 6
plot(t,P_fc)
xlabel('Time (h)');
ylabel('FC power (W)');
xlim([5 17])
%
figure % Plot figure 7
plot(t,P_b)
xlabel('Time (h)');
ylabel('Battery power (W)');
xlim([5 17])
%
figure % Plot figure 8
plot(t,SOC)
xlabel('Time (h)');
ylabel('SOC (Percent)');

```



```

xlim([5 17])
%
figure % Plot figure 9
plot(t,P_el)
xlabel('Time (h)');
ylabel('Electrolyser power (W)');
xlim([5 17])
%
figure % Plot figure 10
plot(t,V_tk)
xlabel('Time (h)');
ylabel('H2 volume (l)');
xlim([5 17])
%
end
%
```

Appendix L: Solving an input-output time-series problem with a time delay neural network

```
% Solve an Input-Output Time-Series Problem with a Time Delay Neural Network
% Script generated by Neural Time Series app.
% Created Sun Feb 26 10:20:45 CAT 2017
%
% This script assumes these variables are defined:
%
% XX - input time series.
% YY - target time series.

[XX, YY, ZZ] = EnergyMgmt;

X = tonndata(XX,false,false);
T = tonndata(YY,false,false);

% Choose a Training Function
% For a list of all training functions type: help nntrain
% 'trainlm' is usually fastest.
% 'trainbr' takes longer but may be better for challenging problems.
% 'trainscg' uses less memory. NTSTOOL falls back to this in low memory
situations.
trainFcn = 'trainlm'; % Levenberg-Marquardt

% Create a Time Delay Network
inputDelays = 1:2;
hiddenLayerSize = 10;
net = timedelaynet(inputDelays,hiddenLayerSize,trainFcn);

% Choose Input and Output Pre/Post-Processing Functions
% For a list of all processing functions type: help nnprocess
net.input.processFcns = {'removeconstantrows','mapminmax'};
net.output.processFcns = {'removeconstantrows','mapminmax'};

% Prepare the Data for Training and Simulation
% The function PREPARETS prepares timeseries data for a particular network,
% shifting time by the minimum amount to fill input states and layer states.
% Using PREPARETS allows you to keep your original time series data
unchanged, while
% easily customizing it for networks with differing numbers of delays, with
% open loop or closed loop feedback modes.
[x,xi,ai,t] = preparets(net,X,T);

% Setup Division of Data for Training, Validation, Testing
% For a list of all data division functions type: help nndivide
net.divideFcn = 'dividerand'; % Divide data randomly
net.divideMode = 'time'; % Divide up every value
net.divideParam.trainRatio = 70/100;
net.divideParam.valRatio = 15/100;
net.divideParam.testRatio = 15/100;

% Choose a Performance Function
% For a list of all performance functions type: help nnperformance
net.performFcn = 'mse'; % Mean squared error

% Choose Plot Functions
```

```

% For a list of all plot functions type: help nnplot
net.plotFcns = {'plotperform','plottrainstate','plotresponse', ...
    'ploterrcorr', 'plotinerrcorr'};

% Train the Network
[net,tr] = train(net,x,t,xi,ai);

% Test the Network
y = net(x,xi,ai);
errors = gsubtract(t,y);
performance = perform(net,t,y)

% Recalculate Training, Validation and Test Performance
trainTargets = gmultiply(t,tr.trainMask);
valTargets = gmultiply(t,tr.valMask);
testTargets = gmultiply(t,tr.testMask);
trainPerformance = perform(net,trainTargets,y)
valPerformance = perform(net,valTargets,y)
testPerformance = perform(net,testTargets,y)

% View the Network
view(net)

% Plots
% Uncomment these lines to enable various plots.
%figure, plotperform(tr)
%figure, plottrainstate(tr)
%figure, plotresponse(t,y)
%figure, ploterrcorr(e)
%figure, plotinerrcorr(x,e)

% Early Prediction Network
% For some applications it helps to get the prediction a timestep early.
% The original network returns predicted y(t+1) at the same time it is given
x(t+1).
% For some applications such as decision making, it would help to have
predicted
% y(t+1) once x(t) is available, but before the actual y(t+1) occurs.
% The network can be made to return its output a timestep early by removing
one delay
% so that its minimal tap delay is now 0 instead of 1. The new network
returns the
% same outputs as the original network, but outputs are shifted left one
timestep.
nets = removedelay(net);
[xs,xis,ais,ts] = preparets(nets,X,T);
ys = nets(xs,xis,ais);
earlyPredictPerformance = perform(net,ts,ys)
% Deployment
% Change the (false) values to (true) to enable the following code blocks.
% See the help for each generation function for more information.
if (false)
    % Generate MATLAB function for neural network for application deployment
    % in MATLAB scripts or with MATLAB Compiler and Builder tools, or simply
    % to examine the calculations your trained neural network performs.
    genFunction(net,'myNeuralNetworkFunction');
    y = myNeuralNetworkFunction(x,xi,ai);
end
if (false)

```

```

% Generate a matrix-only MATLAB function for neural network code
% generation with MATLAB Coder tools.
genFunction(net,'myNeuralNetworkFunction','MatrixOnly','yes');
x1 = cell2mat(x(1,:));
xi1 = cell2mat(xi(1,:));
y = myNeuralNetworkFunction(x1,xi1);
end
if (false)
% Generate a Simulink diagram for simulation or deployment with.
% Simulink Coder tools.
gensim(net);
end
%
```

Appendix M: Matlab code to predict power supplied to the load time-series adaptive neuro-fuzzy interference system

```
% Predict Power Supplied to the Load Time-Series (Code)

%% generates this data
[t, ZZ, ZZ_trn, ZZ_chk] = EnergyMgmt;
time = t;
x = ZZ(:,7);

for ii=19:718,
Data(ii,:)=[ZZ(ii,1) ZZ(ii,2) ZZ(ii,3) ZZ(ii,4) ZZ(ii,5) ZZ(ii,6) ZZ(ii,7)];
end
trnData=Data(1:350,:);
chkData=Data(351:700,:);

%% Training data
fismat = genfis1(trnData);

figure(2)
subplot(3,2,1)
plotmf(fismat, 'input', 1)
subplot(3,2,2)
plotmf(fismat, 'input', 2)
subplot(3,2,3)
plotmf(fismat, 'input', 3)
subplot(3,2,4)
plotmf(fismat, 'input', 4)
subplot(3,2,5)
plotmf(fismat, 'input', 5)
subplot(3,2,6)
plotmf(fismat, 'input', 6)

[fismat1,error1,ss,fismat2,error2] = ...
    anfis(trnData,fismat,[],[],chkData);

figure(3)
subplot(3,2,1)
plotmf(fismat2, 'input', 1)
subplot(3,2,2)
plotmf(fismat2, 'input', 2)
subplot(3,2,3)
plotmf(fismat2, 'input', 3)
subplot(3,2,4)
plotmf(fismat2, 'input', 4)
subplot(3,2,5)
plotmf(fismat2, 'input', 5)
subplot(3,2,6)
plotmf(fismat2, 'input', 6)

%% Plot the error signals
figure(4)
plot([error1 error2]);
hold on; plot([error1 error2], 'o');
xlabel('Epochs');
ylabel('RMSE (Root Mean Squared Error)');
title('Error Curves');
```

```

%% Plot the FIS output versus the training or checking data
figure(5)
anfis_output = evalfis([trnData(:,1:6); chkData(:,1:6)], ...
    fismat2);
index = 21:720;
subplot(211), plot(time(index), [x(index) anfis_output]);
xlabel('Time (hour)');
title('Power Supplied to the Load Time Series and ANFIS Prediction');
subplot(212), plot(time(index), x(index) - anfis_output);
xlabel('Time (hour)');
title('Prediction Errors');
%
```